





Nuclear Science User Facilities 995 MK Simpson Blvd. Idaho Falls, ID 83401-3553

nsuf.inl.gov

Disclaimer

This information was prepared as an account of work sponsored by an agency of the U.S. Government. Neither the U.S. Government nor any agency thereof, nor any of their employees, makes any warranty, expressed or implied, or assumes any legal liability or responsibility for the accuracy, completeness, or usefulness, of any information, apparatus, product, or process disclosed, or represents that its use would not infringe privately owned rights. References herein to any specific commercial product, process, or service by trade name, trade mark, manufacturer, or otherwise, does not necessarily constitute or imply its endorsement, recommendation, or favoring by the U.S. Government or any agency thereof. The views and opinions of authors expressed herein do not necessarily state or reflect those of the U.S. Government or any agency thereof.

Editor: Tiffany Adams

Writers: Tiffany Adams, Karen Bass, Cory Hatch, Paul Menser

Photographers: Wes Agresta, Allison Corona, Manuel Gillispie, Chris Morgan, Andrea Starr

Graphic Designer: Kristyn St. Clair

Cover Image: The Hot Fuels Examination Facility (HFEF) at Idaho National Laboratory

CONTENTS

Nuclear Science User Facilities	
Our NSUF Team	4
From the NSUF Director	7
NSUF by the Numbers	8
NSUF Across the Nation	
Map of NSUF Partner and User Institutions	10
NSUF User Institutions	
NSUF Overview	
IMCL Instrumentation Added	12
Researcher Highlights	
• Cheng Sun	
• Liz Getto	
• Mukesh Bachav	26
• Yutai Katoh	30
Table of FY-18 Awarded Projects	
NSUF Awarded Projects	
Select Project Reports	5 1
•	
Resources	
Acronyms	126
• Index	128

OUR NSUF PROGRAM OFFICE TEAM



J. Rory KennedyDirector
(208) 526-5522
rory.kennedy@inl.gov

Dan Ogden
Deputy Director
(208) 526-4400
dan.ogden@inl.gov



Simon Pimblott
Chief Post-irradiation
Scientist
(208) 526-7499
simon.pimblott@inl.gov



Keith Jewell Technical Lead (208) 526-3944 james.jewell@inl.gov



Thomas Maddock
Technical Lead
(International)
(208) 526-2714
thomas.maddock@inl.gov



Nick Meacham
Experiment Manager
(208) 526-3227
nicholas.meacham@inl.gov



Brenden Heidrich Chief Irradiation Scientist (208) 533-8210 brenden.heidrich@inl.gov



Collin Knight
Post-irradiation
Examination Project Manager
(208) 533-7707
collin.knight@inl.gov



Katie Anderson
Experiment Manager
(208) 526-0049
katie.anderson@inl.gov



Jonathan Kirkham
Nuclear Energy Infrastructure
Database Coordinator
(208) 533-8188
jonathan.kirkham@inl.gov

John Coody
Project Scheduler
(208) 526-2964
john.coody@inl.gov



John Jackson
Industry Program Lead
(208) 526-0293
john.jackson@inl.gov

Lindy Bean
Acting Program
Administrator
(208) 526-4662
lindy.bean@inl.gov





Kelly Cunningham

Nuclear Fuels and Materials Library
Coordinator and RTE Administrator
(208) 526-2369
kelly.cunningham@inl.gov

Travis Howell
Planning and Financial
Controls Specialist
(208) 526-3817
travis.howell@inl.gov





Tiffany AdamsCommunications Liaison
(208) 526-4081
tiffany.adams@inl.gov

Renae Soelberg Administrative Assistant (208) 526-6918 renae.soelberg@inl.gov







FROM THE NSUF DIRECTOR

J. Rory Kennedy
Director
(208) 526-5522
rory.kennedy@inl.gov

nce again (and I never tire of telling you this) our Fiscal Year 2018 was another outstanding year for the Nuclear Science User Facilities (NSUF) program. Overall, we provided about \$17.6 million in new funding for projects, up from \$15.1 million in Fiscal Year 2017, providing even more opportunities to nuclear energy researchers to advance our understanding of the behavior of nuclear fuels and materials under irradiation. Over 62 percent of our new awards went to university researchers and first time applicants represented over 50 percent of our new awards.

We continued to see the number of Rapid Turnaround Experiment (RTE) proposals increase (280 in FY-18 versus 180 in FY-17) and were able to award 105 projects (versus 92 in FY-17). Although the number of awards increased, our awards to proposals ratio decreased. We hope to increase our funding for the RTEs in Fiscal Year 2019. NSUF also awarded almost \$9.5 million in funding to nine Consolidated Innovative Nuclear Research (CINR) projects ranging in costs from about \$180,000 to almost \$2.1 million. These larger and longer term projects will address even more wide reaching questions, covering topics from in-pile instrumentation to additive manufacturing to separate effects and model validation of nuclear fuels to irradiation behavior of core and structural materials.

Interest from industry groups was maintained in FY-18. The NSUF strongly encourages applications from industry and small businesses to better the scientific understanding related to their critical issues. The NSUF works closely with and is a major contributor to the Gateway for Accelerated Innovation in Nuclear (GAIN) initiative whose mission is to address universal issues constraining the domestic nuclear industry. We anticipate that this relationship will foster ever more attention from industry researchers.

The continued increase in both the quantity and quality of NSUF funded research has led to a concomitant increase, yet again, of published articles. In FY-18, research funded by NSUF produced 96 peer reviewed publications and 65 conference proceedings. All totaled, NSUF research has been published in 87 different journals with the Journal of Nuclear Materials by far the journal of choice. Based on acknowledgements to NSUF, we maintain an H-index score of 17.

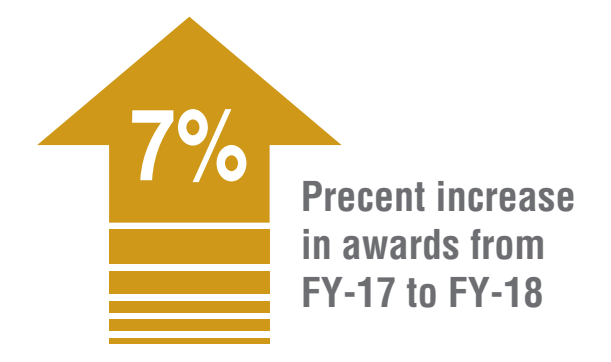
International awareness of NSUF continues to grow. The NSUF became part of the Enabling Technologies
Working Group of the Nuclear Energy
Research and Development Cooperative
Action Plan between the US-DOE and the Department for Business, Energy,

and Industrial Strategy of the UK. In addition, the NSUF was invited by the Organisation for Economic Cooperation and Development's Nuclear Energy Agency (OECD NEA) to speak at the Nuclear Science Committee Workshop "Enhancing Experimental Support for Advancements in Nuclear Fuels and Materials." The goal of this invitation was to showcase the NSUF's success at utilizing experimental infrastructure and serve as a possible template for other international user organizations.

The NSUF will continue to increase its impact and grow the nuclear research community through presentations, exhibits, and dedicated NSUF sessions at conferences and meetings. I am proud of the important role NSUF plays in nuclear energy research and look forward to what is to come such as our deployment of CoMET, the Combined Materials Experiment Toolkit, as an aid to our users in developing projects and the implementation of FaMUS, the Fuels and Materials Understanding Scale, developed to better quantify the state of understanding of materials studied through NSUF research.

J. Rory Kennedy

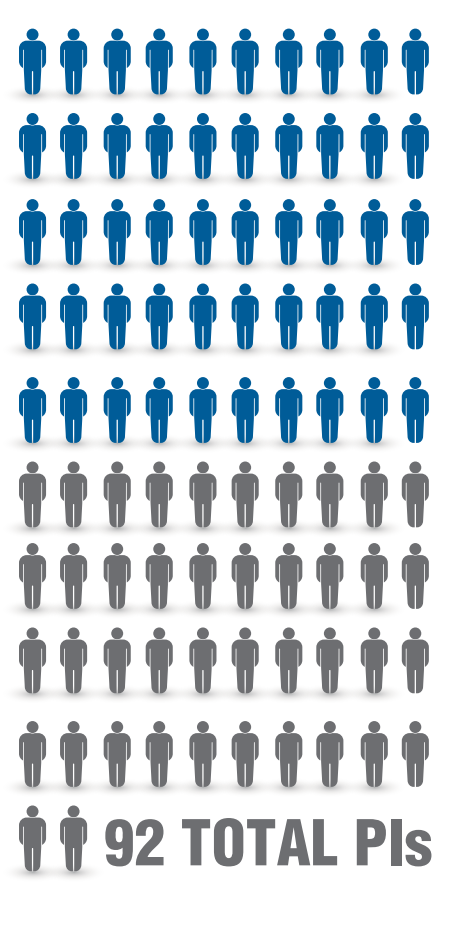
NSUF BY THE NUMBERS



15

NSUF program staff attended 15 conferences and meetings either as organizers, presenters, or exhibit representatives.

50 Number of new Pls



was provided for new awards to researchers around the world

Forty-two user organizations won awards in FY-18 Some organizations were awarded multiple projects.







National Laboratories 5 International Organizations





journal articles were published based on **NSUF-funded research**

NSUF ACROSS THE























































NSUF User Institutions

Alabama

Auburn University

Arizona

University of Arizona

California

Electric Power Research Institute General Atomics Stanford University University of California, Berkeley University of California, Santa Barbara

Florida

University of Florida

Idaho

Boise State University Idaho National Laboratory University of Idaho

Illinois

Argonne National Laboratory University of Illinois

Indiana

Purdue University University of Notre Dame

Kansas

Kansas State University

Maryland

Johns Hopkins University United States Naval Academy

Massachusetts

Massachusetts Institute of Technology

Michigan

Michigan State University University of Michigan

Missouri

Missouri University of Science & Technology

Nebraska

University of Nebraska

New Mexico

Los Alamos National Laboratory

New York

Stony Brook University

North Carolina

North Carolina State University

Ohio

The Ohio State University

Oregon

Oregon State University

Pennsylvania

Pennsylvania State University Westinghouse

Tennessee

Oak Ridge National Laboratory University of Tennessee

Texas

Texas A&M University

Virginia

Aeroprobe

Virginia Polytechnic Institute and State University

Washington

Pacific Northwest National Laboratory

Wisconsin

University of Wisconsin

Belgium

European Commission

Italv

Italian Institute of Technology

United Kingdom

National Nuclear Laboratory University of Liverpool University of Oxford

Germany

European Commission

INSTRUMENTATION ADDED INCL



Thermal Property Measurement Cell

ocated at Idaho National Laboratory's Materials and Fuels ■Complex, the 12,000-squarefoot Irradiated Materials Characterization Laboratory (IMCL) has acquired several key pieces of equipment in 2018, all aimed at enabling researchers to prepare and conduct microstructural-level investigations of the behavior of irradiated nuclear fuels and materials. Completed in 2012, IMCL is the newest building at MFC, longtime home of the Hot Fuel Examination Facility (HFEF), which for decades has performed postirradiation examination of irradiated samples in two large, heavily shielded, argon-filled hot cells.

IMCL was designed from the outset to house state-of-the-art scientific instruments, evolving as instrument capabilities improved over time. Each instrument is housed in an independent modular radiological shielding and confinement system to isolate the user from radiation.

It is no coincidence that the vision for the laboratory dates back to the same time of NSUF's founding with INL's Advanced Test Reactor as the first user facility. Just as ATR is available to users across the United States for irradiation of fuel and material samples, IMCL provides a national resource for post-irradiation examination and analysis.

NSUF has supported the IMCL buildout and invites the worldwide nuclear community to use the capabilities now available to help improve understanding of these complex and difficult-to-handle materials.

"IMCL offers an entirely new way to use instruments in a highly irradiated environment," said Dr. Mitch Meyer, director of INL's Characterization and Advanced Post-Irradiation Examination division. "Our goal is to provide the nuclear energy research community with routine access to the same high-end characterization tools used to advance technology in other industry sectors."

Combined with INL's advanced computer modeling capabilities, the work at IMCL will enable faster development of advanced fuel designs, reducing the time needed for fuel development and licensing as well as the expense involved.

During FY-18, two shielded dual-beam Focused Ion Beam (FIB) systems were placed into service. Of the six FIB instruments in the world capable of characterizing highly irradiated fuel specimens, two are at IMCL, with the third at another building at INL's Materials and Fuels Complex. In addition to the world class FIB capabilities, IMCL offers a complete suite of other material characterization tools.

Current IMCL Capabilities

Thermal Property Measurement Cell

Measuring the thermal properties of nuclear fuels and materials is essential to understanding and predicting the performance of fuels and materials in a reactor system. Detailed plans for the Thermal Property Measurement Cell at IMCL began in 2015, when INL's Thermal Properties Capability Development Workshop was held to identify the capabilities needed by various nuclear programs and the thermal properties instruments needed for nuclear research. As a result, IMCL's shielded Thermal Property Measurement Cell includes four work stations designed to house the following:

- · A laser flash thermal diffusivity.
- · A thermomechanical analyzer.
- A differential scanning calorimeter/ thermogravimetric analyzer.
- An INL-developed thermal conductivity microscope.

These new capabilities are designed to make accurate measurements that provide direct data, feed and validate models, and result in reduced uncertainty and faster licensing times for accident tolerant and advanced fuels.

Electron Probe Micro-Analyzer

The EPMA is an electron beam instrument used primarily for high accuracy, in situ nondestructive chemical analysis of full cross sections of solid fuel and structural material samples. The EPMA acquires quantitative elemental analyses on relatively large samples at high spatial resolution (as little as one to two microns) using wavelengthdispersive spectroscopy. This information is used to understand elemental redistribution, the chemical behavior and migration of solid fission products, fission gas behavior, and the impact of these phenomenon on fuel behavior and fission product release.

Focused Ion Beam (FIB) and Scanning Electron Microscope (SEM)

One of IMCL's most versatile instruments is its combined FIB and SEM. The combination of the FIB and SEM allows three-dimensional reconstruction that is important for understanding material structure at the micrometer scale.

The SEM uses a focused beam of high-energy electrons to generate a variety of signals at the surface of solid specimens. The signals that derive from electron-sample interactions reveal information about the sample including external morphology (texture), chemical composition, crystalline structure and grain orientation.

The primary use of the FIB is as a high-precision "knife" used to cut out small samples from areas identified using SEM. By using the FIB, features often lost using traditional metallurgical sample preparation are preserved. These small samples are then subject to further analysis using a variety of methods.



Electron Probe Micro-Analyzer



Focused Ion Beam and Scanning Electron Microscope



Shielded Sample Preparation Area

The characterization of irradiated fuels and materials depends on the availability of high-quality samples that require great care to produce, which is often a limiting factor in research. IMCL's SSPA provides specialized sample preparation capability for fuels that supplements what is available in the Hot Fuel Examination Facility (HFEF). SSPA includes a shielded

sample preparation cell, an optical microscope, and a sample transfer cell that provides connectivity to HFEF and other facilities with an IMCL shielded container. A glovebox and hood line are also available for preparation and decontamination of lower activity samples.

Shield Sample Preparation Area



Transmission Electron Microscope

Transmission Electron Microscope (TEM)

IMCL's TEM offers an accelerating voltage range of 80 to 200 KV, 0.16 nm resolution, X-FEG high brightness Schottky source, four windowless silicon drift detectors and very fast data acquisition, all to mean that this TEM provides researchers a better, more accurate picture more quickly.

Detectors are interlocked to shutters to shield in case of high gamma dose rate from specimens. It features a piezo-electric specimen stage with single tilt, low background double tilt, high-angle single tilt-rotate tomography holders, and on-axis bright field, dark field and high angle annular

dark field STEM detectors with the capability to display multiple image signals simultaneously.

For imaging, the unit incorporates a 4k x 4k 16-bit CMOS camera. The TEM provides atomic-scale imaging and chemical analysis that is complementary to SEM and Atom Probe Tomography, and provides a platform for many in situ experiments, including mechanical testing, observation of corrosion processes in environmental cells, heating above 1000° C and cooling to cryogenic temperatures. Analyses in the TEM are on a scale consistent with atomistic modeling, and when coupled with modeling and simulation, provide a more fundamental understanding of the processes that drive fuel and material behavior.

Looking Forward

Several new instruments are in the procurement and installation process and will come online in FY-19.

- Local Electrode Atom Probe (LEAP): This new piece of equipment will allow atomic-scale three-dimensional reconstructions and an X-ray computed tomography microscope that will provide three-dimensional images over a wide range of sample sizes and magnifications.
- A Physical Property Measurement System (PPMS) will measure the fundamental electronical, and thermal properties of actinide alloys and compounds that provide a more basic understanding of the performance of these materials.
- IMCL's existing TEM is in the process of being upgraded with an Electron Energy Loss Spectrometer (EELS) and a probe corrector, which will provide information on the chemical state of elements, allow light element analysis and increase resolution to 0.08 nm.

While most of the floor space in IMCL is filled with scientific instruments, space is being left open for the future. "We want to allow the NSUF community to decide what they want to do with that space," Meyer said.

RESEARCHER HIGHLIGHTS



Dr. Cheng Sun

r. Cheng Sun, a staff scientist and principal investigator at Idaho National Laboratory, studies materials irradiated in nuclear reactor environments. One of the biggest challenges guiding nuclear energy is the need to develop advanced materials that can better withstand harsh environments, like high temperatures and neutron/ion bombardment experienced inside a nuclear reactor.

"We are performing fundamental understanding on the irradiation effects on reactor materials," Sun said. "We hope we can design and develop advanced materials that can be used in reactors for longer service time."

Although his interest in nuclear energy research didn't begin until he came to the United States to pursue a doctorate, Sun has always been interested in how materials are formed and changed by their environment. As a child growing up in China, Sun never forgot an interesting grain texture revealed on the surface of a weathered stainless steel structure he once saw. When he began studying materials science and engineering in college, he came across the phenomenon again. "Crystalline metals have grain structures," Sun said. "I didn't know what it was when I was a child, but later on I realized what I had seen."

Today, Sun continues pursuing that interest in materials science as he researches materials performance in extreme conditions. His research is focused on gaining a better understanding of a material's performance under extreme environments, with emphasis on the manufacturingmicrostructure-mechanical property relationships of materials under irradiation. His primary areas of experimental expertise include additive manufacturing of nuclear materials, characterization of irradiated materials via electron microscopy and high-energy X-ray scattering, and small-scale mechanical testing of irradiated materials.

Sun has worked at Idaho National Laboratory since 2016, when he arrived in Idaho as the first Russell L. Heath Distinguished Postdoctoral Associate. The Russell L. Heath postdoctoral appointment was established to attract, recruit, develop and inspire early career researchers who have the potential to develop into INL's future scientific and technical leaders.

At that time, INL's manager of advanced characterization department, Dr. Jian Gan, said Sun's proposal spoke for itself. "His impressive research achievements, supported by his strong publication record, make him a highly talented, early career researcher with great potential to make significant





contributions to INL's nuclear structural materials initiatives." Gan served as Sun's mentor at that time, and the two continue to collaborate on research projects.

Sun's early education was in China (he earned his bachelor's and master's degrees in materials science and engineering from Huazhong University of Science and Technology and the Institute of Metal Research, Chinese Academy of Science, respectively), but he chose to pursue a doctorate at an American school, Texas A&M University. "Obtaining a Ph.D. from the world's best higher-education system helped me distinguish myself from my peers," Sun said. His advisor, Professor Xinghang Zhang, inspired him to focus on nuclear materials research.

Following graduation from Texas A&M, Sun began research on radiation-induced solute redistribution in nuclear structural materials at Los Alamos National Laboratory, where he was a G.T. Seaborg Institute Postdoctoral Fellow. When that fellowship came to an end, Sun set his sights on Idaho. "Idaho National Laboratory is the nation's leading institute for nuclear energy research and development," he said. "INL has many world-class research facilities, like the Advanced Test Reactor, the Irradiated Materials Characterization Laboratory (IMCL) and the Electron Microscopy Laboratory (EML)."

Sun, along with researchers from all over the country, does the majority of his work within the IMCL and EML. Heavily shielded, specialized instruments allow users to safely prepare

irradiated materials (cut, slice and polish very small samples), and then examine them in electron microscopes at the micro, nano and atomic level.

Working with NSUF, Sun continues his research while collaborating with experts and helping train the next generation of researchers. He has mentored several students from universities from across the country who come to INL and do research for their doctoral thesis. "Working at INL is a big plus to their career," Sun said. "They are getting their research done and have published some high-impact journal papers." Sun also works with local students, teaching a course on fundamentals of nuclear materials through the Idaho Falls branch of the University of Idaho.

Sun enjoys working with his colleagues in facilities all across INL, from the Advanced Test Reactor to the Materials and Fuels Complex to the High Performance Computing group in Idaho Falls. "One of the things I really like working at INL is that we always work together," Sun said. "With working on radioactive materials, it's very difficult for people to work alone. It's always teamwork. Some people work on sample transportation, some people work on irradiation, some people work on microstructure characterization, and some people work on mechanical testing. Also, working with the modeling team is a fun part of our research - all of these people are needed to produce world-class research."

"One of the things I really like working at INL is that we always work together,"

Sun said.



Elizabeth Getto

or Elizabeth Getto, a mechanical engineering assistant professor at the U.S. Naval Academy, Rapid Turnaround Experiments (RTEs) funded through the Nuclear Science User Facilities have been essential to research that she and her colleagues would otherwise not have the resources to pursue.

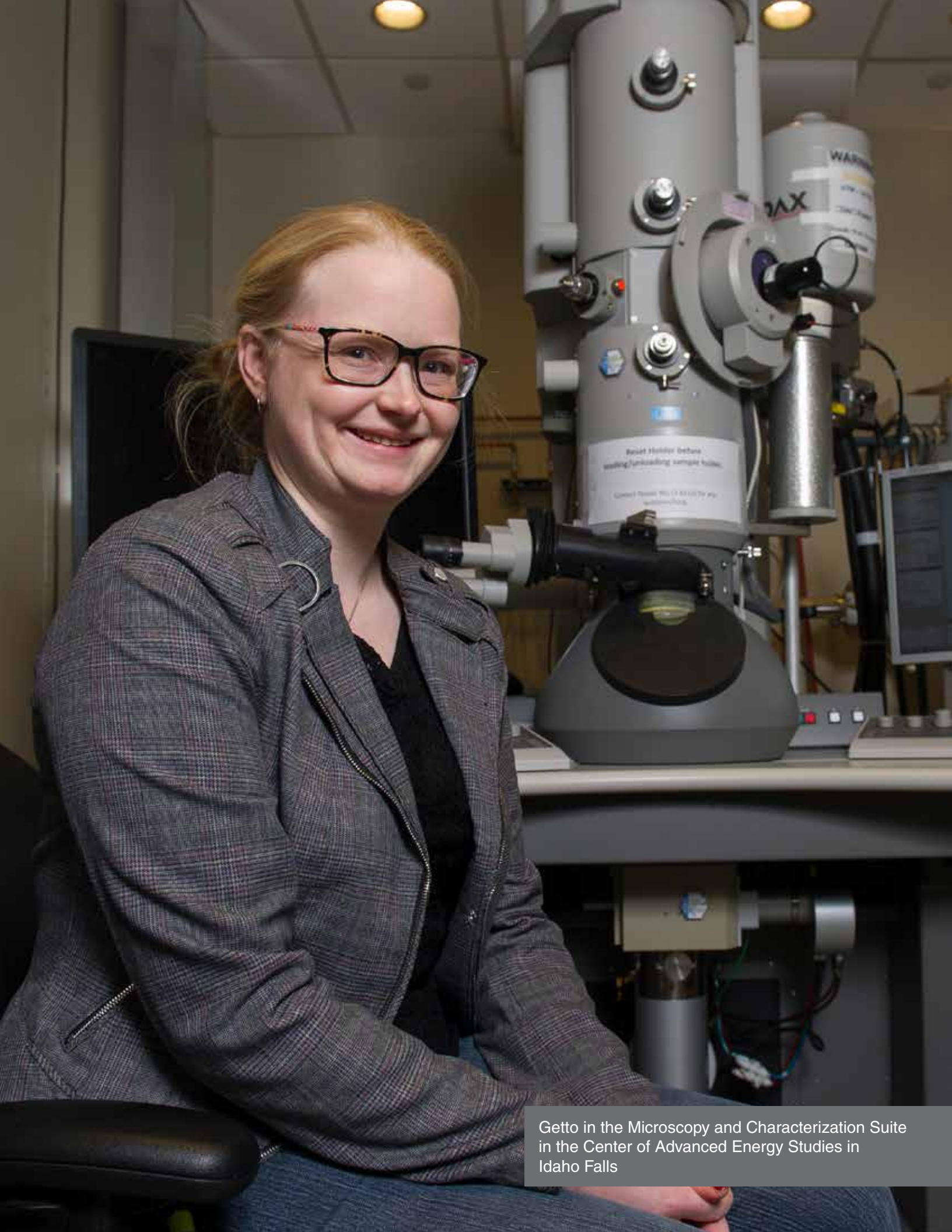
Based on research funded in 2017, the first RTE of three, Getto was the lead researcher on a paper published in the December issue of Journal of Nuclear Materials detailing the effect of friction stir welding and self-ion irradiation on dispersoid evolution in oxide dispersion strengthened (ODS) steel.

To ensure the safety and reliability of small modular reactors, microstructural characterization of the irradiated materials is essential. she wrote. But neutron irradiations are costly, time-consuming, and typically require hot cells for materials examination. Utilizing ion irradiation as a surrogate mitigates many of the challenges associated with neutron irradiation testing, and self-ion irradiations allow for accelerated irradiation testing with well-controlled temperature, pressure, and dose in candidate structural materials.

Getto said the advantage of working through NSUF is that the funding is taken care of, allowing her to focus on the research. "As a new professor at an undergraduate institution, \$50,000 means an awful lot to me," she said.

Her focus has been on the effects of radiation and welding on oxide dispersion strengthened steels, specifically on MA956 ODS alloy, a friction-welded iron-based superalloy that is in relatively short supply. ODS steels are commonly used in reactor vessels. Ultimately, the research will help engineers understand how long a reactor can be run before adverse conditions in the other structural materials need to be addressed.

The experiments detailed in the Journal of Nuclear Materials were to determine systematically the effect of welding and irradiation on ODS steel MA956 at reactor-relevant conditions of 450 degrees Celsius up to 25 displacements per atom (dpa). They found that friction stir welding resulted in the coarsening of the dispersoids relative to the base material, implying that it recovers





lost strength from the welding process. After irradiation, both the diameter and number density increased, which was explained by an irradiation-enhanced diffusion mechanism, reflecting how precipitation and growth of the dispersoid occurs under irradiation.

Future efforts to increase the library of MA956 sample conditions at higher doses within the reactor operating envelope are planned, to provide more evidence for the suitability of MA956 being used in next-generation reactors.

The 2018 RTE was the third, and a continuation of ion irradiation research Getto had done at the University of Michigan's Michigan Ion Beam Laboratory, an NSUF partner facility, and in the Microscopy and Characterization Suite at the Center for Advanced Energy Studies in Idaho Falls, where NSUF has its headquarters. The work is being funded in part by the Defense Threat Reduction Agency (DTRA).

Collaborating with Cmdr. Brad Baker, a professor at the Naval Academy, they plan to conduct further research in spring 2019 at Idaho

National Laboratory's Materials & Fuels Complex (MFC).

Getto joined the Naval Academy faculty in 2016 after receiving her master's and doctorate in nuclear engineering from University of Michigan. She quickly became aware of NSUF and the opportunities represented by RTEs, and the opportunities for the Naval Academy, which has about nine faculty and 45 people on staff focused on nuclear research plus a wealth of materials. Born into a nuclear Navy family, Getto teaches in Rickover Hall, named after Adm. Hyman Rickover, the admiral who directed the original development and use of nuclear in its fleet. She believes the Navy has a special leadership position in the nuclear research community.

"The next generation has some new ideas," she said. "We're much more willing to reach across the aisle to environmentalists, and more open to new technologies. It's one thing for a professor to say, 'Nuclear energy is the solution,' but to get buy-in from midshipmen at the Academy is another matter."



Mukesh Bachhav

r. Mukesh Bachhav has done research on three continents, but Idaho National Laboratory is where he has found the tools essential to his efforts at high-resolution characterization of irradiated nuclear materials.

Bachhav is an Atom Probe Tomography (APT) lead in INL's Irradiated Materials Characterization Laboratory (IMCL) at the Materials & Fuels Complex (MFC), an integral part of the NSUF network.

A native of Nashik, India, he earned his doctorate in materials science from France's University of Rouen and his master's in physics from India's University of Pune. While doing postdoctoral work at University of Michigan (another NSUF partner), Bachhav made use of the resources available at MFC and also in the Microscopy and Characterization Suite (MaCS) at the Center for Advanced Energy Studies (CAES), where NSUF leadership has its home.

INL turned out to be "a perfect fit," Bachhav said. NSUF's Nuclear Fuels and Materials Library (NFML) and INL's interest in elucidating irradiated nuclear materials at a nanoscale level to understand irradiation performance provided a rare opportunity to work in the Characterization and Advanced Post-Irradiation Examination Division at MFC. Much of his work is done with the APT instrument at CAES, a

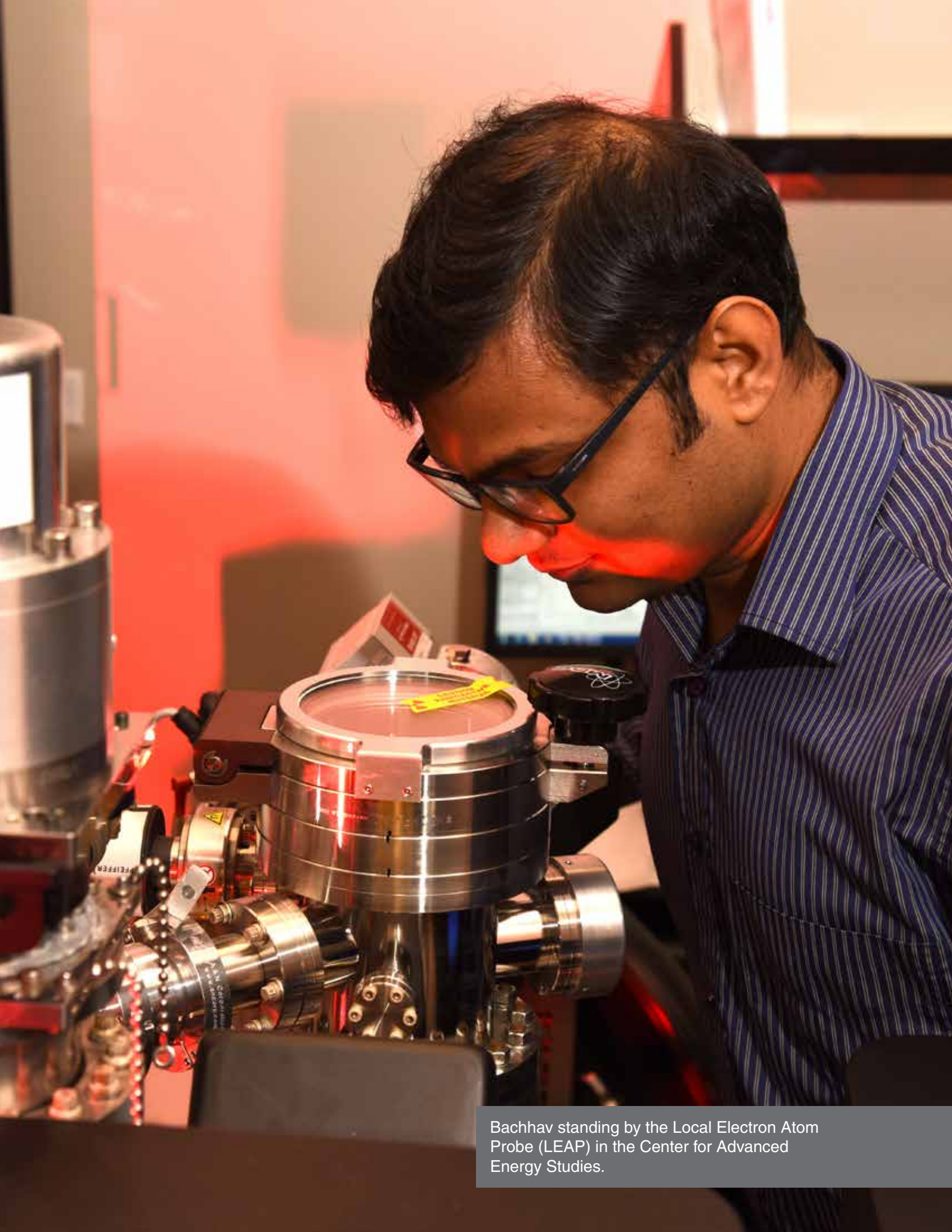
unique facility that allows analysis of "hot," meaning radioactive, materials with ease. This enables research on nuclear fuels and materials to be performed on a routine basis.

Bachhav was the lead author of an article, "Challenges and Opportunities on Elucidating Irradiated Fuels with Atom Probe Tomography," published Aug. 1, 2018, in the journal Proceedings of Microscopy & Microanalysis. Co-authors included his IMCL colleagues Dr. Jian Gan, Dr. Lingfeng He and Dr. Brandon Miller, as well as Dr. Dennis Keiser of INL.

The paper lays out the advantages that APT can bring to understanding microstructural evolution in nuclear fuel materials that have been subjected to extreme conditions. One of the main mechanisms guiding the microstructural changes in fuels is damage associated with the formation and migration of fission products.

This can lead to void formation and grain boundary segregation, which can cause fuel to lose integrity, they wrote. During irradiation in aggressive reactor conditions, interaction can occur between the fuel particle and the matrix in a dispersion fuel that results in the development of an interaction layer that is unstable under irradiation, which can contribute to fuel plate failure.

To understand migration of fission products and their effect on fuel performance, APT is a unique





technique to provide 3D distribution of microstructures in materials at nano-length scale, along with near exact chemistry mapping of the elements. The APT work done in the past to analyze irradiated metallic and oxide fuels for correlating microstructure with the performance of fuel has been limited.

However, Bachhav and his colleagues described in the paper how they carried out systematic APT study on Uranium-Molybdenum (U-Mo) alloy fuel particles coated with a diffusion barrier layer of zirconium nitride (ZrN) and dispersed in an aluminum matrix. APT analysis on irradiated U-Mo fuel revealed a uniform distribution of spherical-shaped clusters enriched with fission products such as ruthenium, palladium and cadmium. Quantification of the fission products relied on the operating conditions of the APT instrument (base temperature, pulse rate, detection rate, laser and mode of operation). They found that low-base temperature and voltage mode during APT analysis offered better spatial resolution and quantification of the fission products formed in irradiated U-Mo fuel Transmission Electron Microscopy (TEM) analysis offered high-resolution images of bubbles, along with the distribution of uranium and molybdenum, though it has some limitation when it comes to quantification of fission products.

Although APT offers high chemical and spatial resolution that no other technique can match, the team said there are still challenges involved with multicomponent materials and interfaces, such as what is called the local magnification effect, arising from differences in evaporation fields of adjacent phases. "These differences can lead to ion trajectory overlaps near the interface and loss of spatial resolution," the researchers wrote.

Bachhav has been awarded with several DOE-NE NSUF proposals, which are in close collaboration with universities such as University of Wisconsin, University of Florida, United States Naval Academy and Massachusetts Institute of Technology. While he is a recognized reviewer for several publications, including Journal of Applied Physics Letters, Journal of Nuclear Materials, and Materials Science & Engineering B, Bachhav is also a member of the International Youth Nuclear Congress. IYNC's goal is to provide a global network for young professionals in the nuclear field, especially when it comes to the transfer of knowledge from the current generation of leading scientists and engineers to a new generation.



Yutai Katoh

aterials scientist Yutai
Katoh credits an elementary school science experiment—the construction of a simple radio from a germanium diode and a crystal earphone—with sparking his love of science and engineering.

His resume since then includes working with teams that developed plasma-facing materials for a fusion reactor at Japan's National Institute for Fusion Science (NIFS), and a high-density silicon carbide matrix that led to accident tolerant fuels for conventional and advanced light water reactors.

Now, in Katoh's current job as a program manager for fusion materials science and advanced nuclear materials at Oak Ridge National Laboratory, he hopes his contributions will continue to promote the safety and acceptance of nuclear power.

Katoh grew up in Tokyo, Japan, the son of a real estate developer and a pharmacist. In high school, his heroes included Soichiro Honda and Masaru Ibuka, the founders of Honda Motor Company and Sony, respectively.

In college, he developed an interest in fusion and eventually began pursing a degree in materials science engineering. "I read introductory books and articles about fusion energy and realized that superconducting materials are among the key technologies," Katoh said. "This was the time when the high temperature superconductor boom was in its beginning."

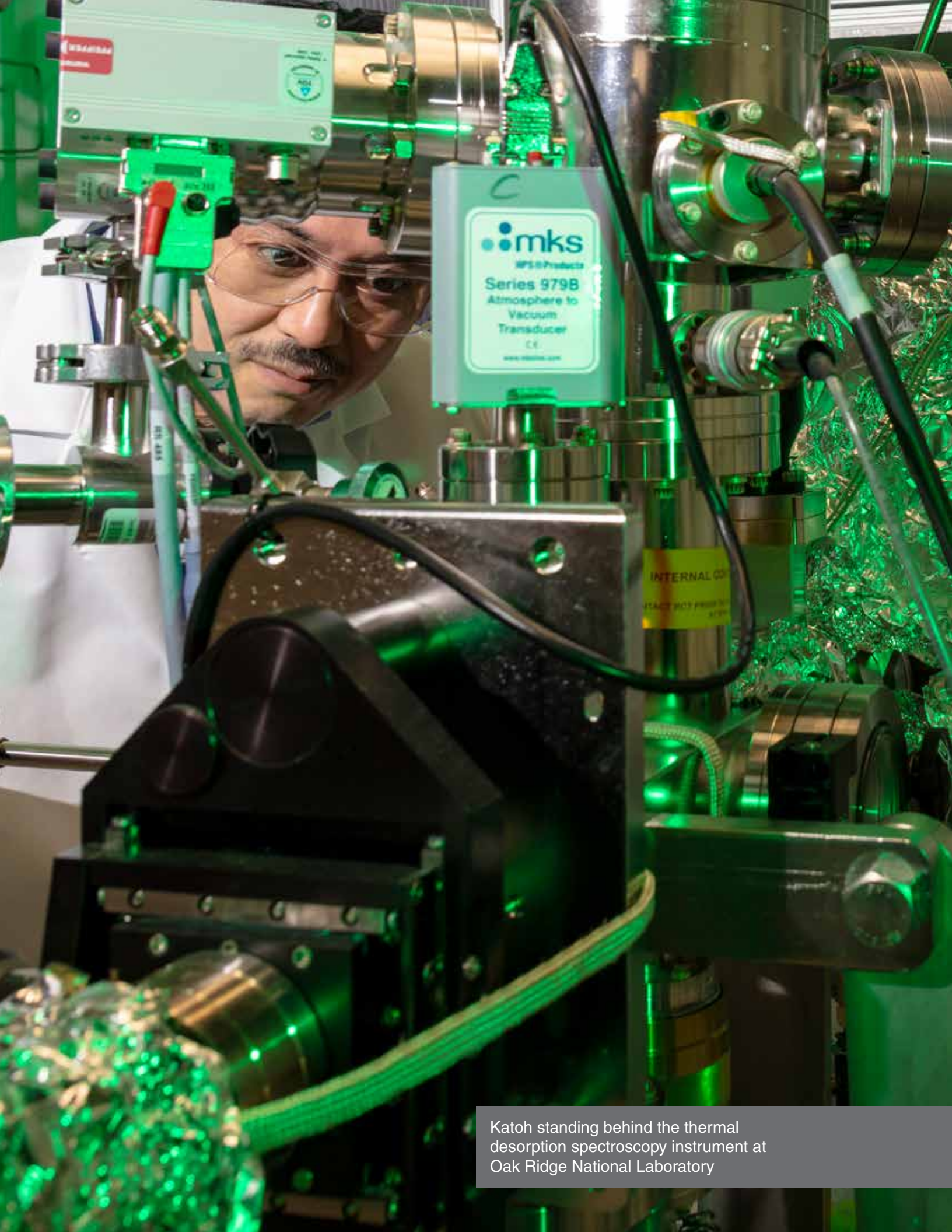
During his junior year, a professor noticed Katoh's ability to design and build electronic circuits and offered to become his graduate adviser.

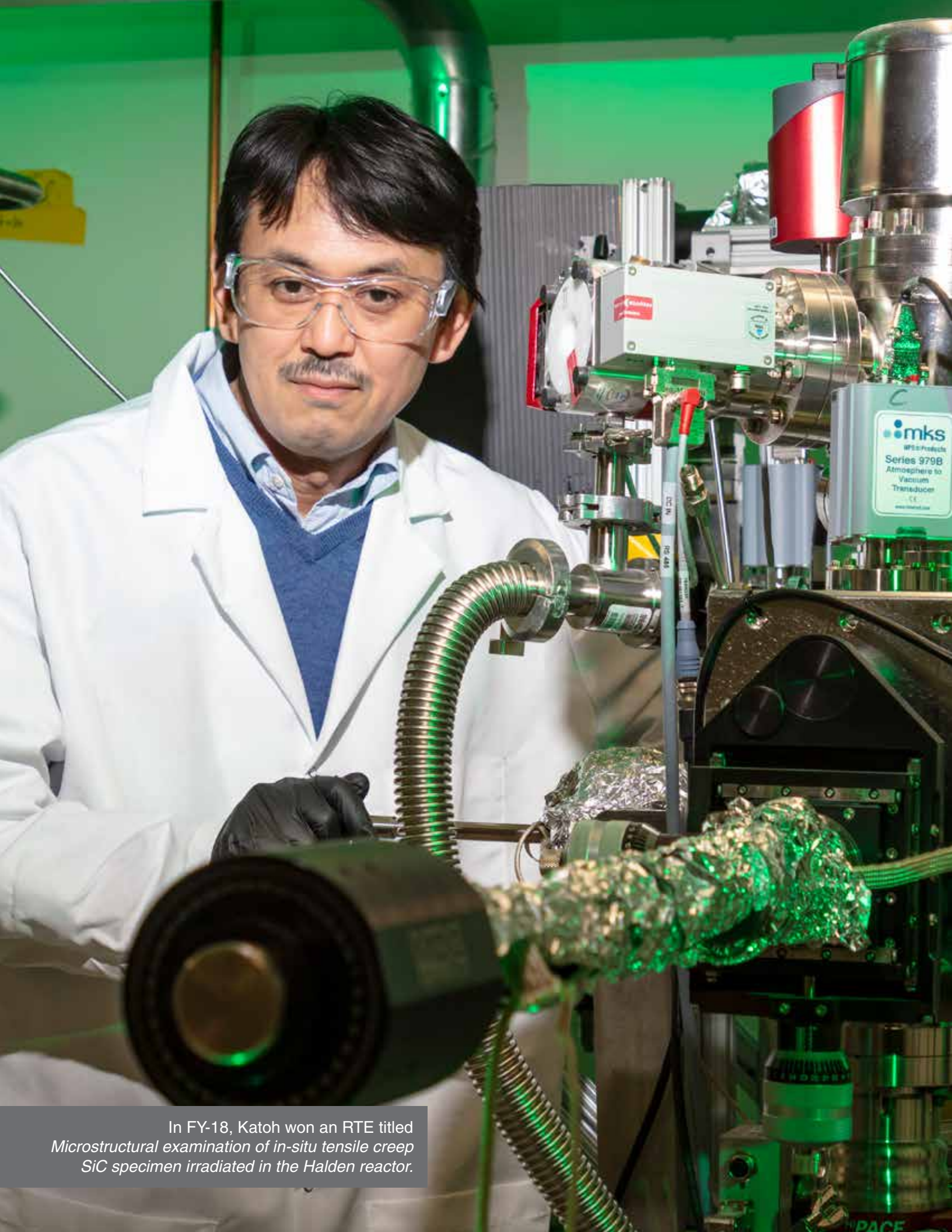
"The group was studying radiation effects in fusion materials, which resonated with my interest," Katoh said. "The group was building a new ion irradiation facility, and my project had a side focus on building electronics for beam current profiling and electron beam heating."

Katoh stayed with the group as he earned his Ph.D. studying radiation effects in steels for nuclear applications.

From there, Katoh went to the newly founded NIFS. His job was to assist with plasma-facing components (PFC) engineering in support of experiments using the Large Helical Device stellarator, a nuclear fusion research device that uses magnetic fields to control fusion plasma.

"There was a huge gap between materials science and PFC engineering," Katoh said. "I didn't realize at that time that the gap would stay as a challenge for fusion energy development for decades to come."





When Katoh's adviser moved to Kyoto University, Katoh decided to join him. The pair soon had a proposal accepted for the development of silicon carbide composites for high temperature energy applications.

"One of the notable inventions from the project was the NITE silicon carbide composite," Katoh said. "This invention produced a new class of silicon carbide composites at that time, and later led to invention of the Fully Ceramic Microencapsulated fuel for light water and advanced reactors."

In 2003, after years of involvement in U.S.-Japanese partnerships at both Pacific Northwest National Laboratory and Oak Ridge National Laboratory (ORNL), a collaborator at ORNL offered Katoh a job, and he accepted.

Since then, he has served as primary investigator for numerous fission and fusion materials science projects, including development and characterization of ceramics, graphite, composites and other advanced materials for high temperature and severe environment applications; neutron irradiation effects in metals, alloys and ceramics; and development of accident tolerant fuel materials and technologies for nuclear reactors.

Over the course of his career, he has authored or co-authored nearly 400 journal articles.

More recently, he's started developing new programs and gotten more involved with management.

"I am hoping to contribute to making nuclear energy safer, more widely accepted, and utilized to its potential through helping develop advanced fuels and materials," Katoh said.

AWARDED PROJECTS

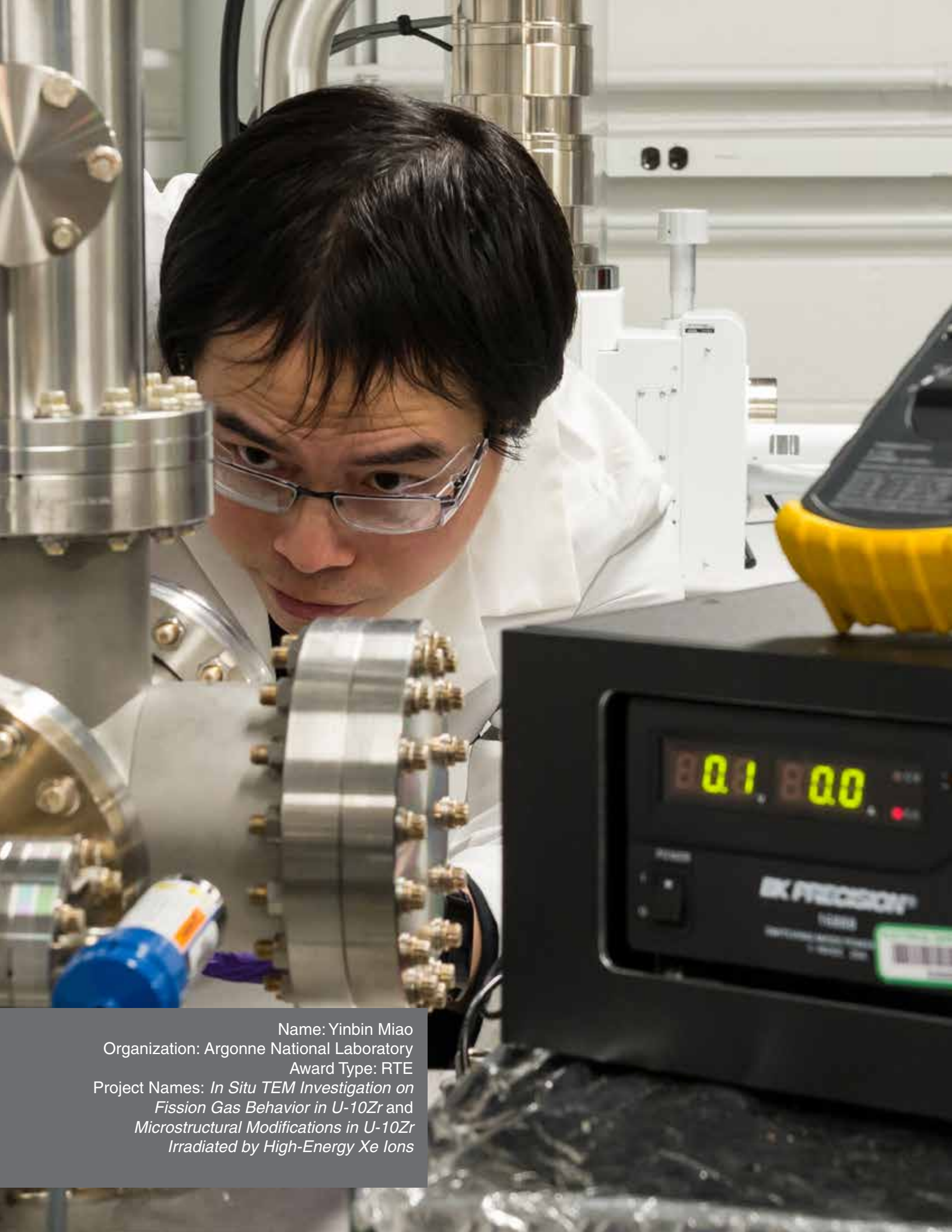
RTE 1st Call

PI Name	Institution	Title	Facility
Nathan Almirall	University of California, Santa Barbara	Atom Probe Tomography Investigations of nm-Scale Precipitates in Reactor Pressure Vessel Steels in the UCSB Advanced Test Reactor (ATR-2) Neutron Irradiation Experiment	Center for Advanced Energy Studies
Maria Auger	University of Oxford	Post-irradiation analysis at the nanoscale of 14YWT after high dose (16.6 dpa) neutron irradiation at 386C and 412C	Oak Ridge National Laboratory
Mukesh Bachhav	Idaho National Laboratory	Understanding the role of grain boundary character in segregation behavior of solute elements in neutron irradiated 304 SS using Atom Probe Tomography.	Center for Advanced Energy Studies
Nicholas Brown	Pennsylvania State University	Kinetics of irradiation defect annealing and thermal conductivity recovery in silicon carbide at high temperature	Oak Ridge National Laboratory
Matthew Cook	University of Florida	Fission Product Distribution Comparison in Irradiated and Safety Tested AGR-1 and AGR-2 TRISO Fuel Particles	University of Florida
James Edgar	Kansas State University	Transmutation doping of hexagonal boron nitride	Ohio State University
David Estrada	Boise State University	Ion irradiation of Aerosol Jet Printed Cu, Ag, and Ni Structures	University of Michigan
Rodney Ewing	Stanford University	In situ study of "rim effect" microstructure modification of nuclear fuels (resubmitted)	Argonne National Laboratory
David Frazer	University of California, Berkeley	Elevated Temperature In-situ SEM micro compression of UO_2	University of California, Berkeley

PI Name	Institution	Title	Facility
Jian Gan	Idaho National Laboratory	Investigation of gas bubble behavior in metals using in-situ Ne, Ar and Kr ion irradiation	Argonne National Laboratory
Lingfeng He	Idaho National Laboratory	Characterization of grain boundaries of Alloy X-750 irradiated in EBR-II	Idaho National Laboratory
Kathy Lu	Virginia Polytechnic Institute and State University	In situ TEM observation of microstructural evolution of silicon carbide (SiC)-nanostructured ferritic alloy (NFA) composite under high temperature ion irradiation	Argonne National Laboratory
Yutai Katoh	Oak Ridge National Laboratory	Microstructural examination of in-situ tensile creep SiC specimen irradiated in the Halden reactor	Oak Ridge National Laboratory
Takaaki Koyanagi	Oak Ridge National Laboratory	Pair distribution function analysis on recovery of irradiation induced defects in SiC	Brookhaven National Laboratory
Edward Lahoda	Westinghouse	Evaluation of Irradiated Cr Coatings on Zirconium Alloys	Westinghouse
Ju Li	Massachusetts Institute of Technology	Quantification of porosity evolution in ion irradiated metal-1D/2D nanocomposites and gas-embrittled steels via Positron Annihilation Spectroscopy	North Carolina State University
Subhashish Meher	Idaho National Laboratory	Electron Tomography for Three- Dimensional Characterization of Intragranular Fission Product Transport in Neutron-Irradiated Silicon Carbide in TRISO Fuel	Idaho National Laboratory
Yinbin Miao	Argonne National Laboratory	In Situ TEM Investigation on Fission Gas Behavior in U-10Zr	Argonne National Laboratory

PI Name	Institution	Title	Facility
Maria Okuniewski	Purdue University	Synchrotron X-ray Characterization of the Microstructural Evolution of U Alloys Irradiated to Low Fluences	Brookhaven National Laboratory
Riley Parrish	University of Florida	Microstructural characterization of \sim 7% burn-up MOX fuel	Idaho National Laboratory
Ramprashad Prabhakaran	Pacific Northwest National Laboratory	Mechanical characterization of three heats (ORNL, LANL and EBR II) of HT-9 after side-by-side neutron irradiation at LWR and fast reactor relevant temperatures	Pacific Northwest National Laboratory
Koroush Shirvan	Massachusetts Institute of Technology	Understanding the Mechanism of Thermal-Hydraulic Enhancement On Gamma Irradiated Nuclear Materials Interfaces	Sandia National Laboratories
Michael Short	Massachusetts Institute of Technology	Investigation of radiation-generated phases in FeCrSi alloys for multimetallic layered composite (MMLC) for LWR fuel cladding	Center for Advanced Energy Studies
Charlyne Smith	University of Florida	Atom probe tomography of fission gas bubble superlattice in U-Mo fuel	Center for Advanced Energy Studies
James Spicer	Johns Hopkins University	Understanding the mechanism for mesopore development in irradiated graphite by high resolution gas adsorption measurements (N2 and Kr at 77 K)	Oak Ridge National Laboratory
James Stubbins	University of Illinois	Microstructure characterization of neutron-irradiated Fe-Cr-C model alloys	Idaho National Laboratory
Matthew Swenson	University of Idaho	Irradiation-induced solute clustering behavior in ferritic/martensitic alloy T91	Center for Advanced Energy Studies
Jonova Thomas	Purdue University	Microstructural Phase Characterization of Irradiated and Control U-10Zr Fuels	Idaho National Laboratory
Kevin Tolman	Idaho National Laboratory	Towards characterizing the microstructural evolution in nuclear fuel via neutron diffraction	Massachusetts Institute of Technology

PI Name	Institution	Title	Facility
Julie Tucker	Oregon State University	Micro-mechanical characterization of long range order in Ni-Cr alloys and their response to radiation damage	University of California, Berkeley
Jean Claude Van Duysen	University of Tennessee	In Situ Straining of 10-dpa Neutron Irradiated Austenitic Stainless Steels using Scanning Electron Microscope Electron Backscatter Diffraction	Oak Ridge National Laboratory
Isabella Van Rooyen	Idaho National Laboratory	In-situ High Temperature Ion Irradiation Sandia National Laboratorio Transmission Electron Microscopy to Understand Fission Product Transport in Silicon Carbide of TRISO Fuel	
Janelle Wharry	Purdue University	Extension and Validation of Rate Theory Model of Nanocluster Irradiation Evolution: An Atom Probe Tomography Study	Center for Advanced Energy Studies
Karl Whittle	University of Liverpool	Interfacial Effects, Damage and Recovery in Binary Carbides	Argonne National Laboratory
Yong Yang	University of Florida	Understand the Fission Products Behavior and Irradiation Effects in UCO Fuel Kernels of Irradiated AGR-1 and AGR-2 TRISO Fuel Particles Using Titan Themis 200 with ChemiSTEM Capability	Idaho National Laboratory
Kayla Yano	Purdue University	TEM in situ 4-point bend fracture testing of irradiated ODS alloys	Center for Advanced Energy Studies
Tom Zega	University of Arizona	In situ Ion Irradiation of a SiC composite using a MEMS-based Heating Holder	Argonne National Laboratory
Xinghang Zhang	Purdue University	Radiation response of nanostructured steels with various types of defect sinks	Argonne National Laboratory
Steven Zinkle	University of Tennessee	Irradiation-induced precipitation/ segregation in dual-phase Al0.3CoCrFeNi alloy	Center for Advanced Energy Studies



RTE 2nd Call

PI Name	Institution	Title	Facility
Thomas Blue	Ohio State University	High Fluence Irradiation Testing of Fiber Optic Material Transmission	Oak Ridge National Laboratory
Nicholas Brown	Pennsylvania State University	Novel Microstructure Characterization of Pre-Hydrided ZIRLO® at Low Neutron Doses	Oak Ridge National Laboratory
Timothy Burchell	Oak Ridge National Laboratory	TEM investigation of irradiation, irradiation creep and thermal annealing effects in nuclear graphite	Oak Ridge National Laboratory
Mahmut Cinbiz	Oak Ridge National Laboratory	Characterization of Neutron-Irradiated Zr-1Nb-O Using Scanning Transmission Electron Microscopy	Idaho National Laboratory
Fabio Di Fonzo	Italian Institute of Technology	Controlling the kinetics of radiation induced crystallization in nanoceramics by doping	Argonne National Laboratory
Ben Eftink	Los Alamos National Laboratory	Study on defect evolution and stability of Y-Ti-O nano-oxides in 14YWT alloys under heavy ion irradiation	Argonne National Laboratory
Mohamed Elbakhshwan	University of Wisconsin	Radiation Damage in High Entropy Alloys	University of Wisconsin
David Frazer	University of California, Berkeley	High temperature in-situ small-scale mechanical testing of fast reactor mixed oxide (MOX) pins.	Idaho National Laboratory
Elizabeth Getto	United States Naval Academy	Radiation Tolerance of Advanced Joining Techniques for Oxide Dispersion Strengthened Steels under Ion Irradiation	Center for Advanced Energy Studies
Lingfeng He	Idaho National Laboratory	Microstructural characterization of trans- mutation nitride fuels for fast reactors	Idaho National Laboratory
Maik Lang	University of Tennessee	The study of local atomic structure and formation of ceramic phase in a simplified nuclear waste glasses	Brookhaven National Laboratory
Ju Li	Massachusetts Institute of Technology	In-situ TEM study of radiation and oxidation tolerance of MAX-phase-like materials	Argonne National Laboratory
Dong Liu	University of Oxford	In situ Study of the Irradiation Anisotropy in Fine Grain Nuclear-grade Graphite	Argonne National Laboratory

PI Name	Institution	Title	Facility
Xiaoyuan Lou	Auburn University	Heavy ion irradiation on SCC resistant austenitic stainless steel made by laser additive manufacturing	University of Michigan
Casey McKinney	University of Florida	EPMA Characterization of Actinide Redistribution and Fission Product Composition in MOX Fuels	Idaho National Laboratory
Yinbin Miao	Argonne National Laboratory	Microstructural Modifications in U-10Zr Irradiated by High-Energy Xe Ions	Center for Advanced Energy Studies
Michael Moorehead	University of Wisconsin	TEM and APT Characterization of Ion-Irra- diated High-Entropy Alloys for Sodium- Cooled Fast Reactors	Center for Advanced Energy Studies
Riley Parrish	University of Florida	TEM analysis of Irradiated MOX fuel	Idaho National Laboratory
Christian Petrie	Oak Ridge National Laboratory	Active Irradiation Testing of Temperature Sensing Capability of Clad Sapphire Optical Fibers with Type 2 Bragg Gratings using Optical Backscatter Reflectometry	Ohio State University
Pradeep Ramuhalli	Pacific North- west National Laboratory	Post-irradiation Piezoelectric Property Characterization of Radiation-Tolerant Piezoelectric Materials	Pacific Northwest National Laboratory
Niyanth Sridharan	Oak Ridge National Laboratory	Evaluating void swelling and microstructure evolution of additively manufactured HT9	University of Michigan
James Stubbins	University of Illinois	A comparative study of the radiation response of Fe–12Cr, Fe–14Cr, Fe–19Cr model alloys and a Fe–14Cr ODS alloy	Center for Advanced Energy Studies
Qing Su	University of Nebraska	Atom Probe Tomography Study of Helium precipitates in amorphous/crystalline SiOC/Fe nanocomposites	Center for Advanced Energy Studies
Matthew Swenson	University of Idaho	Characterization and modeling of secondary phase evolution in an irradiated Zr-1.0Nb alloy	Center for Advanced Energy Studies
Ming Tang	Los Alamos National Laboratory	Radiation Stability Study on Nuclear Waste Materials	Argonne National Laboratory

PI Name	Institution	Title	Facility
Jonathan Tatman	Electric Power Research Institute	Advanced microstructural and nano- hardness characterization of low penetra- tion pulsed-laser weldments performed on highly activated neutron irradiated stainless steel	Oak Ridge National Laboratory
Athanasia Tzelepi	National Nuclear Laboratory	Electron Tomography Characterisation of Porosity in IG-110 and NBG-17 Nuclear Graphite Grades	Oak Ridge National Laboratory
Haiming Wen	Missouri University of Science & Technology	Nanostructuring to enhance irradiation tolerance of ferritic/martensitic Grade 91 steels	University of Wisconsin
Janelle Wharry	Purdue University	Irradiated Microstructure Evolution in Cast Compared to PM-HIP Alloy 625	Westinghouse
Walter Williams	Purdue Univer- sity	In-Situ Phase Analysis of Phase Transitions in U-(6, 10, 20, 30) wt%Zr Fresh Fuels.	Los Alamos National Laboratory
Ge Yang	North Carolina State University	Positron annihilation lifetime spectroscopy investigation of vacancy-related defects in room-temperature radiation detector material CdZnTe	North Carolina State University
Zefeng Yu	University of Wisconsin	TEM/EDS study of Nb redistribution in ZrNb alloys following proton irradiation	Idaho National Laboratory
Dalong Zhang	Oak Ridge National Laboratory	Effects of Welding on Radiation-Enhanced Precipitation in FeCrAl Alloys	Center for Advanced Energy Studies

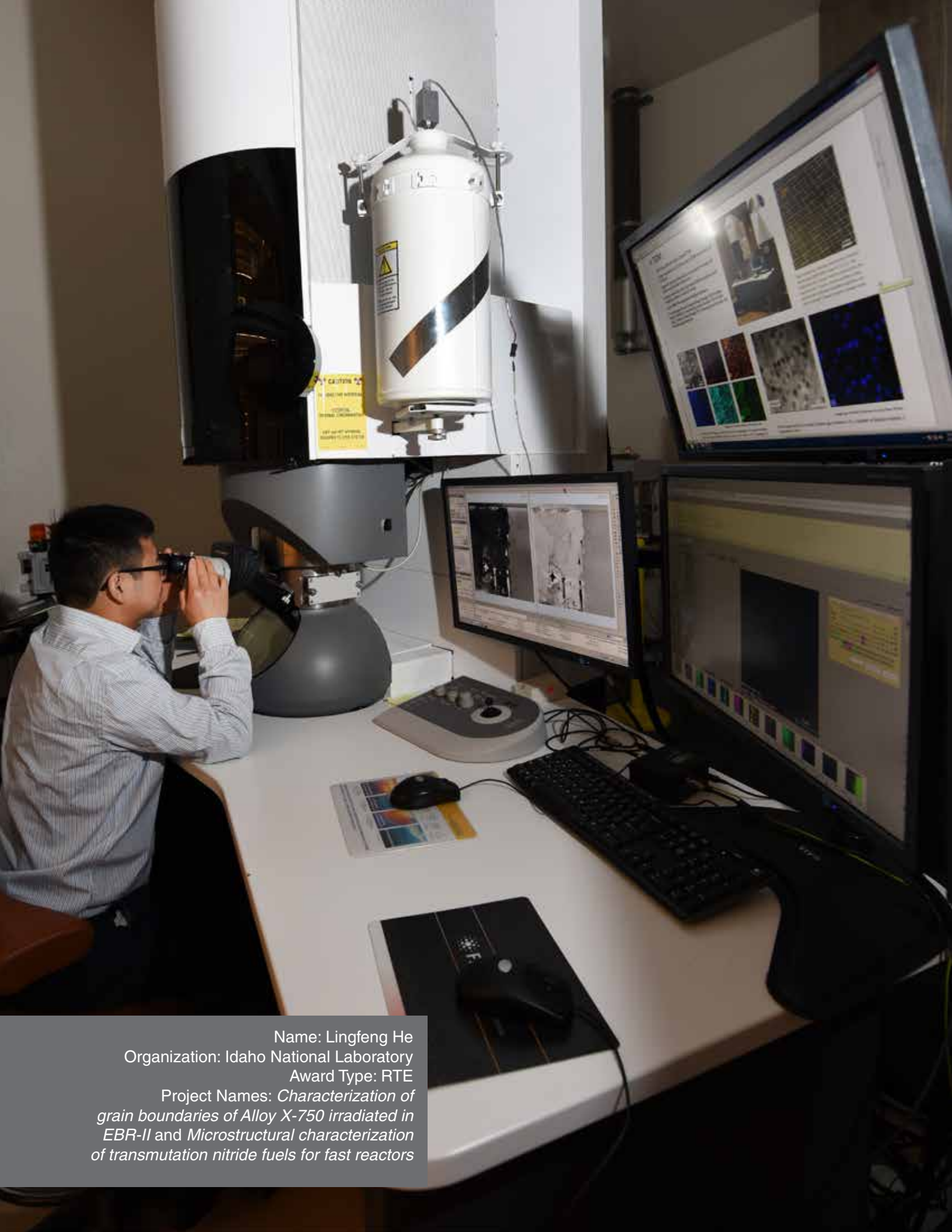
RTE 3rd Call

PI Name	Institution	Title	Facility
Assel Aitkaliyeva	University of Florida	Investigation of fuel-cladding chemical interaction (FCCI) in irradiated U-Pu-Zr fuel	Idaho National Laboratory
Brad Baker	United States Naval Academy	Characterization of Radiation Tolerance of Advanced Joining Techniques for Oxide Dispersion Strengthened Steels under Ion Irradiation	Center for Advanced Energy Studies
Carl Boehlert	Michigan State University	In-situ investigation of the Threshold Incubation Dose for the formation of c-component loops in additively manufactured and powder metallurgy rolled Ti-6Al-4V Argonne National Laboratory	
Leonard Brillson	Ohio State University	Neutron Irradiation of Ga2O3 to Identify Native Point Defects	Ohio State University
Fabiola Cappia	Idaho National Laboratory	Electron microscopy characterization of fast reactor MOX joint oxyde-gaine (JOG)	Idaho National Laboratory
David Carpenter	Massachusetts Institute of Technology	Microstructural characterization of grain boundaries in Hastelloy N corroded in molten FLiBe salt under neutron irradiation	Idaho National Laboratory
Cristian Contescu	Oak Ridge National Laboratory	Micro-structural investigation of the pore Oak Ridge National Labo structure of uncrept and crept irradiated PCEA graphite specimens with SEM and FIB tomography	
Bai Cui	University of Nebraska	Irradiation Damage in (Hf0.2Zr0.2Ta0.2Nb0.2Ti0.2)C High- Entropy Ceramics	Center for Advanced Energy Studies
Christian Deck	General Atomics	Non-destructive X-ray computed tomography analysis of SiC composite tubes neutron-irradiated with and without a high radial heat flux	Oak Ridge National Laboratory
Philip Edmondson	Oak Ridge National Laboratory	Understanding the local atomic structure in variable composition, irradiated perovskites	Brookhaven National Laboratory
David Estrada	Boise State University	Neutron Irradiation and Activation of Fe, Co and Ni Aerosol Jet Printed Structures	Massachusetts Institute of Technology



PI Name	Institution	Title	Facility
Zhenyu Fu	University of Florida	Understand the Fission Products Behavior and Irradiation Effects in UCO Fuel Kernels of Irradiated AGR-1 and AGR-2 TRISO Fuel Particles by Using Atom Probe Tomography	Center for Advanced Energy Studies
Djamel Kaoumi	North Carolina State University	Correlation between In-situ TEM Observations of Radiation Damage of an Advanced Ferritic/Martensitic Alloy under Dual-Beam Ion Irradiation and its Mechanical Properties through In-situ Nanomechanical Testing	
Takaaki Koyanagi	Oak Ridge National Laboratory	Post-irradiation examinations of SiC Oak Ridge National Laborato composites neutron irradiated at 300°C to 30dpa	
Xiang Liu	Idaho National Laboratory	Investigation of the synergistic effects of dual beam irradiation in an austenitic-ferritic duplex alloy	Argonne National Laboratory
Ben Maier	University of Wisconsin	in-situ Transmission Electron Microscopy during Ion-Irradiation Studies of Cold Spray Coatings for Accident Tolerant Cladding	Argonne National Laboratory
Brandon Miller	Idaho National Laboratory	In-situ high temperature Transmission Electron Microscopy (TEM) of radiogenic He in high burnup fast reactor MOX	Idaho National Laboratory
Calvin Parkin	University of Wisconsin	IVEM Investigation of Defect Evolution in Bulk High Entropy Alloys under Single- and Dual-beam Heavy-ion Irradiation	Argonne National Laboratory
Riley Parrish	University of Florida	TEM Characterization of High Burnup MOX Fuel	Idaho National Laboratory
Emmanuel Perez	Idaho National Laboratory	Investigation of Ag, Pd, I, Ru, and Sr fission products in bulk and grain boundaries of neutron irradiated SiC	Center for Advanced Energy Studies
Michael Short	Massachusetts Institute of Technology	In situ investigation of the thermome- chanical performance of HCP metals and Zircaloy-4 under ion beam irradiation	Sandia National Laboratories
Tyler Smith	University of Tennessee	Microstructural investigation of hydride reorientation in zirconium based spent nuclear fuel cladding	Oak Ridge National Laboratory

PI Name	Institution	Title	Facility
Lance Snead	Stony Brook University	Determining Annealing Kinetics of SiC to Enable in LWR Accident Modeling	Massachusetts Institute of Technology
Qing Su	University of Nebraska	Radiation tolerance of nanostructured amorphous/crystalline SiOC/Fe(Cr) nanocomposites	Texas A&M University
Jonova Thomas	Purdue University	3D Microstructural Assessment of Irradiated and Control U-10Zr Fuels	Idaho National Laboratory
Julie Tucker	Oregon State University	Synchrotron XRD characterization of long range order in Ni-Cr alloys formed by isothermal aging or irradiation	Brookhaven National Laboratory
Gary Was	University of Michigan	Microstructure Analysis of High Dose Neutron Irradiated Alloys	Oak Ridge National Laboratory
Walter Williams	Idaho National Laboratory	Phase Evolution of Uranium-Zirconium Alloys Under In-Situ TEM Heating	Idaho National Laboratory
Thierry Wiss	European Commission	Grain Size Effects on He and Xe behavior in UO_2 and ThO_2	Argonne National Laboratory
Takuya Yamamoto	University of California, Santa Barbara	APT Characterization of RPV Steels from the UCSB ATR-2 Neutron Irradiation Experiment	Center for Advanced Energy Studies
Xuan Zhang	Argonne National Laboratory	Investigation of the Tensile-Deformed Microstructure of a Neutron-Irradiated Type 316 Stainless Steel Specimen	Center for Advanced Energy Studies
Dalong Zhang	Oak Ridge National Laboratory	In-situ TEM deformation of neutron irradiated FeCrAl alloys	Center for Advanced Energy Studies
Steven Zinkle	University of Tennessee	Investigation of neutron irradiation effects on Zr based bulk metallic glass (BMG) via advanced in situ mechanical testing and microstructural analysis	Oak Ridge National Laboratory

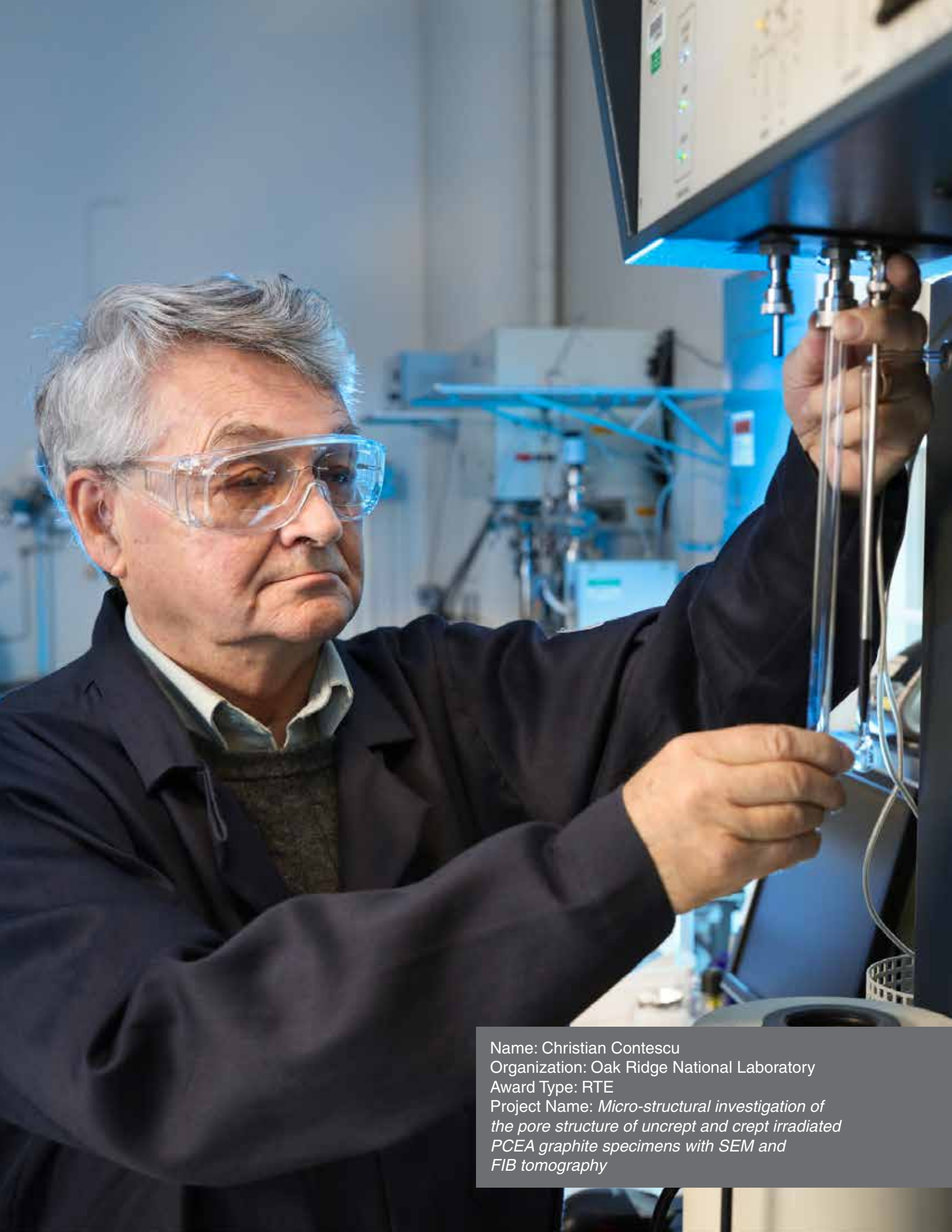


CINR - Joint R&D with NSUF

Organization	Title	Project Description
Aeroprobe	18-14788: Irradiation Testing of Materials Produced by Additive Friction Stir Manufacturing	Researchers will perform irradiation and post-irradiation examination of materials produced by the MELD manufacturing process (FKA additive friction stir (AFS)) and analogous advanced manufacturing technologies. Compared with other additive manufacturing technique, MELD is much faster, generates a refined equiaxed structure, and does not require the post-manufacturing treatments needed for processes based on melting and solidification.
Idaho National Laboratory	18-14772: Understanding Swelling- Related Embrittlement of AISI316 Stainless Steel Irradiated in EBR-II	Researchers will investigate the swelling-related embrit- tlement behavior of AISI 316 stainless steels irradiated in fast reactor EBR-II at high neutron fluences.
Massachusetts Institute of Technology	18-14783: Nanodispersion Strengthened Metallic Composites with Enhanced Neutron Irradiation Tolerance	Researchers will study the neutron irradiation tolerance of nanodispersion strengthened composites produced by an innovative manufacturing method at low cost. The prolific internal interfaces between 1D/2D nanodispersions and the metal matrix provide radiation defect recombination venues to heal radiation damage. The success of this work will provide the novel concept of developing an innovative manufacturing method for advanced nuclear fuels and materials at low cost for long-term operation.
Ohio State University	18-14749: Irradiation Behavior of Piezoelectric Materials for Nuclear Reactor Sensors	The objective of this project is to perform a focused investigation of the irradiation behavior of piezoelectric aluminum nitride, a material considered as a highly attractive candidate for ultrasonic sensors in nuclear applications. In previous irradiation tests it has been identified as highly irradiation tolerant. The experiment will be designed to allow measurement of irradiation effects while isolating effects caused by transducer design.
University of Notre Dame	18-14730: High-performance nanostructured thermoelectric materials and generators for in-pile power harvesting	This project aims to develop radiation-resistant nano- structured bulk thermoelectric materials and devices for in-pile power harvesting and sensing. The thermo- electric power harvesting technology has crosscutting significance to expand nuclear reactor sensing, instru- mentation and offer major cost savings and enhanced safety for all reactor designs & fuel cycle concepts.

CINR - NSUF Access Only

PI Name	Organization	NEUP Title	Project Description
Assel Aitkaliyeva	University of Florida	18-14704: Facilitating MARMOT Modeling of Radiation Phenomena in U-Pu-Zr fuels through experiments (MORPH experiment)	Researchers will increase the fundamental understanding of irradiation-induced metallic U-Pu-Zr fuel behavior and to obtain data needed for the development of irradiation models for metallic fuels in MARMOT. The project requests access to PIE facilities at NSUF partner facility to conduct examination of irradiated metallic fuels with the goal of providing foundational understanding of the radiation behavior in metallic fuels needed to inform the development of MARMOT models.
Kevin Field	Oak Ridge National Laboratory	18-14717: Rapid Simulation of Irradiation Damage in PWR Internals	Researchers will demonstrate that ion irradiation can grow an existing damage microstructure to higher dose levels such that the doses provided by self-ion and neutron irradiation produces the same microstructure.
Ramprashad Prabhakaran	Pacific Northwest National Laboratory	18-14787: High-dose ion irradiation testing and relevant post-irradiation examination of friction-stir-welded ODS MA956 alloy	Researchers will perform higher-dose ion irradiation on neutron irradiated and unirradiated friction stir welded (FSW) MA956 alloy to understand microstructural evolution and radiation-hardening. The study will use ion irradiations and examination to understand and compare the effects of ion, neutron and neutron+ion irradiations.





Select Project REPORTS

This section contains reports on projects awarded through the NSUF and completed in FY 2018.

since its inception, the NSUF has awarded over 400 access awards. Projects awarded through this program have resulted in several scientific gains.

These select project reports in the following pages detail several previously awarded projects including

- High Fluence Embrittlement Database and ATR Irradiation Facility for LWR Vessel Life Extension (FY08, #139)
- Development of Ultrasonic Thermometer at INL (FY15, CINR-15-8489)
- Radial Heat Flux Irradiation Synergism in SiC ATF Cladding (RPA-10468)

- Additive Manufacturing of Thermal Sensors for In-pile Thermal Conductivity Measurement (FY17, CINR-17-12527)
- Post-irradiation examinations of annular mixed oxide (MOX) fuel pins for sodium fast reactors (FY18, CINR-18-12876)
- Availability of well-characterized, highly-irradiated 304 stainless steel for NSUF-supported studies (FY17, RTE #938)
- Neutron Irradiation Performance of Fe—Cr Base Alloys (FY08, RTE #92)
- Disc Irradiation for Separate Effects
 Testing with Control of Temperature (DISECT)

The NSUF UCSB-1 Library ATR Irradiation Experiment

G. R. Odette - University of California, Santa Barbara - odette@engineering.ucsb.edu

This experiment was designed to create a new and unprecedented library of alloys and irradiation conditions to facilitate understanding of and modeling to ultimately predict and improve the behavior of structural materials used in nuclear energy systems.

he NSUF University of California at Santa Barbara (UCSB)-1 Library Advanced Test Reactor (ATR) irradiation experiment was designed to create a new and unprecedented library of alloys and irradiation conditions to facilitate understanding of and modeling to ultimately predict and improve the behavior of structural materials used in nuclear energy systems. The UCSB-1 experiment comprised ≈1400 specimens of various types composed of 40 alloys that included tempered martensitic, nanostructured ferritic, dual phase stainless, maraging, and bainitic RPV steels. The irradiation also included Fe-Cr, Fe-Cu-Mn-Ni-Si ferritic and Cu-Nb multilayer model alloy systems. The four-cycle (145A to 146B) irradiation in the A10 position in the ATR represented 210 effective full power days. Thirty-two isothermal temperature packets contained in nine capsules were irradiated from ≈ 1.8 to 6.8 displacements per atom (dpa) at seven temperatures, ranging from \approx 320 to 750°C. The side-by-side irradiation of so many alloys under so many conditions has provided a unique library that is enabling a campaign of wide ranging collaborative research studies.

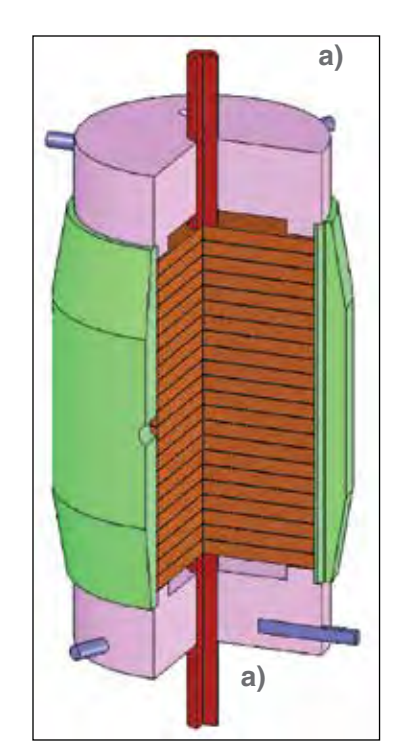
Project Description

UCSB-1 was a drop-in experiment, and so did not have thermocouples to directly monitor temperatures. Instead, a specified packet temperature was achieved by a combination of nuclear heating and a partially insulating gas gap (comprising a mixture of helium and argon). To minimize temperature uncertainties, researchers at UCSB carried out an extensive finiteelement-based thermal-design study. The packets were hollow, profiled cylinders, containing multipurpose disc specimens, or cylindrical holders for other specimens. Each packet had an individual gas-gap profile designed to yield a uniform specimen centerline target temperature. Stainless steel pins provided interpacket thermal isolation and forced the heat flow to be primarily in the radial direction, crossing a minimum number of interfaces. This packet concept is illustrated in Figure 1a; the temperature-dpa profile is shown in Figure 1b. One capsule was removed from its centerline position after one reactor cycle when the contents reached a damage level of 1.8 dpa, and a replacement capsule was inserted where it remained for the rest of the irradiation. An identical packet to that irradiated at the centerline position during

the first cycle was irradiated in a lower-flux position to reach 1.8 dpa at the end of the experiment—i.e., after four cycles, providing some dpa-rate variation. The maximum damage level the experiment could reach was determined by the period of irradiation. Unfortunately, this time was limited by a reactor-power increase after the fourth cycle that would have resulted in higher temperatures. Finally, a postirradiation adjustment of the nuclear heating rates resulted in temperature estimates being somewhat higher than planned; for example, Capsule 6 ran at ≈593 K versus the planned 563 K.

The alloys, including proper certifications, were acquired by UCSB from various sources. UCSB also fabricated all the specimens in the irradiation and loaded them into packets under the supervision of an INL quality assurance engineer. The packets were sent to INL to be loaded into capsules.

Mechanical properties of the alloys have been (or will be) variously assessed, both prior to and after irradiation by nanoindentation, microhardness, shear punch, tensile, compression, chevron wedge, and fracture toughness subsized-specimen tests. Sample specimens are shown in Figure 1c. Microstructural char-



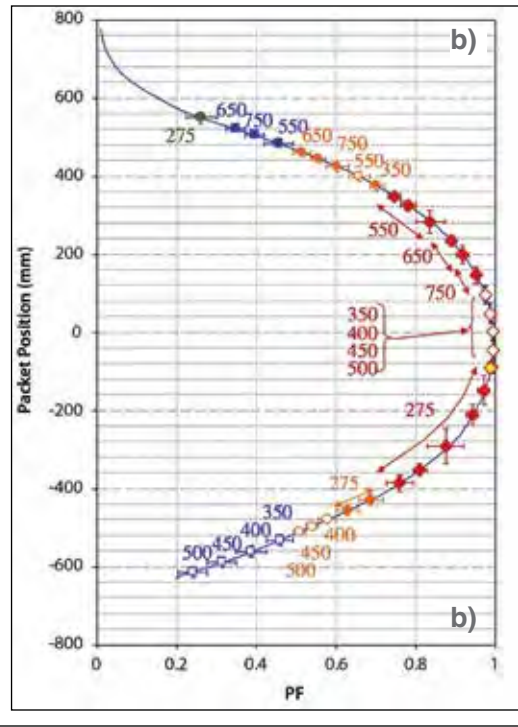
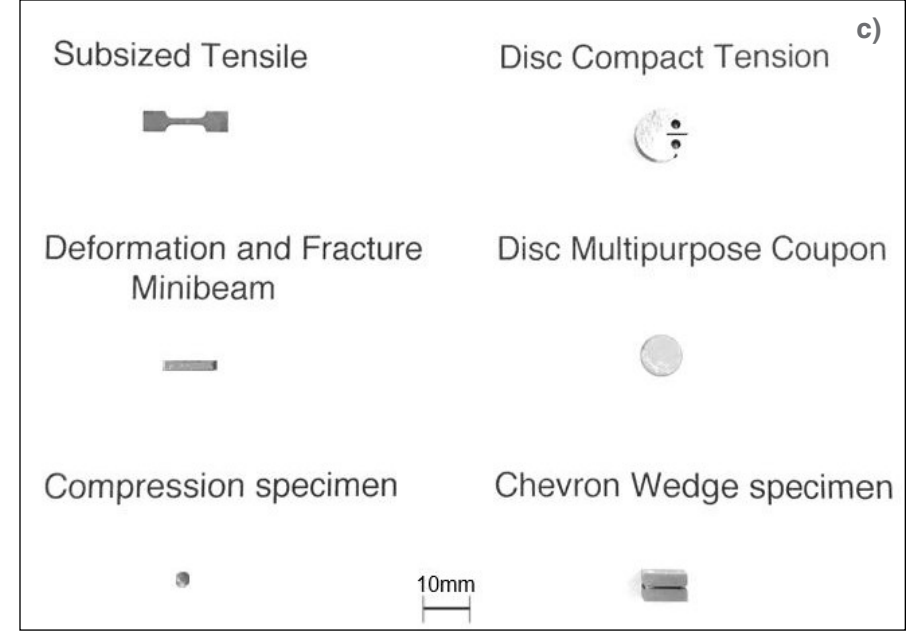
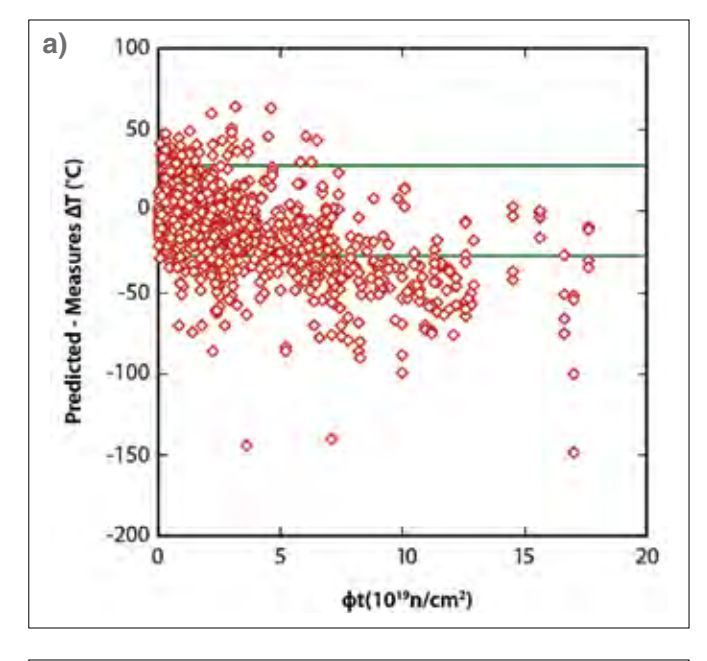
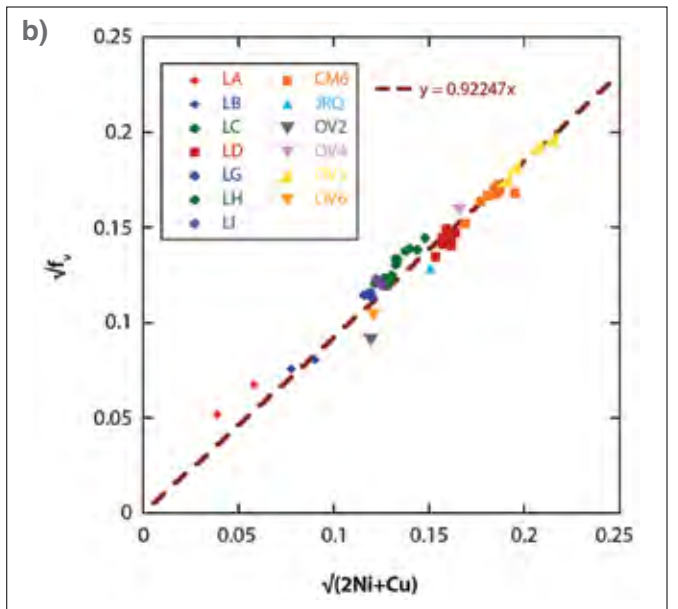
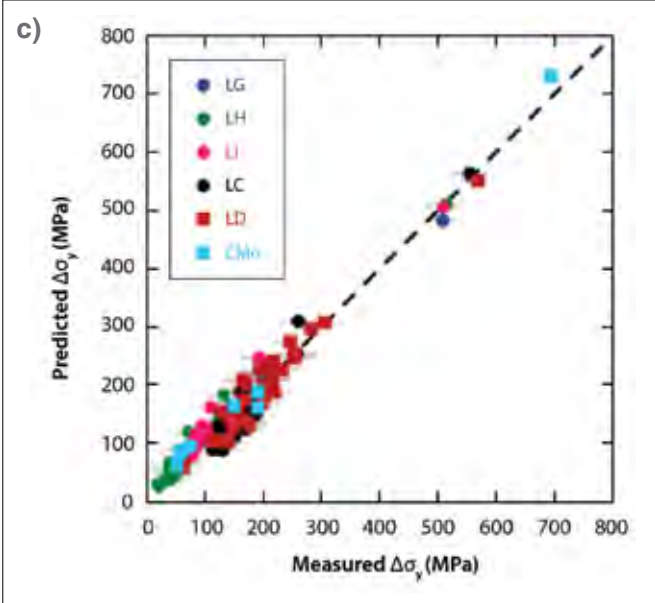


Figure 1. a) A schematic drawing of the profiled packet concept; b) the flux profile showing the packet temperatures; c) the types of specimens contained in the experiment.









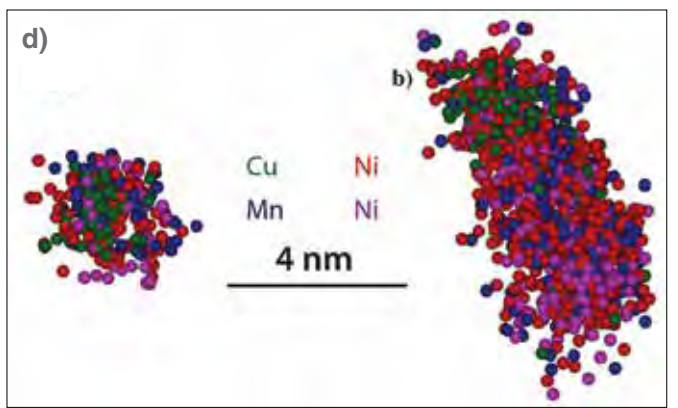


Figure 2. a) The predicted minus measured ΔT as a function of fluence for a large body of test-reactor data; b) the $\sqrt{(2Ni+Cu)}$ versus \sqrt{f} in the UCSB-1 irradiation to 1.8 dpa at 593 K; c) measured versus predicted Δ_y based on APT measured f in ATR-1 and other lower-fluence irradiation experiments; d) the evolution of core-shell CRPs to CRP-MNSP precipitates.

acterization techniques available include small-angle neutron and X-ray scattering (SANS and SAXS), transmission electron microscopy (TEM), atom probe tomography (APT), and X-ray diffraction (XRD). UCSB-1 also included two lab-on-a-chip experiments, including diffusion multiples, to characterize multi-constituent alloy thermo-kinetics under irradiation, and in situ He injection assemblies to produce samples to evaluate the effects of a wide range of He/dpa ratios.

The library concept irradiation was extended to what might best be described as a "reading-club" experimental campaign. UCSB organized various collaborations around different sub-experiments, with researchers expert in different post-irradiation examination (PIE) techniques. As an example, the Fe-Cr series sub-experiment for one irradiation condition involved APT studies led by Professor Emmanuelle Marquis at the University of Michigan (UM). TEM characterization was led by Dhriti Bhattacharyya at the Australian Nuclear Science and Technology Organization (ANSTO), and irradiation hardening measurements were performed at UCSB. These data were then combined and analyzed by UCSB to develop a new microstructurebased hardening model that has been successfully extended to predict yield stress changes (Δ) in tempered martensitic structural steels. The

combination of expertise and insight provided by a reading-club approach resulted in a whole that is greater than the sum of its parts.

Accomplishments

High-fluence Embrittlement of RPV Steels

Light-water reactor pressure vessels (RPVs) are exposed to a low flux of neutrons that cause irradiation hardening and embrittlement, which manifests as a growing degradation of their fracture resistance with increasing fluence. Plant life extension of up to 80 years requires rigorous proof that the RPV maintains a very large safety margin to protect against brittle fracture under all conceivable conditions, including severe accident transients.

Embrittlement manifests as an upward shift in the temperature marking the transition from brittle cleavage to ductile fracture. RPV embrittlement is reasonably well understood and predicted up to the normal licensed plant life of 40 years; however, limited surveillance data is available for extended life, and current regulatory models underpredict accelerated testreactor data at high fluence, as shown in Figure 2a. Current embrittlement regulations reflect the strong effect of Cu and Ni on embrittlement and are associated with the rapid formation of Cu-rich precipitates (CRPs) that harden and embrittle the steel. Theoretical models long ago predicted a new embrittlement mechanism, associated with the formation of so-called "late blooming" Mn-Ni-Si precipitates (MNSPs), which cause severe and unexpected hardening and embrittlement at high fluence, even in nominally radiation-tolerant, Cu-free RPV steels. As studies from UCSB long ago confirmed, the MNSPs are real and highly embrittling. The multifaceted question is this: at what combination of fluences, alloy compositions, irradiation temperatures and fluxes do MNSPs form? Further, it is important to know what MNSPs are, how much of them develop, and how they relate to hardening and embrittlement?

The UCSB-1 experiment was enormously successful in addressing this challenge. Work by then Ph.D. student Peter Wells considered split melt alloys with controlled variations in Cu and Ni contents. APT and SANS showed large volume fractions (f) of MNSPs, which are approximately independent of the alloy Cu content at the high UCSB-1 experiment fluence [1]. The MNSP f increases approximately linearly with the Ni and Cu content of the alloy

 $f \approx 0.92(2Ni + Cu),$

consistent with the observation that MNSPs contain roughly equal fractions of Ni and Mn + Si, a result which is characteristic of the compositions of nearby G and 2 phases. These results are also consistent with CALPHAD

It is important to emphasize that there are a large number of untapped opportunities remaining in the UCSB-1 library, and what has been accomplished to date can be considered just the tip of the iceberg.

thermodynamic predictions [2] and with XRD measurements [3] of the composition and structure of MNSPs. As illustrated in Figure 2b, the squareroot total-precipitate volume fraction (\sqrt{f}) scales with the $\sqrt{2}$ Ni(MNSP) + Cu(CRP)], and the corresponding strengthening contribution scales with the \sqrt{f} in a dispersed-barrier hardening model. Figure 2c compares measured versus predicted (Δ_{v}) for a number of alloys irradiated in various experiments, including UCSB-1. Figure 2d shows that in Cu-bearing alloys, the precipitates evolve from Cu-core-Mn-Ni shell structures to Cu-appendage structures, as predicted by a recent model based on the analysis of UCSB-1 APT data [4]. The UCSB-1 data also played a key role in developing a detailed thermo-kinetic model of precipitation hardening and embrittlement in Cu-free RPV steels [5].

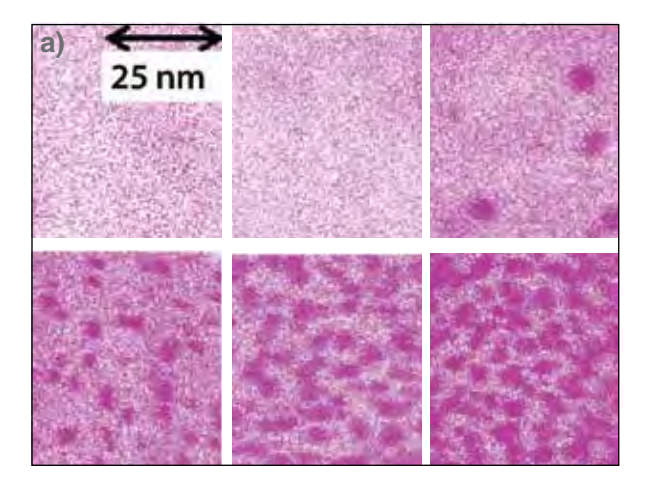
In summary, while the fluxes and fluences are higher than directly pertinent to extended RPV service, the UCSB-1 library provided tremendous insight on late blooming phase MNSPs. Remaining questions center on the effects of lower flux and fluence and improved predictive embritlement models. These are being addressed in the ongoing program of studies on the UCSB-2 experiment library.

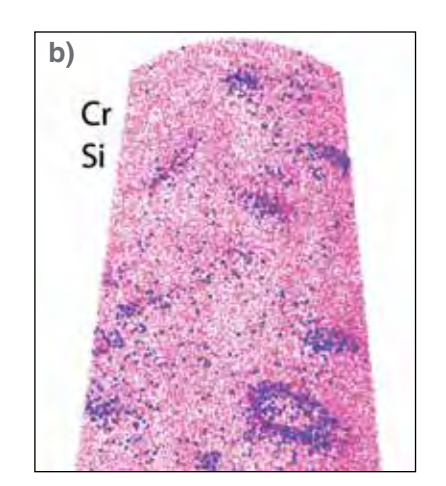
Microstructural and Microstructural Evolutions in Fe-Cr Model Alloys
Fe-8Cr to Fe-18Cr tempered martensitic and ferritic steels are the leading candidate structural alloy system for a wide range of advanced nuclear applications. While more damage resistant than fcc austenitic stainless steels, these bcc alloys experience neutron irradiation that drives complex nm-scale microstructural and microchemical evolutions that lead

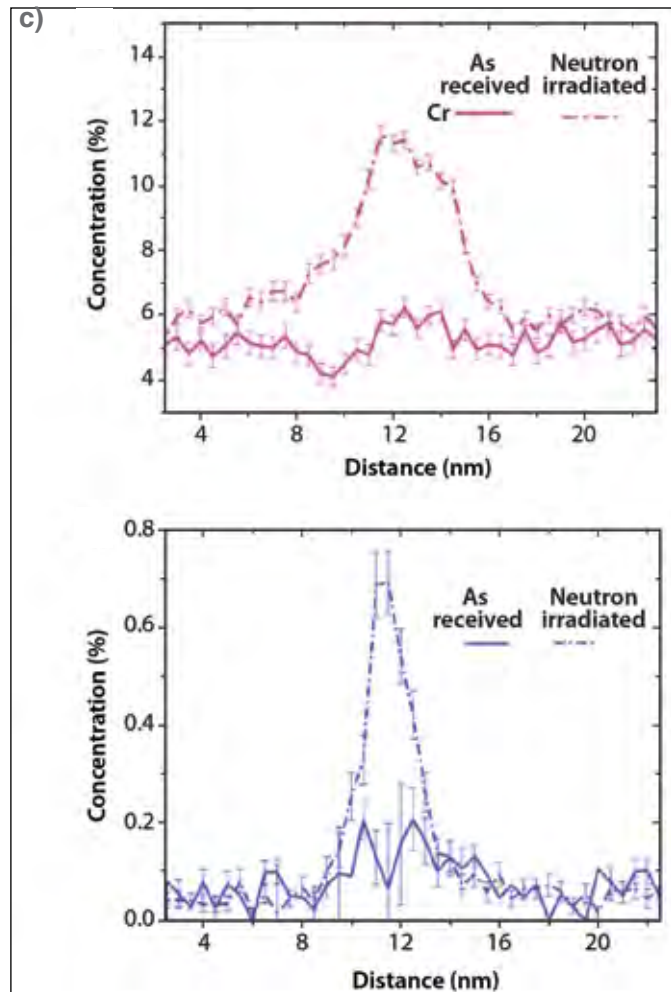
to hardening and embrittlement, as well as dimensional instabilities like irradiation creep and even swelling at very high fluence. The features that develop under irradiation include dislocation loops, '(Cr-rich) precipitates, Mn, Ni, Si, Cr, P solute clusters, solute segregation, helium bubbles and, in some cases, growing voids at high fluence. Thus, one objective of developing the UCSB-1 library was to explore a number of these phenomena in a series of model Fe-3Cr to Fe-18Cr binary alloys that were irradiated sideby-side under the same conditions.

Figure 3a compares APT examinations of Fe-3Cr to Fe-18Cr binary alloys irradiated at 593 K to 1.8 dpa [6]. Precipitation of 'was observed in all of the alloys containing more than 9% Cr. APT was used to fully quantify the number densities, size distributions, average radii, and mole fraction of ', and indicated nearly full 'to decomposition. Both mole fraction and the matrix Cr compositions are in good agreement with the 593 K solvus boundary predicted in a recently published, first-principles guided, Fe-Cr phase diagram (which, notably, deviates substantially from earlier Cr-solubility limits based on classical CALPHAD thermodynamics). The number density and mean radius increase and decrease, respectively, with increasing Cr. These observations are consistent with classical nucleation and growth mechanisms of thermal precipitation, that are greatly accelerated by radiation-enhanced diffusion at the low irradiation temperature.

Figure 3b shows that in the sub-saturated Fe-6Cr alloy, Si and Cr segregate, both in small clusters and visible interstitial dislocation loops [7]. The primarily Si and Cr clusters are likely







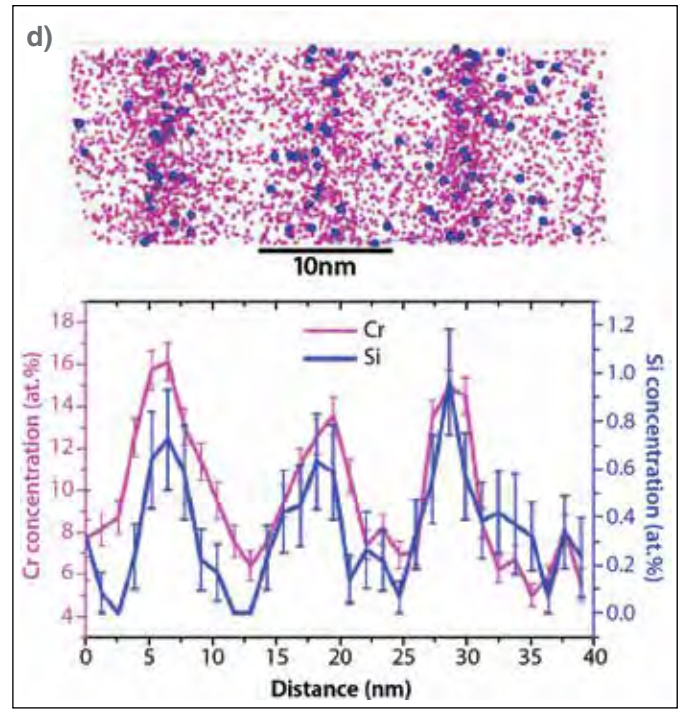
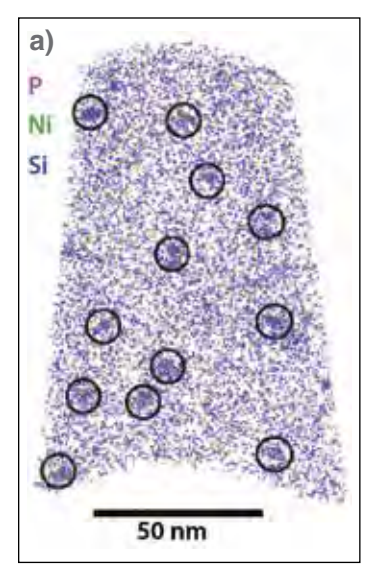
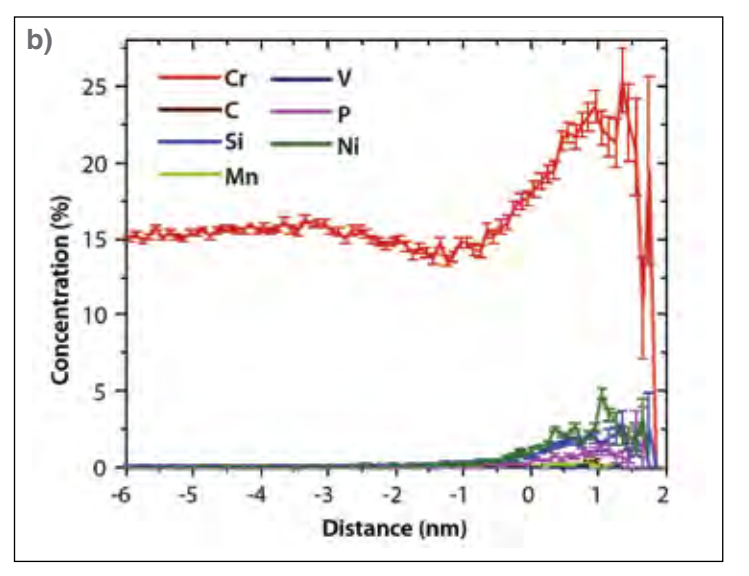
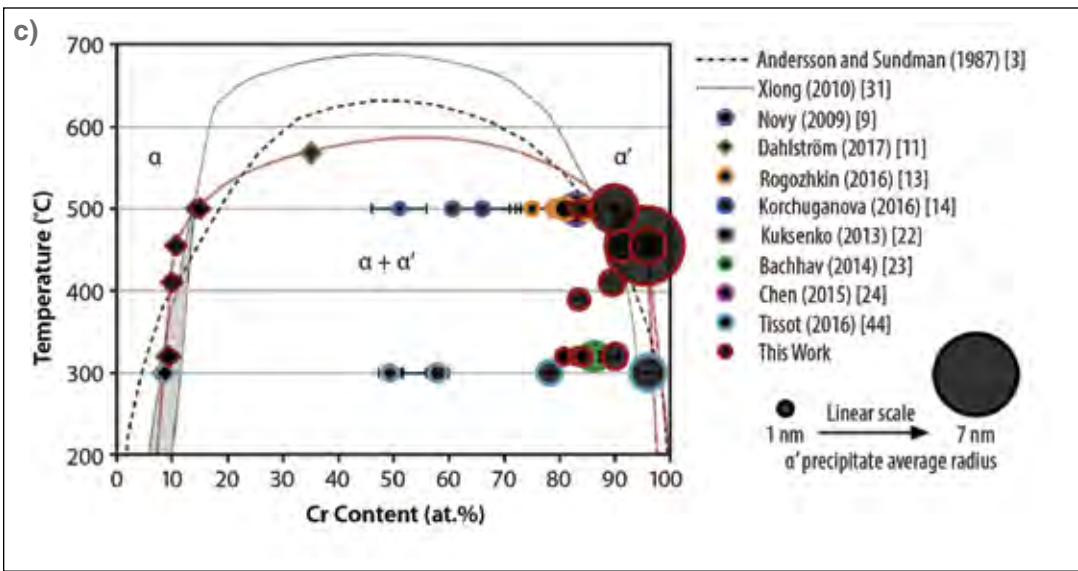


Figure 3. a) APT reconstructions of 'precipitation in Fe-9Cr to Fe-18Cr alloys in 3Cr increments; b) dislocation loops decorated with Si and Cr segregants; c) Cr (top) and Si (bottom) segregation at grain boundaries; d) Cr and Si segregation to dislocations forming a low-angle tilt boundary.







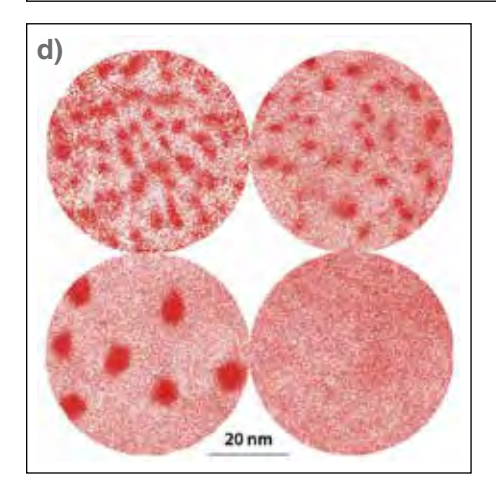


Figure 4. a) Cr-Si-P- solute clusters formed by segregation to small loops in the UCSB-1 irradiated Fe-15Cr alloy; b) a proxigram showing the corresponding enrichment of Cr and other solutes to the segregated loop; c) the and 'solvus boundaries showing good agreement with a revised Fe-Cr phase diagram for sufficiently large precipitates, with sizes represented by the radius of the circles; d) APT reconstructions showing coarsening of 'precipitates at 773 K and dissolution at 873 K.

associated with the smallest loops. At intermediate size, the Cr segregates to the outside of the loops while Si segregates to both the inside and outside. Both solutes segregate to the outside of the loops at larger sizes. The loops were analyzed in terms of their number density, size, habit plane and spatial distribution. Larger numbers of visible loops are observed near grain boundaries. The data from the 593 K irradiation also show segregation (enrichment) of Cr, Si (and P) at grain boundaries (Figure 3c). The C concentration is also slightly increased by irradiation, likely due to co-segregation effects with the higher Cr. Dependence of segregation on the type of grain boundary and solute enrichment at the individual dislocations were observed in low angle tilt boundaries, as demonstrated in Figure 3d.

APT studies on the Fe-15Cr alloy presented in Figure 4a show a high density of very small Cr-Si-Ni-P clusters, again likely associated with small loops [8]. These solute clusters are believed to play a critical role in irradiation hardening of Fe-9Cr tempered martensitic steels, especially at higher dpa. In addition to the expected solute clusters and 'precipitates, grain-boundary Cr-carbide and nitride precipitates were also observed in Fe-15Cr alloy, which altered the local alloy chemistry. In general, less segregation of Cr at grain boundaries was observed in the 15Cr alloy, although this might be affected by nitride and carbide precipitates. Si, Ni and P generally segregate to all types of interfaces.

Examination of 'precipitation over a range of irradiation temperatures and dpa, as well as following postirradiation annealing (PIA) at both 773 and 873 K [9] has been used to establish the full Cr solvus line. Figure 4c shows that the nominal 'Cr content measured by APT is generally less than predicted by the Cr-rich thermodynamic phase boundary and is a function of the 'precipitate size. However, a proxigram analysis (interface-to-center concentration profile) presented in Figure 4b showed that the Cr composition at the 'core approaches equilibrium values in sufficiently large precipitates, especially at higher temperatures. This demonstrates, once again, that such matrix element enrichment in precipitates is an APT artifact. Note, the interface composition may be affected by chemistry-dependent interface energies, as well as by cascade ballistic mixing at lower temperatures. Figure 4d shows that PIA results in 'coarsening at 773 K, and full 'dissolution at 873 K, again consistent with the phase diagram.

These results show the effect of neutron-irradiation-enhanced diffusion on accelerating thermally driven ' precipitation in Fe-Cr alloys with ≥9% Cr. However, 'precipitation is modified in similar alloys under ion irradiation at high dpa rates. Figure 5 (top) shows 'formation in an Fe-18Cr alloy following both ion and neutron irradiations at around 593 K and dose rates from ≈10⁻⁷ to 10^{-4} dpa/s [10]. The steady-state Cr content of the 'depends on the ion irradiation dose and dose rate, confirming the contribution of ballistic mixing to diluting nonequilibrium 'precipitates at high dpa rates.

These APT data were used to guide the development and calibration of a model on the effects of the irradiating-particle type and dpa rate on 'formation [11]. The model was based on the Cahn-Hilliard phasefield theory, which includes dparate-dependent radiation-enhanced diffusion and cascade ballistic mixing to simulate 'evolution under neutrons, heavy ions, and electron irradiation at 573 K. As shown in Figure 5 (bottom), the model predicts that higher dpa rates increase the number density of precipitates while decreasing their radius, volume fraction, and Cr content. Furthermore, the model predicts that 'formation is completely suppressed above about 10⁻⁵dpa/s. In contrast to the ion and neutron irradiations, with high ballistic mixing rates associated with displacement cascades, electron irradiation with weak mixing had little effect on 'formation up to 10^{-3} dpa/s. These results show that both cascade mixing and radiation-enhanced diffusion must be accounted for, along with many other confounding factors, when attempting to emulate neutronirradiation effects using accelerated cascade-inducing ion irradiations.

Neutron Irradiation Effects on The Constitutive Properties of Fe-Cr Ferritic Martensitic Steels and Fe-Cr Model Alloys: Property-Property-Microstructure Relations

True stress-true strain constitutive relations, (), are the most important mechanical property used in engineering analysis and design, as a required input to finite-element calculations. The UCSB-1 irradiation included sub-sized tensile specimens for a variety of ferritic-martensitic and several other steels. The test results for subset of six of these alloys, five 9Cr to12Cr tempered martensitic

steels and one 14Cr oxide-dispersionstrengthened nanostructured ferritic alloy, are shown in Figure 6 [12]. Engineering stress-strain s(e) curves for tests at 298 and 573 K were analyzed using a finite-element-based inverse method developed to derive the corresponding () curves, both before and after irradiation. Increases in yield stress (Δ_v) and reductions in uniform strain ductility (Δ_u) were observed in all cases. The effect of irradiation on can be understood in terms of the flow instability condition d(u)/d = (u). The irradiated () curves fall into three categories of post-yield behavior: initial strain softening, followed by perfectly plastic, nearly perfectly plastic, and reduced or unaffected strain hardening. The irradiation-induced increases in the average plastic flow stress in the range of 0 to 10% strain, $\Delta_{\rm f}$, is generally smaller than the corresponding $\Delta_{\rm v}$ due to the reduction in strain hardening. The tensile data were also analyzed to establish relations between $\Delta_{\rm y}$ and corresponding changes in the ultimate stress, $\Delta_{\rm u}$, as well as the effects of both test temperature and the unirradiated yield stress (yu). The latter shows that higher yu correlates with lower Δ_{v} , due to quadratic dispersedbarrier strengthening superposition effects.

In five out of six cases, the effects of irradiation are generally consistent with previous results on these types of alloys. However, the particular heat of the 12Cr HT-9 tempered martensitic steel in this study has a much higher irradiated strainhardening rate and uthan observed in earlier heats. This difference is likely due to the correspondingly

high strain-hardening rate in the unirradiated condition. The u in the 14Cr oxide-dispersion-strengthened nanostructured ferritic alloy was even less affected by irradiation, and the strain-hardening rate was remarkably unchanged. Again, this is likely due to the high rate of strain hardening in both conditions, primarily due to the very fine-grained microstructure, which promotes the formation of geometrically necessary dislocations.

The use of accelerated charged-particle irradiations as a surrogate for neutron irradiation, while potentially advantageous, is not without challenges. One significant challenge is extracting Δ_{v} [or more generally, ()] data from ion-implantation depths of only a few μm. In principle, this type of analysis can be done using nano-indentation (NI) methods. However, it is critical that techniques to transfer NI to bulk () be developed and validated. To this end, small disc specimens punched from the end tabs of the tensile specimens of the same six samples considered in Figure 6, plus two additional UCSB-1 library irradiated steels, were subjected to NI measurements [13] to develop correlations between NI at various depths, and the bulkirradiated steels tensile properties. The NI and tensile data were analyzed with various property-property correlation models. As shown in Figure 7a, a reasonably good correlation was found between high-load Berkovich microhardness (H_{μ} , somewhat akin to Vickers microhardness) and two measures of NI hardness taken at a sufficient penetration depth to avoid size effects. Unfortunately, the correlation between NI hardness and tensile properties was more scattered and the corresponding Δ_y were not well predicted by the NI measurements. These results underscore the caution required in interpreting NI data and demonstrate that additional research is needed to develop better property-property correlations.

The microstructure and mechanical behavior of the Fe-6Cr in the unirradiated, self-ion-irradiated and neutron-irradiated conditions were measured and compared [14]. Ion irradiations were performed to the same dpa (≈1.8) and similar temperatures, but at much higher dpa rates. The mechanical property characterization involved both NI and microcantilever bend tests for a wide range of beam dimensions to study the interrelationships between irradiation hardening and plasticity size effects. TEM found dislocation loop densities about $3 \times 10^{22}/\text{m}^3$ for the neutronirradiated condition versus only 1.4×10^{22} /m³ for the ion-irradiated alloy, although these differences are within typical scatter. Notably, Cr segregation to loops was only found for the neutron-irradiated case. The NI hardness increase due to neutron irradiation was about ≈3 GPa, which is roughly similar to an estimate of ≈2.6 GPa, based on Vickers microhardness data. The corresponding ion-irradiation hardening was much less, at about 1 GPa. The large difference was judged to be only partly due to the effects of dpa rate and corresponding microstructural differences.

TEM has been used to characterize

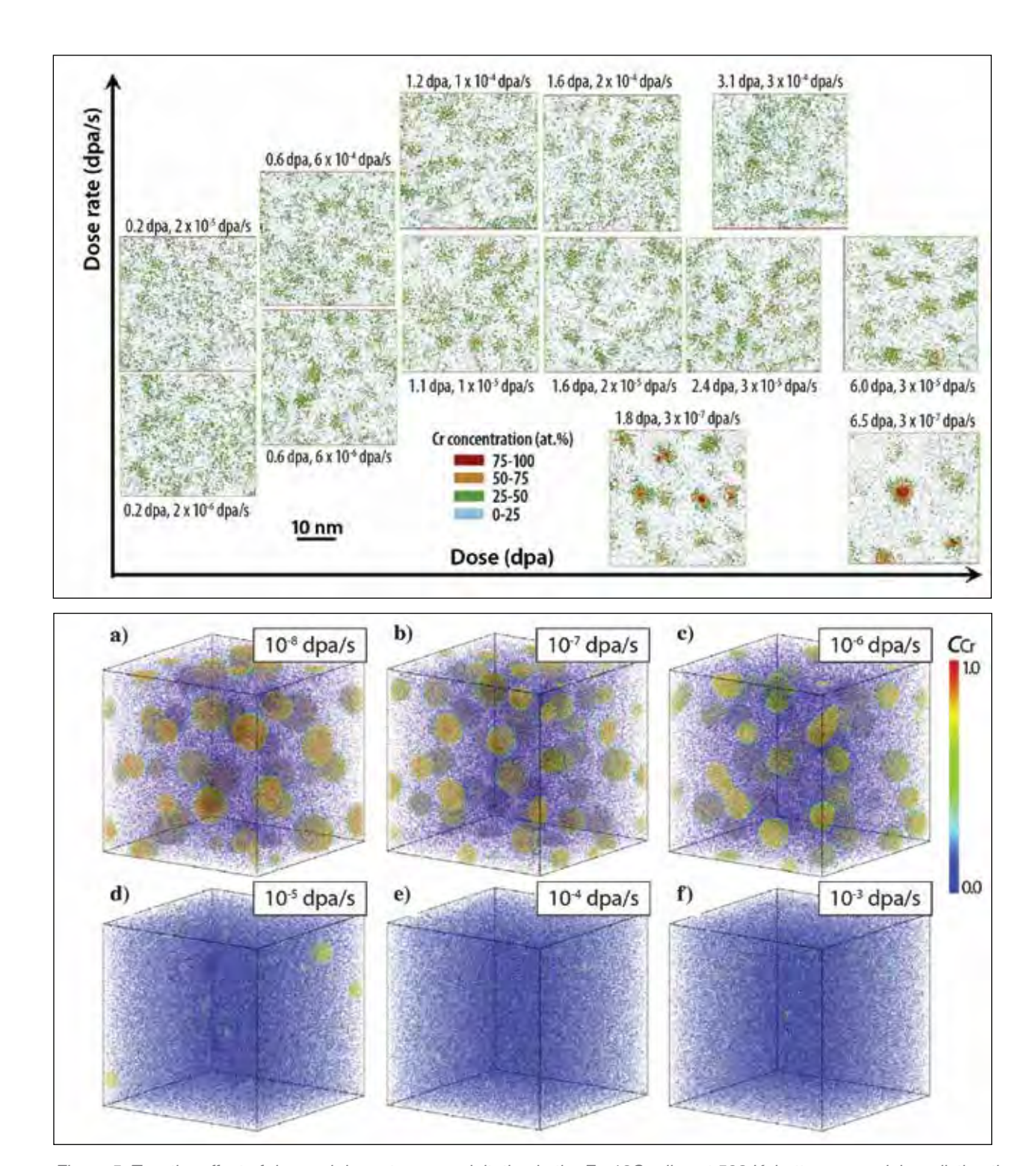


Figure 5. Top, the effect of dpa and dpa rate on precipitation in the Fe-18Cr alloy at 593 K; bottom, a model predicting the effect of dpa rate on the precipitation in a Fe-15Cr alloy at 573 K.

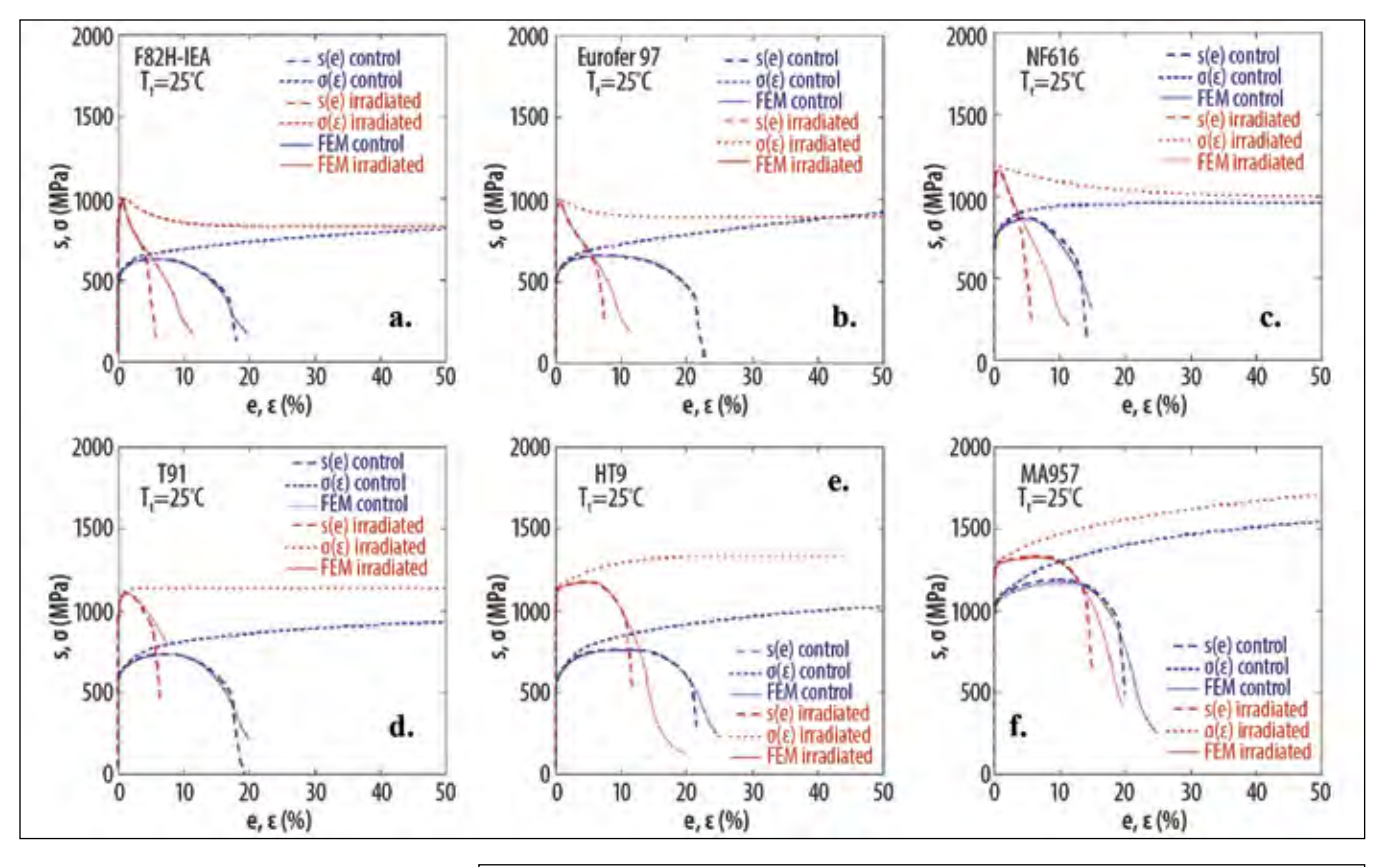
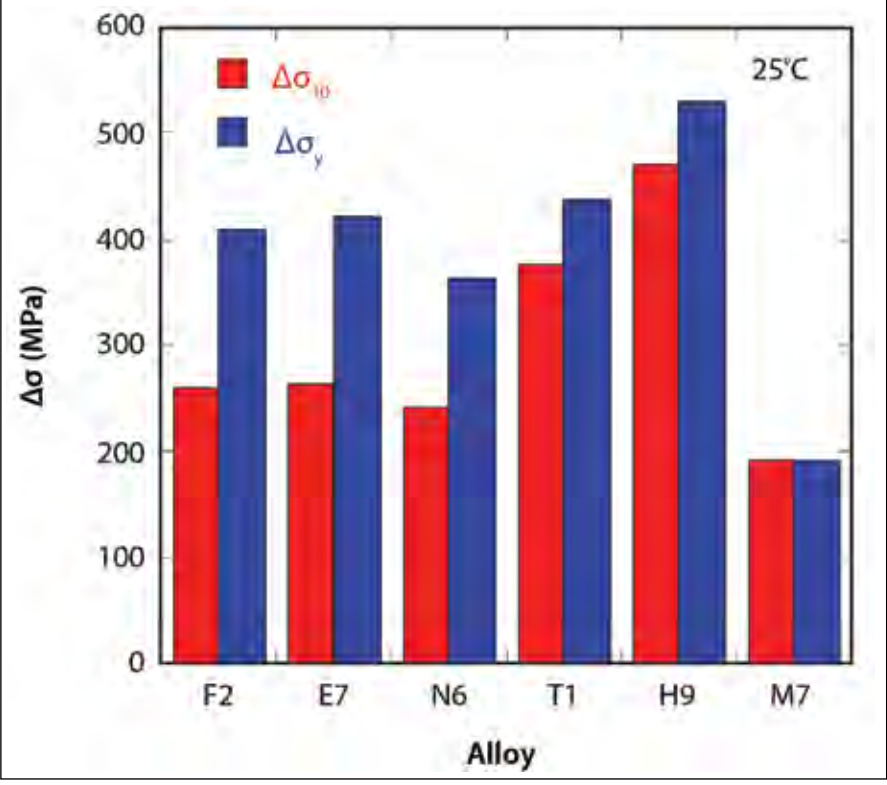
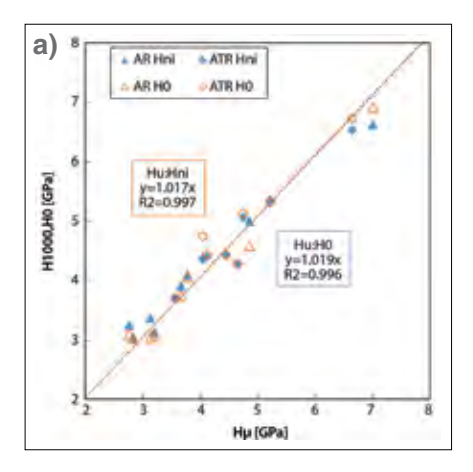
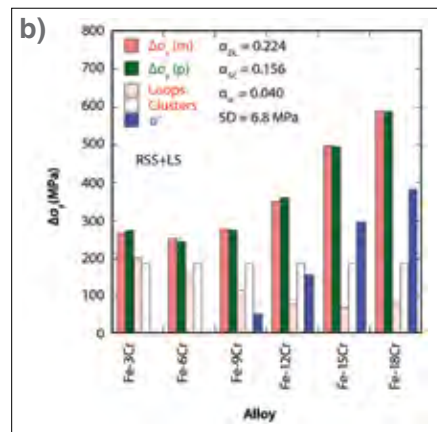
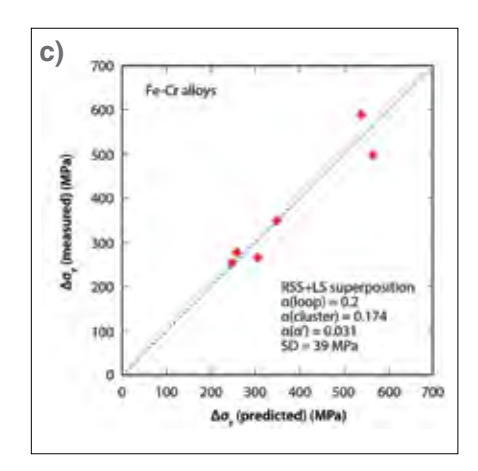


Figure 6. Top, room-temperature engineering s(e) and truestress-strain () curves for six alloys in unirradiated and UCSB-1 irradiated materials 6.5 dpa at ≈593 K; bottom, the corresponding increases in the yield and flow stresses.









dislocation loops in the Fe-3Cr to Fe-18Cr alloys irradiated at 593 K to about 1.8 dpa [15] to estimate the obstacle strength factors (i) for loops, solute clusters and 'precipitates. This study involved analyzing the combined microstructural and $\Delta_{\rm v}$ measurements (based on Vickers microhardness, ΔH_v) by least-square fitting the dispersed barrier strength factors i and an independently derived strength superposition model. As shown in Figures 7b and c, the optimized hardening predictions are in good agreement with experiment, within expected uncertainties. Sequential 168 h isochronal anneals of the Fe-6Cr alloy from 573 to 673 K, in 25 K increments, coarsened the loop size distribution by a factor of three, and decreased the number density by a factor of 8. TEM also showed that isothermal 300 h anneals at 773 and 873 K, coarsened and dissolved the precipitates, respectively, qualitatively consistent with APT observations [9]. Coarsening was shown to be consistent with bulk diffusion controlled kinetics (aka Ostwald Ripening).

Nanostructured Ferritic Alloys (NFA)

Nanostructured ferritic alloys (NFA) are Fe-12Cr to Fe-18Cr ferritic stainless steels, which are dispersion strengthened by an ultrahigh density of Y-Ti-O nano-oxide precipitates. These materials have both remarkable high-temperature strength and irradiation tolerance. As shown in Figure 8, advanced TEM (through focal series, exit wave and STEM diffraction) techniques demonstrate that largeand medium-sized oxide nanoparticles produce all the expected extra spots in the fast Fourier transformation averaged power spectra for the fcc pyrochlore Y₂Ti₂O₇ complex oxide [16]. Figure 8c shows the corresponding spot pattern for the matrix without the oxide particles. Figure 8d and e show that the spot patterns for larger selected areas containing populations of much smaller oxide nanoparticles are the same in both as-fabricated and UCSB-2 library irradiated MA957. While the extra spots are blurred or streaked, and all are not visible, these patterns are also consistent with the presence of Y₂Ti₂O₇. Figure 8e shows similar spot patterns in another unirradiated NFA.

Future Activities

Figure 7. a) the correlation between high load and two measures of NI hardness using a Berkovich indenter; b) a bar graph showing the predicted and measured Δy for the optimized dispersed barrier model for the fitted indicated strengthening factors for loops, solute clusters and 'precipitates, along with their individual contributions; c) a scatter plot of the predicted versus measured Δy .

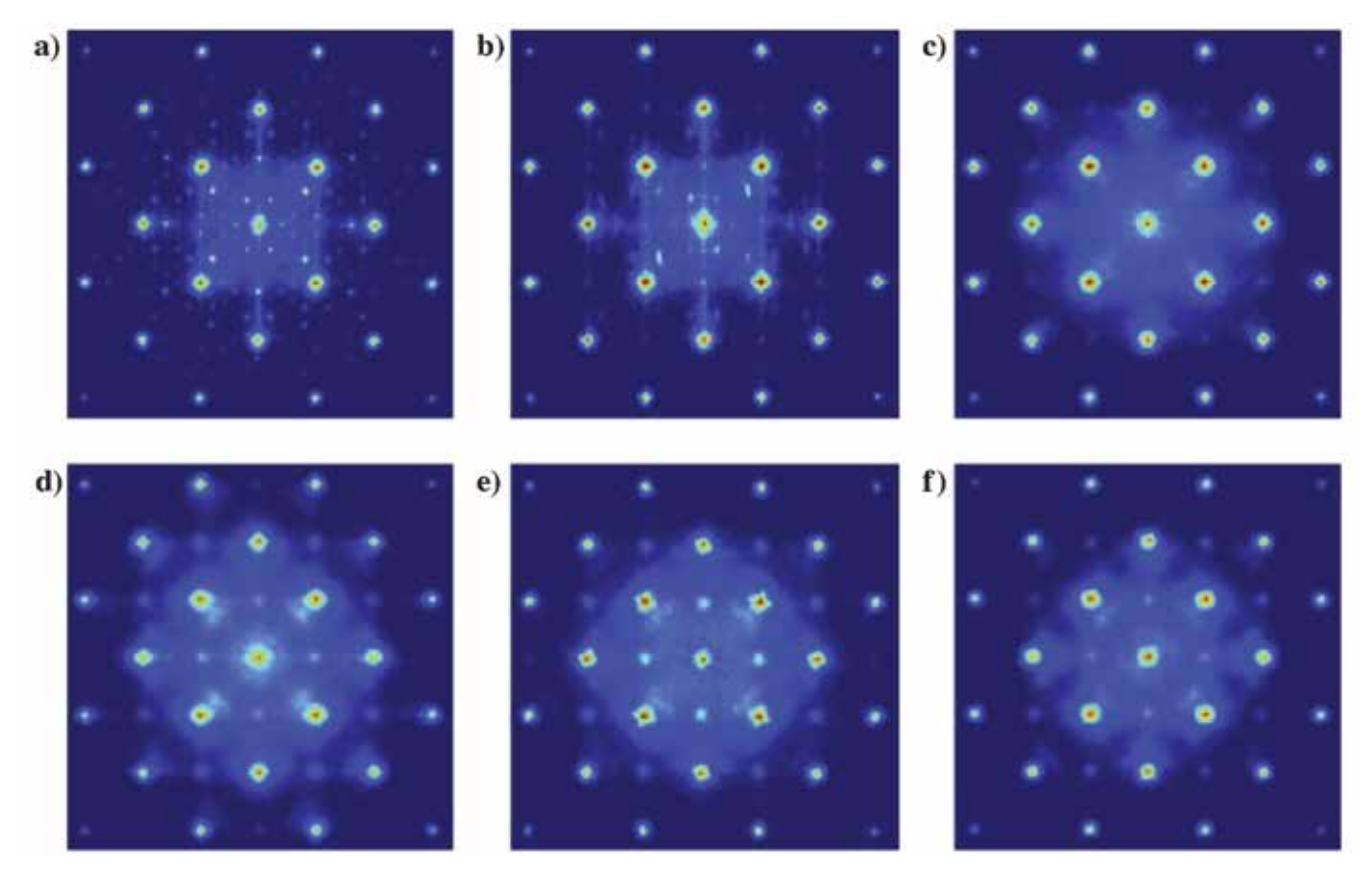


Figure 8. Fast Fourier transformation power spectra patterns for the oxide nanoparticles in indicating the presence of Y₂Ti₂O₇. Figure 8e is for MA957 following irradiation in the UCSB-2 experiment.

A number of additional papers have been submitted or are nearly ready for submission, while a significant amount of post-irradiation examination and research is ongoing utilizing UCSB-1 library material in collaboration with Oxford (Roberts), UM (Marquis), LANL (Maloy), UC Berkeley (Hosemann). It is important to emphasize that there are a large number of untapped opportunities remaining in the UCSB-1 library, and what has been accomplished to date can be considered just the tip of the iceberg.

Publications

[1.] PB Wells, T Yamamoto, B Miller, T Milot, J Cole, Y Wu and GR Odette, Evolution of manganesenickel-silicon-dominated phases in highly irradiated reactor pressure vessel steels, Acta Materialia 80 (2014) 205-219 (40)

- [2.] W Xiong, HB Ke, R Krishnamurthi, P Wells, L Barnard, GR Odette and D Morgan, Thermodynamic models of low-temperature Mn-Ni-Si precipitation in reactor pressure vessel steels, MRS Communications 4-3 (2014) 101-105 (10)
- [3.] DJ Sprouster, J Sinsheimer, E Dooryhee, SK Gosh P Wells, T Stan, GR Odette and L Ecker, Structural characterization of nanoscale intermetallic precipitates in highly neutron irradiated reactor pressure vessel steels, Scripta Materialia 113 (2016) 18-22 (14)
- [4.] S Shu, PB Wells, N Almirall, GR Odette, and DD Morgan, Thermodynamics and kinetics of coreshell versus appendage co-precip-

- itation morphologies: An example in the Fe-Cu-Mn-Ni-Si system, Acta Materialia 157 (2018) 298-306. (0)
- [5.] H Ke, P Wells, PD Edmondson, N Almirall, L Barnard, GR Odette and D. Morgan, Thermodynamic and kinetic modeling of Mn-Ni-Si precipitates on low-Cu reactor pressure vessel steels, Acta Materialia 138 (2017) 10-26 (8)
- [6.] M Bachhav, GR Odette and EA Marquis, Alpha prime precipitation in neutron-irradiated Fe-Cr alloys, Scripta Materialia 74 (2014) 48-51(49)
- [7.] M Bachhav, L Yao, GR Odette and EA Marquis, Microstructural changes in a neutron-irradiated Fe-6at%Cr alloy, Journal of Nuclear Materials 453 1-3 (2014) 334-339 (14)
- [8.] M Bachhav, GR Odette and EA Marquis, Microstructural changes

- in a neutron-irradiated Fe-15at%Cr alloy, Journal of Nuclear Materials 454 1-3 (2014) 381-386 (14)
- [9.] ER Reese, M Bachhav, PB Wells, TYamamoto, GR Odette, EA Marquis, On 'precipitate composition in thermally annealed and neutron-irradiated Fe- 9-18Cr alloys, Journal of Nuclear Materials 500 (2018) 192-198. (2)
- [10.] ER Reese, N Almirall, T Yamamoto, S Tumey, GR Odette,
 EA Marquis, Dose rate dependence of Cr precipitation in an ion-irradiated Fe 18Cr alloy",
 Scripta Materialia 146 (2018)
 213-217. (2)
- [11.] JH Ke, ER Reese, EA Marquis, GR Odette, DD Morgan. Flux effects in precipitation under irradiation – Simulation of Fe-Cr alloys, Acta Materialia 164 (2019) 586-601(0)

- [12.] SA Maloy, TA Saleh, O Anderoglu, TJ Romero, GR Odette et al., Characterization and comparative analysis of the tensile properties of five tempered martensitic steels and an oxide dispersion strengthened ferritic alloy irradiated at approximate to 295 degrees C to approximate to 6.5 dpa, Journal of Nuclear Materials 468 (2016) 232-239 (7)*
- [13.] DL Krumwiede, T Yamamoto, TA Saleh, SA Maloy, GR Odette, P. Hosemann, Direct comparison of nanoindentation and tensile test results on reactor- irradiated materials, Journal of Nuclear Materials 504 (2018) 135-143. (2)
- [14.] CD Hardie, GR Odette, Y. Wu, S. Akhmadaliev, SG Roberts, Mechanical properties and plasticity size effect of Fe-6% Cr irradiated by Fe ions and by neutrons, Journal of Nuclear Materials 482 (2016) 236-247 (2)
- [15.] D Bhattacharyya, T Yamamoto, P Wells, E Marquis, M Bachhav, Y Wu, J Davis, A Xu, GR Odette, Microstructural changes and their effect on hardening in neutron irradiated Fe-Cr alloys, Journal of Nuclear Materials (2019) accepted
- [16.] Y Wu, J Ciston, S Kraemer, et al, The crystal structure, orientation, relationships and interfaces of the nanoscale oxides in nanostructured ferritic alloys, Acta Materialia 111 (2016) 108-115 (19)

Distributed Partnership at a Glance			
NSUF and Partners	Facilities and Capabilities		
Idaho National Laboratory	Advanced Test Reactor (ATR)		
Collaborators			
Australian Nuclear Science and Technology Organisation	Dhriti Bhattacharyya (collaborator)		
Brookhaven National Laboratory	D. J. Sprouster (collaborator), Lynne Ecker (collaborator)		
Idaho National Laboratory	Jim Cole (principal investigator)		
Los Alamos National Laboratory	Stuart Maloy (collaborator)		
University of California, Santa Barbara	G. R. Odette (principal investigator), Nathan Almirall (collaborator), Peter Wells (collaborator), Takuya Yamamoto (collaborator)		
University of Michigan	Emmanuelle Marquis (collaborator)		
University of Wisconsin	Dane Morgan (collaborator)		

Development of Ultrasonic Thermometer at INL

Joshua Daw - Idaho National Laboratory - joshua.daw@inl.gov

S DOE-NE programs are investigating new fuels and materials for advanced and existing reactors. A primary objective of these programs is to characterize the irradiation performance of fuels and materials. Examples of the key temperatures needed to evaluate fuel performance, as well as the desired accuracies and resolutions, are shown

in Table I [1] . Similar measurement requirements exist for other parameters (i.e. fission-gas pressure). Ultrasonic technologies can be used to measure most of the key parameters of interest, but temperature was selected for initial development, as this is the most common measurement requested of irradiation programs.

	Estimated Peak Value	Desired Accuracy and Spacial Resolution
	Ceramic Light Water Reactor (LWR): 1400°C	
	Ceramic Sodium Fast Reactor (SFR): 2600°C	2%
Fuel Temperature	Metallic SFR: 1100°C	1-2 cm (axially) 0.5 cm (radially)
	Tristructural-isotropic (TRISO) High Temperature Gas Reactor (HTGR): 1250°C	
	Ceramic LWR: <400°C	
Cladding Temperature	Ceramic SFR: 650°C	1-2 cm (axially)
	Metallic SFR: 650°C	

Table I. Summary of desired fuel measurement parameters for irradiation testing.

Project Description

Ultrasonic thermometry

Ultrasonic thermometry has the potential to improve upon temperature sensors currently used for in-pile fuel temperature measurements. Current methods for in-pile temperature detection primarily rely on either thermocouples or post-irradiation examination methods (such as melt wires). Commercially-available thermocouples (e.g., Type K, Type N, Type C, etc.) are widely used and cover a wide temperature range. However, their use is limited. Type K and Type N thermocouples decalibrate at temperatures in excess of 1100°C. Material transmutation causes decalibration in tungsten/rhenium (e.g., Type C) or platinum/rhodium (e.g., Type R or S) thermocouples in neutron-radiation environments. Although largerdiameter, multipoint thermocouples are available, most thermocouples only measure temperature at a single location. Melt wires and other post-irradiation methods only allow estimation of maximum test temperatures at the point of installation. The labor and time to remove, examine, and return (if necessary) irradiated samples for each measurement also makes this

out-of-pile approach very expensive. Prior ultrasonic thermometry applications have demonstrated the viability of this technology, but in-pile applications were primarily limited to high-temperature fuel damage tests, which ceased several decades ago [2].

Theory of Operation

Waveguide based ultrasonic thermometers (UTs) work on the principle that the speed at which sound travels through a material (acoustic velocity) is dependent on the temperature of the material. The average acoustic velocity of a material can be measured by sending an ultrasonic pulse through a thin rod of known length and measuring the time between the initial pulse and the reflection of the pulse from the opposite end of the rod. By introducing acoustic discontinuities such as notches or sudden diameter changes into the rod, the probe may be segmented into multiple zones (the average acoustic velocity of each segment derived from timing of the successive reflections). If the ultrasonic waves are non-dispersive (the rod having a diameter of less than one tenth of the signal wavelength

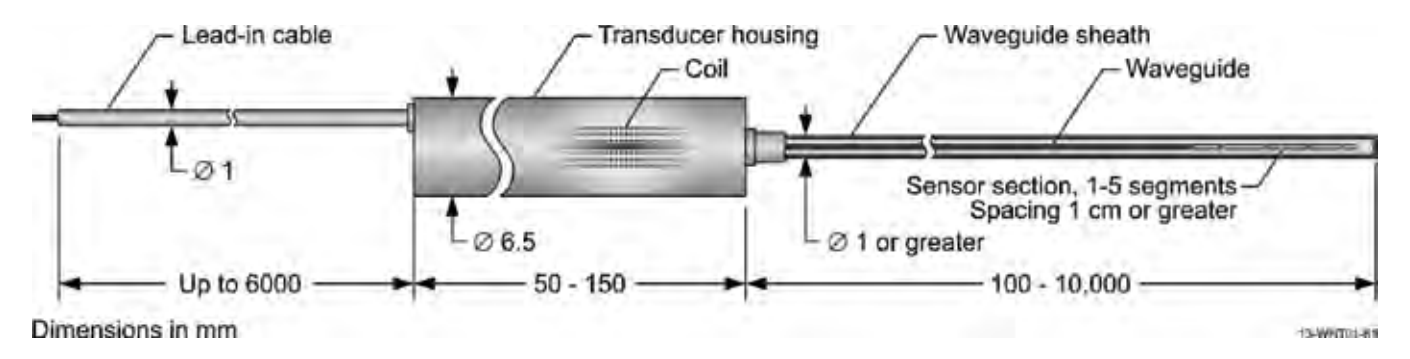


Figure 1. Schematic diagram of magnetostriction based ultrasonic thermometer.

[3]), the temperature-dependent acoustic velocity of the sensor material, c(T), is related to the density, $\rho(T)$, and the elastic (Young's) modulus, E(T), (both properties are also temperature dependent) of the sensor material through the following equation:

$$c(T) = \sqrt{\frac{E(T)}{\rho(T)}} \ (1)$$

A typical multisensor UT system with key components identified is shown in Figure 1. As indicated in this figure, a narrow ultrasonic pulse is generated in a magnetostrictive rod by a short-duration magneticfield pulse produced by an excitation coil. The ultrasonic pulse propagates to the sensor wire, where a fraction of the pulse energy is reflected at each discontinuity (notches or diameter change). Each reflected pulse is received by the excitation coil, transformed into an electrical signal, amplified and evaluated in a start/stop counter system. The

time interval between two adjacent echoes is evaluated and compared to a calibration curve to give the average temperature in the corresponding sensor segment. When a number of notches are available on the wire sensor, the various delay time measurements give access to a temperature profile along the probe.

Irradiation Testing

Until recently, INL-developed UTs had been tested at high temperatures in furnace environments (i.e., inert gas or vacuum atmosphere), but not in an irradiation environment. In-core qualification of a new sensor is a necessary step prior to deployment in irradiation test campaigns.

ULTRA

To generate and receive ultrasonic pulses and signals, two of the most commonly used technologies are piezoelectric and magnetostrictive transducers. Only the magnetostrictive transducers will be discussed here. The current capabilities of magnetostrictive transducers are typically limited

These technologies, which have performed successfully in out-of-pile tests, have not been well qualified in a test-reactor environment. The first in-core sensor, based on ultrasonic technologies and targeted for deployment, is the ultrasonic thermometer (UT), which can provide a temperature profile in candidate metallic and oxide fuels and would provide much-needed data for validating new fuel performance models.

to operation at frequencies up to the order of 100 kHz. However, mechanical coupling and guided-wave-mode generation makes magnetostrictive transduction ideal for low-frequency measurements, such as ultrasonic thermometry [4]. The irradiation behavior of magnetostrictive materials has not previously been studied in depth, leaving their appropriateness for use in irradiation tests unknown.

An NSUF-funded irradiation, dubbed the ULtrasonic TRAnsducer (ULTRA) irradiation test, led by Pennsylvania State University and executed at the Massachusetts Institute of Technology Research Reactor allowed for longterm irradiation testing of both piezoelectric and magnetostrictive transducers and evaluation of their survival within a high-radiation environment. The magnetostrictive transducer designed for this test was based on research by Lynnworth [5] and Daw [6]. The magnetostrictive transducers consist of a small driving/ sensing coil, a biasing magnet, and a magnetostrictive waveguide. The

ultrasonic signal is generated when a high frequency alternating-current pulse is driven through the coil. The induced magnetic field causes magnetic domains within the material to oscillate. The domains are prebiased by the magnet to maximize the response. Received echoes are detected through the reciprocal effect.

The design of the transducers was identical to the UT shown in Figure 1, except the entire waveguide consisted of the magnetostrictive alloy being evaluated.

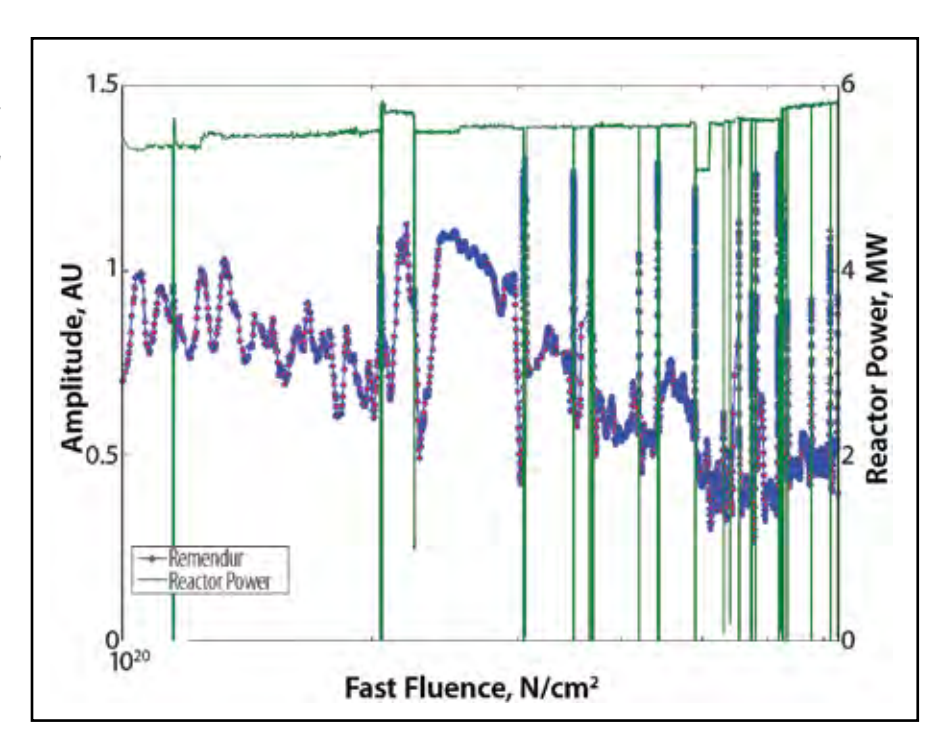
Candidate Materials

The magnetostrictive transducer materials were selected based on previous use in radiation environments, amounts of neutron sensitive materials, Curie temperature, and saturation magnetostriction.

Remendur

Remendur has the most history of use in nuclear applications of all magnetostrictive alloys, having been used previously for short-duration thermometry applications. Remendur

Figure 2. Remendur-element transducer-signal amplitude as a function of accumulated fast fluence.



has a high Curie temperature (950°C) and relatively high-saturation magnetostriction (\sim 70 ρ strains). Remendur is an alloy composed of approximately 49% iron, 49% cobalt, and 2% vanadium. Because of its cobalt content, Remendur was not considered to be an ideal choice (due to concerns about the production of Cobalt-60 during irradiation). However, its successful prior use was deemed sufficient reason to warrant inclusion.

Figure 2 shows the normalized amplitude for the Remendur transducer as a function of accumulated fluence. There is a generally decreasing trend, but signal recovery after temperature transients indicates that some of the signal attenuation is due to temperature effects, in this case binding of

the wire against the coil bobbin (see Figure 1 for transducer component diagram). As with the Galfenol transducer, increased noise after the first reactor restart post refueling may indicate an intermittent short in the drive/sense coil.

Galfenol

Galfenol is a relatively new alloy of iron and gallium (approximately 13% gallium). Galfenol is a member of the "giant" magnetostrictive alloys and has a very large saturation magnetostriction (100–400 ρ strains). It also has an appropriately high Curie temperature (700°C). Neither of its constituent elements reacts strongly with neutron radiation. These factors made Galfenol a very appealing magnetostrictive material candidate.

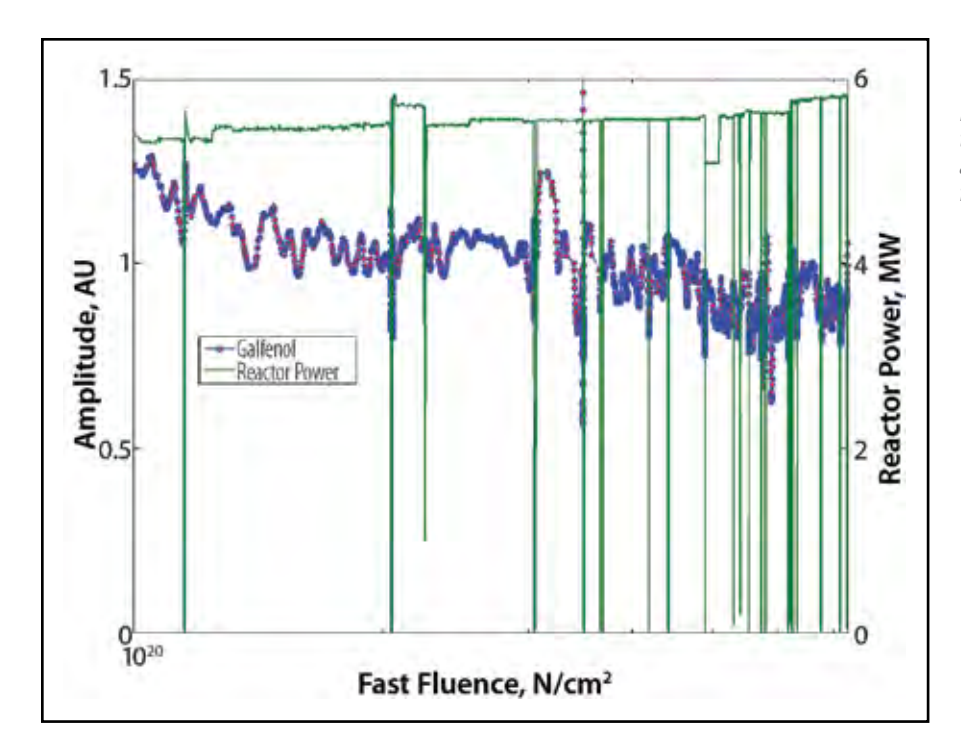


Figure 3. Galfenol element transducer signal amplitude as a function of accumulated fast fluence.

Performance of the magnetostrictive transducers was characterized using the normalized magnitude of the fast Fourier transform (FFT) of the first reflected acoustic signal (normalized to the time when the reactor first reached full power). The frequency-transformed signal is used because it is less sensitive to the interference effects of noise and signal transients

The Galfenol transducer was stable over the course of the irradiation, though the total peak-to-peak signal amplitude was typically on the order of one third that observed for Remendur. Figure 3 shows the normalized peak-to-peak amplitude for a Galfenol transducer as a function of accumulated fluence. The

green trace shows the reactor power history. The Galfenol transducer shows steady operation during periods when the reactor power level was stable. There is little decrease in the signal strength over these periods. The decreases in signal strength observed when reactor power is increased appear to be due to increases in operating temperature, as the signal strength stabilizes shortly after each power increase.

The transducers were irradiated to a fast fluence of $8.8 \times 10^{20} \, \text{n/cm}^2$ (E>1 MeV). Post-irradiation examination of each irradiated material indicated negligible effects on the magnetostrictive behavior of either

Figure 4. Single-segment Inconel sensor results

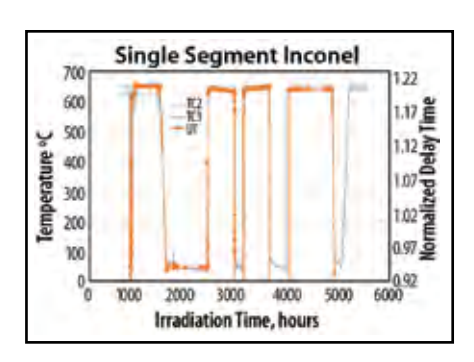


Figure 5. Multi-segment Inconel sensor results.

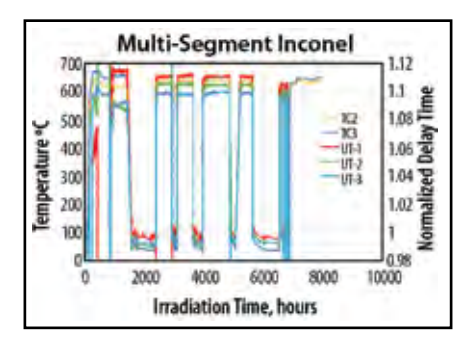
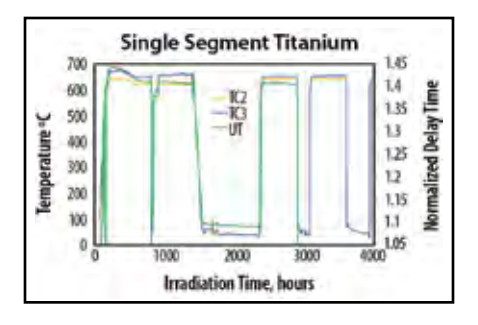


Figure 6. Single-segment titanium results.



tested material. Observed online signal changes were deemed to have been caused by thermal and mechanical effects within the transducers.

ULTRA2

Based on the results of the ULTRA irradiation test, a follow-on irradiation (ULTRA2) was selected for funding by NSUF. This test included INL-developed UTs and fiber-optic sensors provided by the French

Atomic and Alternative Energy Commission (CEA) and by the University of Pittsburgh (only the UTs will be discussed here). Three UTs were included in the ULTRA2 irradiation test. Two of the experimental UTs use Inconel 606 wire as the sensing element; one had a single measurement zone, and the other had three zones. The third UT had a single zone and used commercially pure titanium wire as the sensing element. Spatial constraints of the MIT test capsule restricted the length of these UTs. As such, the UTs could not be directly calibrated without damaging the transducers. Performance was determined by examining the trends in measured delay times against temperatures measured by included thermocouples.

Each of the three UTs included in this test experienced failures of the driver coil before the completion of the test. This is likely due to a material change in a ceramic cement used to fill the transducer housing that was made between the original ULTRA experiment and ULTRA2. The new cement likely lost cohesion, allowing the coil wire to move during temperature transients and during refueling operations. All UTs survived for between ~5000 and 7000 hours and produced reasonable signals over that time.

Figure 4 shows the normalized delay time and thermocouple (TC) temperature of the single segment Inconel sensor. The data during initial reactor start-up were unusable, possibly due to a mechanical

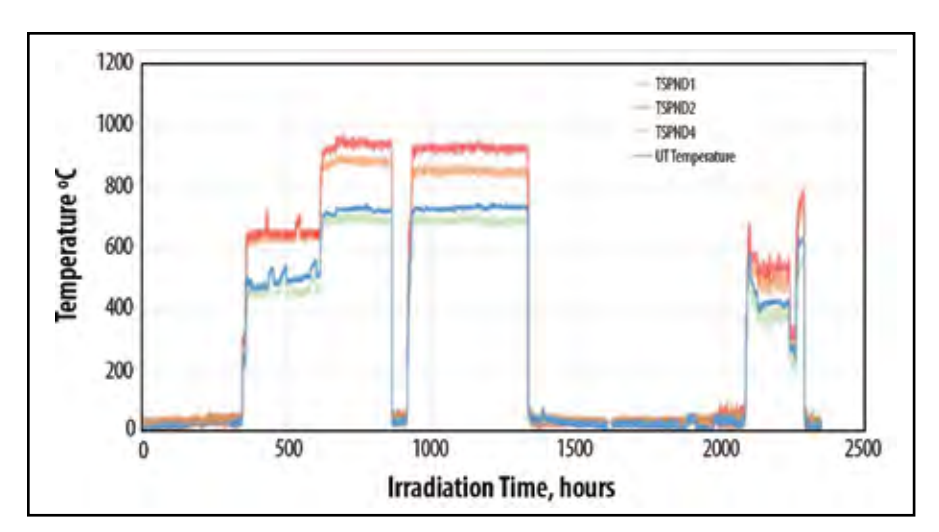


Figure 7 AGR 5/6/7 UT results

pinch in the sensor's wire that cleared up after temperature cycling. The signal follows the reactor temperature well, for most of the test. Some intermittent signal loss was observed over the last few reactor cycles. This is evidence that the coil was the component that failed, as any other component failing would not allow for a recovery.

Figure 5 shows the normalized delay time and TC temperature of the three-segment Inconel sensor. As with the single-segment sensor, for most of the irradiation, the signal closely matches the reactor temperature. Some anomalous behavior can be observed during the early part of the irradiation, seen as an opposing response between the first and second segments (as one signal increases, the other decreases proportionately). It is unclear at this point if this is a physical phenomenon or an artifact of the signalacquisition process. This sensor also failed intermittently before finally failing after ~7000 hours.

Figure 6 shows the normalized delay time and TC temperature of the single-segment titanium sensor. This sensor performed well through almost 3000 hours before failure. Unlike the Inconel sensors, there was observed a slow decrease in measured delay time. The likely explanation of this drift is fast-neutron damage causing a slow increase in the elastic modulus of the titanium. The effect appears to have saturated by the last operational reactor cycle, but this behavior may make titanium a poor material for UTs.

AGR 5/6/7

Also based on the results of the ULTRA irradiation, one UT, using molybdenum as the sensing waveguide, was included in the Advanced Graphite Reactor (AGR)-5/6/7 irradiation test at INL's Advanced Test Reactor (ATR). This UT has performed very well through the early irradiation. This thermocouple was calibrated prior to installation in the experiment. Figure 7 shows the temperatures measured

Ultrasonic technologies offer the potential for high accuracy and resolution for in-pile measurement of a range of parameters, including geometry changes, temperature, crack initiation and growth, gas pressure and composition, and microstructural changes.

by the UT and by several thermocouples located near the UT. The thermocouple labeled TCSPND4 is closest to the UT, and offers the best comparison. The standard deviation of the UT temperature is $\sim 2^{\circ}\text{C}$ at the maximum test temperatures.

Future Activities

The results of testing to date have been very promising, but some work remains in order to consider the UT completely qualified for in-core deployment. The issue observed in the ULTRA2 test is likely due to changes made to a ceramic cement used to fill the transducer housing, but this has not been verified through PIE. This issue may be solved by identifying a better potting compound or by making the coil wire more robust, either by changing materials or wire diameter.

A planned NSUF-sponsored irradiation test, DISECT, will be performed in the Belgian BR2 reactor in collaboration with Studiecentrum voor Kernenergie/Centre d'Étude de l'énergie nucleaire (SCK•CEN). DISECT is meant to study metallic fuel foils arranged along a ~1 meter test vehicle. Multi-point temperature measurements along the length of the DISECT capsule are needed in order to fully characterize the experiment. Multipoint thermocouples are

planned as primary instrumentation, but an INL UT will also be included in the test, along with a promising fiber-optic sensor. The expected temperatures are relatively low for a UT, less than 300°C for the first phase of testing, but the need for a temperature-profile measurement makes the test ideal for demonstration of the performance of the UT because the temperatures measured by the single UT can be directly compared to those of the multipoint thermocouples. The UT designed for this application will have 10 measurement zones along the length of the test, making this the most complicated irradiation yet for the sensor.

This article documents the development of a multipoint ultrasonic thermometer and the progress, to date, toward regular deployment in irradiation experiments. The largest hurdle a new in-core sensor must overcome to be considered qualified is demonstration in prototypic irradiation conditions. The reactor access provided by NSUF has been critical in progressing the UT through several stages of design improvement, and has shown that the UT is a viable option for making multipoint temperature measurements in extreme irradiation environments such as those experienced in the ATR.

Publications

- [1.] B. G. Kim, J. L. Rempe, J-F Villard, and S. Solstad, "Review of Instrumentation for Irradiation Testing of Fuels and Materials," Nuclear Technology, 176, p 155-187, 2011.
- [2.] M. Laurie, et al., "Ultrasonic High Temperature Sensors: Past Experiments and Prospective for Future Use," Proc. International Symposium on Temperature and Thermal Measurements in Industry and Science (TEMPMEKO), Portorož, Slovenia, June 2010.
- [3.] E.P. Papdakis, L.C. Lynnworth, D.R. Patch, E.H. Carnevale, "Ultrasonic Thermometry in LMFBR Systems," Final Report NYO-3906-13, Panametrics Inc. 1972.

- [4.] H.A. Tasman, M. Campana, D. Pel, J. Richter, "Ultrasonic Thin-Wire Thermometry for Nuclear Applications," Temperature: Its Measurement and Control in Science and Industry, Vol. 5, Part 2, pp. 1191-1196, 1982.
- [5.] L.C. Lynnworth, E.H. Carnevale, M.S. McDonough, S.S. Fam, "Ultrasonic Thermometry for Nuclear Reactors," IEEE Transactions on Nuclear Science, Vol. NS-16, 1968, pp. 184-187.
- [6.] J. Daw, J. Rempe, S. Taylor, J. Crepeau, and S.C. Wilkins, "Ultrasonic Thermometry for In-Pile Temperature Detection," Proceedings of NPIC&HMIT 2010, 2010.

Distributed Partnership at a Glance			
NSUF and Partners	Facilities and Capabilities		
Massachusetts Institute of Technology	Nuclear Reactor Laboratory		
Collaborators			
Idaho National Laboratory	Joshua Daw (principal investigator)		

Radial Heat Flux – Irradiation Synergism in SiC ATF Cladding

Yutai Katoh - Oak Ridge National Laboratory - katohy@ornl.gov

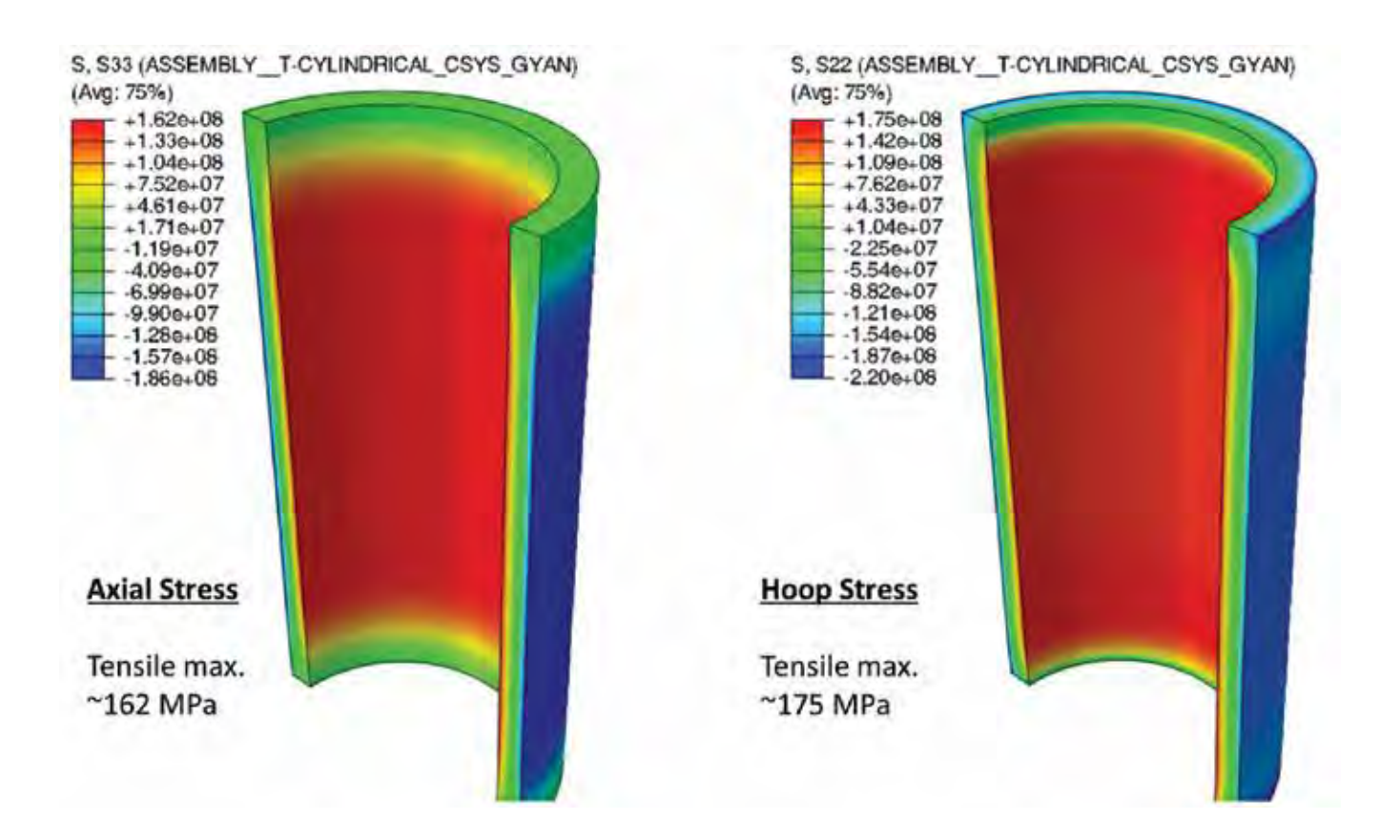


Figure 1. The "inverse thermal stress" predicted by multiphysics finite element thermomechanical analysis to develop in SiC/SiC tube as the synergistic effect of radial heat flux and neutron irradiation. Assumed conditions include radial heat flux 0.6 MW/m2 and outer surface temperature 573K.

silicon carbide fiber-reinforced silicon carbide matrix (SiC/SiC) composite is an enabling materials technology for the ultimate accident-tolerant fuels for light-water reactors (LWRs) and the core structures for advanced high-temperature reactors of various concepts. This ceramic composite combines the intrinsic benefits of SiC (e.g., outstanding irradiation

tolerance and steam-oxidation resistance) and the engineered benefits of fiber composites (e.g., damage tolerance and design flexibility).

The unique set of benefits for SiC/SiC composite comes with a unique set of challenges. This project addresses one of the most critical challenges, this material's inability to maintain fission-product-gas containment.

This project is intended to experimentally verify the irradiation-induced inverse stress behavior and determine its impact of the stress on the performance of SiC/SiC as the LWR fuel cladding.

Project Description

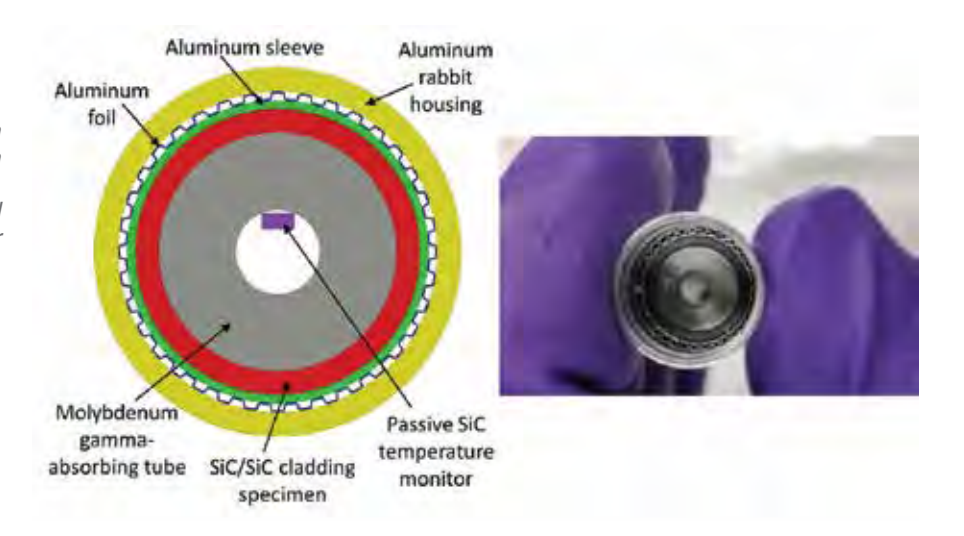
Among the unique challenges for fuel cladding made from SiC/SiC composite is internal stress arising from differential irradiation strain. SiC swells rather rapidly during the first week or two of operation as the LWR fuel cladding until the point-defect accumulation saturates. The swelling of SiC accompanies a decrease in the thermal conductivity, resulting in a steep temperature drop across the cladding-wall thickness due to high heat flux from fuel to coolant. The saturated swelling strain exhibits negative dependence on temperature. The results are the tensile stress at the inner surface and compressive stress at the outer surface of the cladding wall i.e., the opposite effect from normal thermal stress (Figure 1).

The implications of the predicted "inverse thermal stress" range from significant (such as microcracking initiating from the inner surface) to severe (crack networking leading to a loss of hermeticity and a threat to structural integrity) for the fuel cladding. This R&D project is

intended to experimentally verify the irradiation-induced inverse stress behavior and determine its impact of the stress on the performance of SiC/ SiC as the LWR fuel cladding [1].

The project consists of three technical tasks: 1) design and build an irradiation vehicle that enables neutron irradiation of small tubular specimens under an LWR-relevant radial heat-flux condition, 2) experimentally verify the thermal gradient through the tube wall thickness, and 3) examine the damage in the irradiated tubes and other effects of neutron irradiation under a steep temperature gradient. Each task is first-of-a-kind development involving significant technical obstacles that have to be overcome. However, success of the project will have implications beyond its immediate objectives because this innovative approach will enable studies on irradiation effects accompanying significant dimensional instability and irradiation behavior of any material under a steep temperature gradient.

Figure 2. Design and construction of the Fire Rabbit irradiation vehicle developed in the project, enabling simultaneous high radial heat flux and neutron exposure for tubular test specimens.



Accomplishments

The irradiation engineering challenge in this project is to develop a low-cost "Fire Rabbit" capsule that accommodates SiC/SiC tube specimens, enabling a radial heat flux relevant to LWR fuel claddings, and maintaining the specimen temperature constant [2]. The heat flux was produced by placing a concentric gamma-absorbing tube as a heat source inside the specimen (Figure 2). The need to maintain the specimen outer-surface temperature is the most significant challenge when SiC swells linearly by $\sim 0.7\%$ while a gap of a few microns causes unacceptable temperature deviations due to high heat flux. Moreover, any excessive mechanical constraint on the specimen has to be avoided.

Our team came up with the idea of using an embossed metallic foil sleeve surrounding the specimen, so that a constant heat conduction from the specimen to the capsule housing is maintained during and after the specimen swelling. Thus, an expandable thermal homogenizer sleeve was inserted between the foil and the specimen to minimize radial perturbation of temperature. The embossing pattern was optimized through a series of ex-pile experiments involving the measurement of heat conduction as a function of the compressive deformation of the foil layer. The actual radial build of the irradiation capsule is shown in Figure 2.



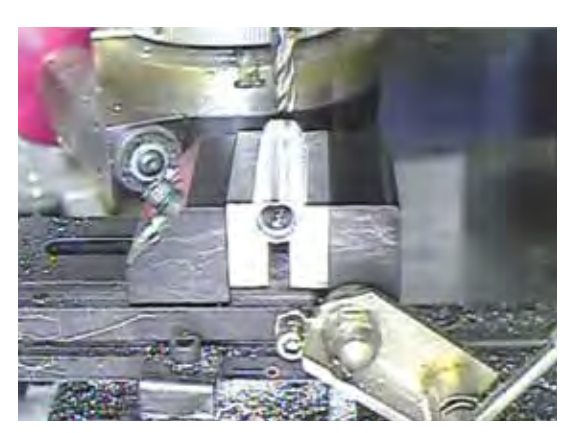


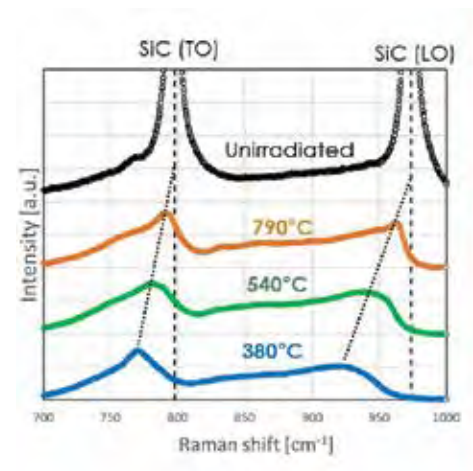


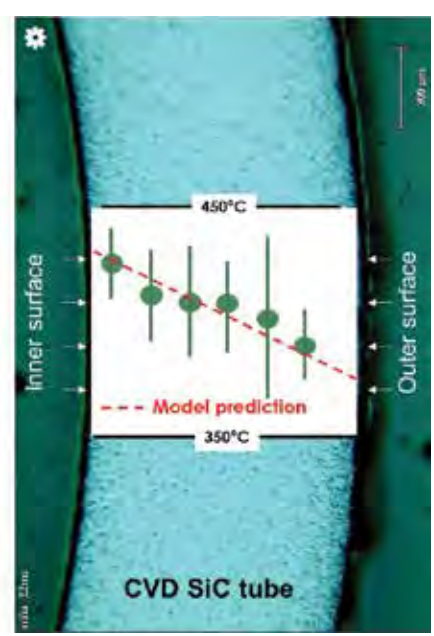
Figure 3. Disassembly of Fire Rabbit at the Irradiated Materials Examination and Testing Laboratory following neutron irradiation in the High Flux Isotope Reactor. Top left: a hot-cell operator opening the capsule; top right: capsule housing being carefully milled to retrieve the delicate samples; bottom: retrieved specimens with aluminum thermal homogenizer jacket (left), SiC/SiC composite tube with centering thimbles (middle), and monolithic SiC tube (right).

The capsules were irradiated in the Flux Trap facility of the High Flux Isotope Reactor for one full cycle following approval of the entirely new capsule design for the reactor. During this irradiation, the SiC sample accumulated the damage level of \sim 2 displacement per atom, achieving the swelling-saturation dose. The irradiated capsules were then carefully opened using a precision milling tool in the Irradiated Materials Examination and Testing Laboratory. The capsule-opening operation, including the capsule being milled while gently clamped in fixture, and the specimens being successfully retrieved are shown in Figure 3

Verifying the actual temperature of irradiation is essential for this experiment because the temperature profile defines stress distribution within each specimen. Sources of potential deviations from design temperature include poor thermal contact at any interface between the specimen and the housing, poor specimen quality, and unexpected axial heat loss from the heating tube. Passive temperature monitors were used to verify the temperature of the heating tube, and the average irradiation temperatures of individual specimens were confirmed by swelling measurements.

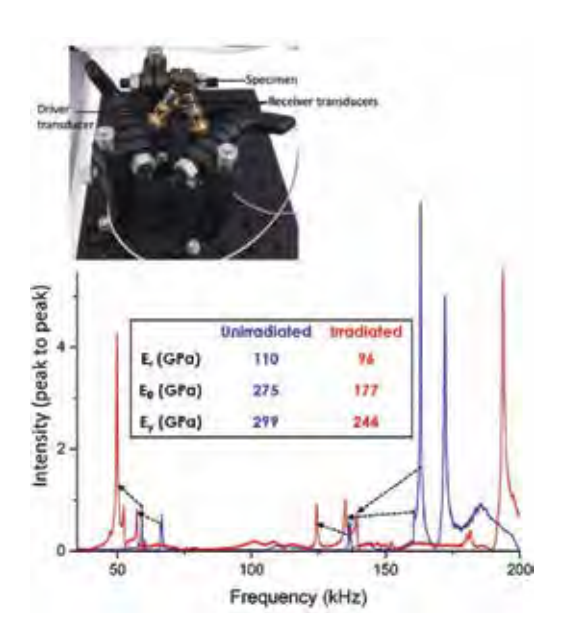
Figure 4. Development of a laser micro-Raman technology to map the irradiation temperature of SiC by post-irradiation thermometry (left), and application of the technology in verifying the temperature gradient across tube-wall thickness during neutron irradiation of SiC samples in Fire Rabbit (right).

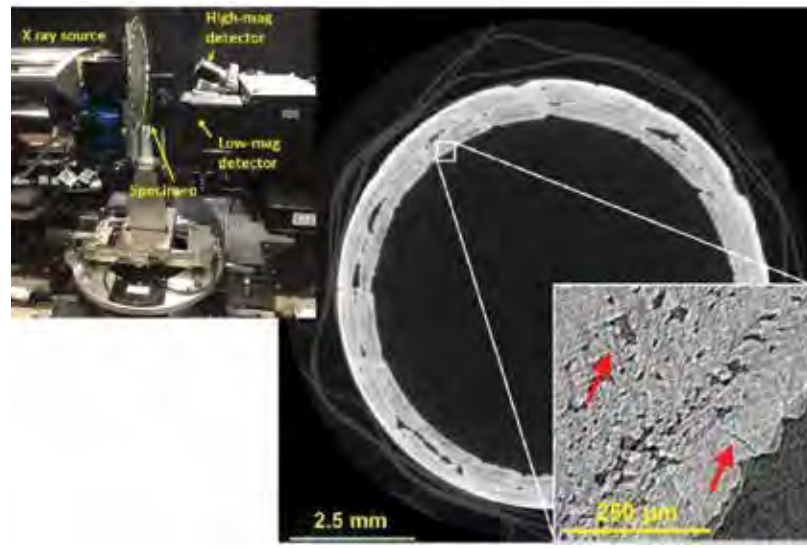




Moreover, a novel experimental technique for mapping irradiation temperature in specimens was developed. In this technique, the one-to-one correlation of certain Raman peaks and the lattice swelling of irradiated SiC was established [3,4] then successfully applied to determine the radial temperature profile within a thin-walled tube. Despite its limited accuracy due, partly, to the small laser spot size used for the mapping, the developed approach was able to prove the presence of a temperature slope consistent with the predicted for a CVD SiC specimen as shown in Figure 4.

The project plans an extensive set of post-irradiation characterization, starting with non-destructive evaluations (NDE) and followed by destructive evaluations such as cross-sectional microscopy and stress state-characterization involving elevated-temperature annealing. NDEs are focused on detecting and characterizing microcracking behavior and the possible resultant changes in gas permeability. Because microcracking due to irradiation-heat-flux synergy is anticipated at or near the inner surface of the tubes, where stress is primarily in tension, sonic or X-ray-probe NDEs are particularly useful.





The technique of ultrasonic-resonance spectroscopy (RUS) was utilized to evaluate the collective effects of microcracks on the elastic properties of the tubes [5]. Without changes in crack microstructures, ~6% reduction in Young's modulus is anticipated in SiC due to neutron irradiation alone. However, as shown in Figure 5 (left), more significant and anisotropic decreases in elastic constants are observed after irradiation in the Fire Rabbit, implying more-

extensive microcracking across the circumferential and axial orientations than radial. High-resolution X-ray computed tomography (XCT) examination revealed the presence of radial microcracks, which were not found in unirradiated tubes. The microcrack shown in Figure 5 (right) appears to be slightly open at the inner surface and extends to the mid-plane of the tube wall, where the inverse thermal stress is anticipated to be neutral.

Figure 5. Observation and characterization of microcracks present in the SiC/SiC composite tubes following neutron irradiation in Fire Rabbit: Resonant ultrasonic spectrometry showing significant decreases in circumferential and axial elastic moduli after irradiation (left) and X-ray computed tomography identifying radial microcracks near the inner surface of an irradiated tube (right).

The results obtained by NDE characterizations are consistent with those predicted by computational modeling incorporating the known effects of irradiation in SiC/SiC composites.

Future Activities

The results obtained by NDE characterizations are consistent with those predicted by computational modeling incorporating the known effects of irradiation in SiC/SiC composites. Within the present project, additional experimental data, including thermal conductivity, stress state, and helium permeation will be generated to further validate the multiphysics model and computation. The study will contribute toward fully establishing predictive capability regarding failure probability and behavior of SiC-based fuel cladding and core structures during the normal and offnormal operation of nuclear reactors.

Publications

[1.] Y. Katoh, K.A. Terrani, T. Koyanagi, C.M. Petrie, G. Singh, L.L. Snead, C. Deck, Irradiation – High Heat Flux Synergism in Silicon Carbide-Based Fuel Claddings for Light Water Reactors, in: LWR Fuel Perform. Meet. TopFuel 2016, Boise, Idaho, USA, 2016: pp. 823–831.

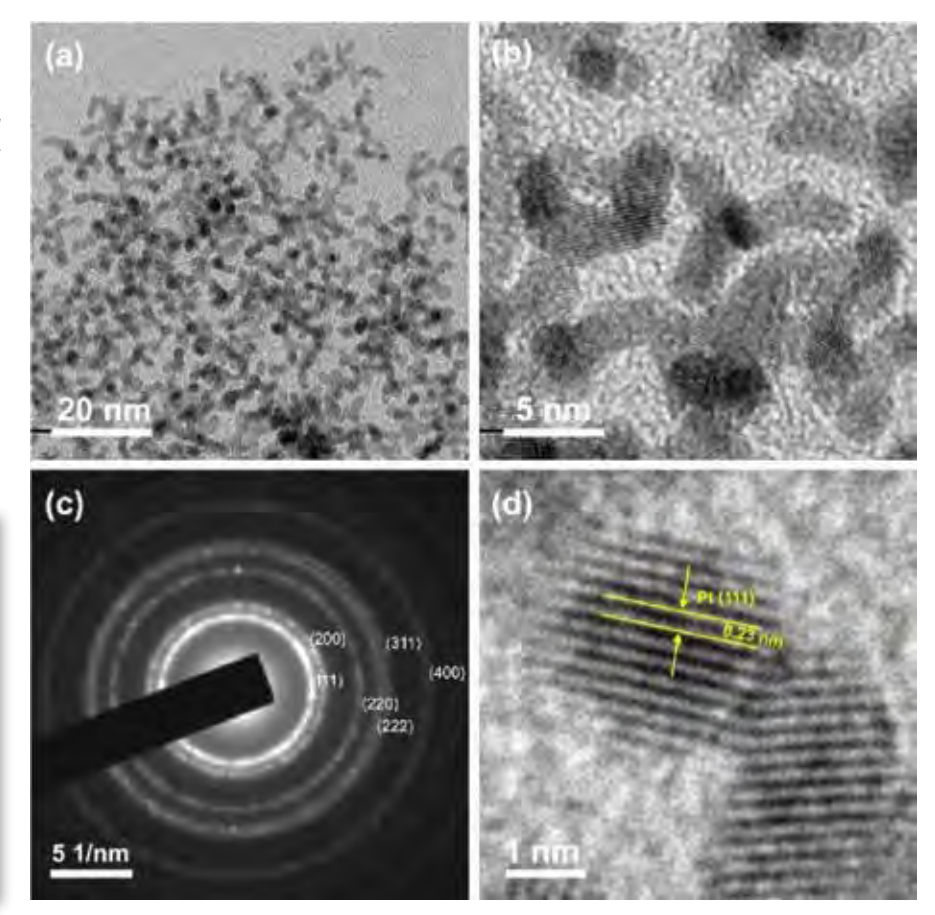
- [2.] C.M. Petrie, T. Koyanagi, J.L. McDuffee, C.P. Deck, Y. Katoh, K.A. Terrani, Experimental Design and Analysis for Irradiation of SiC/SiC Composite Tubes under a Prototypic High Heat Flux, J. Nucl. Mater. 491 (2017) 94–104.
- [3.] T. Koyanagi, M.J. Lance, Y. Katoh, Quantification of irradiation defects in beta-silicon carbide using Raman spectroscopy, Scr. Mater. 125 (2016) 58–62. doi:10.1016/j.scriptamat.2016.08.004.
- [4.] T. Koyanagi, Y. Katoh, M.J. Lance, Raman spectroscopy of neutron irradiated silicon carbide: Correlation among Raman spectra, swelling, and irradiation temperature, J. Raman Spectrosc. (2018) 1686– 1692. doi:10.1002/jrs.5425.
- [5.] G. Singh, T. Koyanagi, C. Petrie, K. Terrani, Y. Katoh, Evaluating the irradiation effects on the elastic properties of miniature monolithic SiC tubular specimens, J. Nucl. Mater. 499 (2018) 107–110. doi:10.1016/j.jnucmat.2017.10.060.

Distributed Partnership at a Glance			
NSUF and Partners	Facilities and Capabilities		
Oak Ridge National Laboratory	High Flux Isotope Reactor (HFIR), Irradiated Materials Examination and Testing Facility (IMET) Hot Cells, Low Activation Materials Design and Analysis Laboratory (LAMDA)		
Collaborators			
General Atomics	Christian Deck (collaborator), Christina Back (collaborator)		
Oak Ridge National Laboratory	Chris Petrie (collaborator), Gyanender Singh (collaborator), Hsin Wang (collaborator), Joel McDuffee (collaborator), Kurt Terrani (collaborator), Takaaki Koyanagi (collaborator), Xunxiang Hu (collaborator), Yutai Katoh (principal investigator)		

Additive Manufacturing of Thermal Sensors for In-pile Thermal Conductivity Measurement

Yanliang Zhang - University of Notre Dame - yzhang45@nd.edu

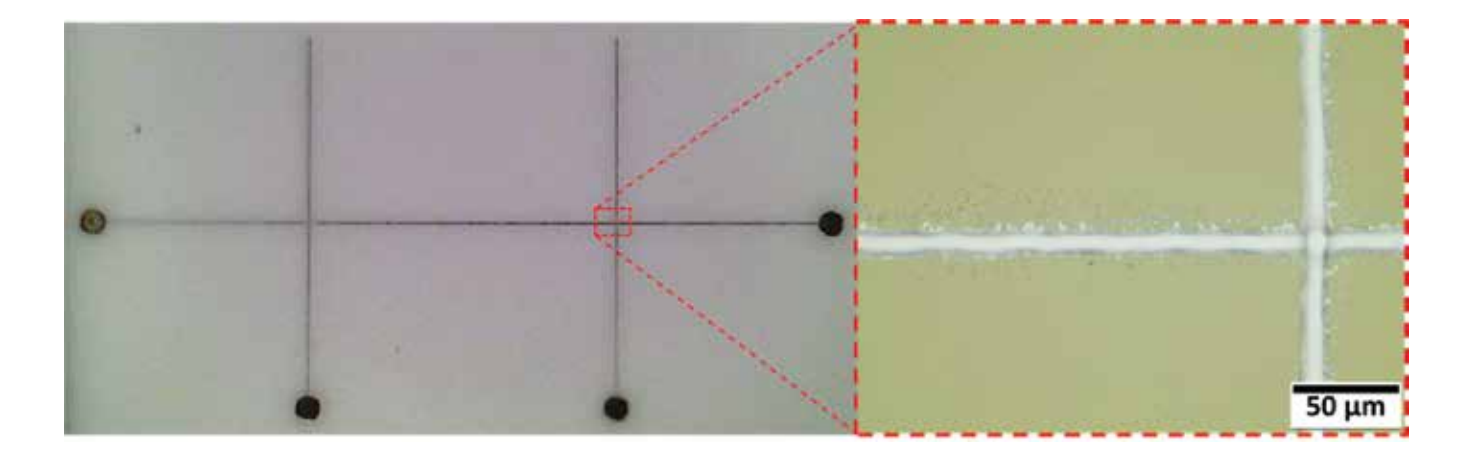
Figure 1. a, b)TEM and HRTEM d) images of the as-fabricated Pt nanoparticles. The corresponding SEAD pattern c) is also given.



The printed 3-omega sensors have great potential for improving the understanding of fuel thermal transport properties through in-pile thermal conductivity measurement.

hermal conductivity is one of the most important fuel properties driving heat transfer performance as well as temperature distribution in nuclear fuel [1]. Thermal conductivity is determined by materials' physical structure, chemical composition, and thermodynamic state. These factors are strongly affected by a variety of physical processes in nuclear fuels, such as large temperature variations,

species diffusion, neutron capture, and microstructure evolution [2,3]. Fuel thermal conductivity may also change substantially after removal from the reactor due to resulting changes in the material after the dynamic conditions of irradiation are removed. As a result, it becomes important to gain a more complete understanding of thermal transport as a function of time-temperature-burnup [4]. To do so requires accurate, spatially resolved



in-pile thermal conductivity measurements. The majority of the fuel thermophysical properties measurements to date, including thermal conductivity, have been performed out of pile in a hot cell. In-pile measurement of thermal conductivity presents a significant challenge due to the space constraints, the difficulties to realize nonintrusive sensor implementation and the extreme environment of in-pile irradiation and temperature. Hence, very few thermal conductivity methods have been implemented in-pile, and these methods are often intrusive and fail to yield accurate fuel thermal conductivity.

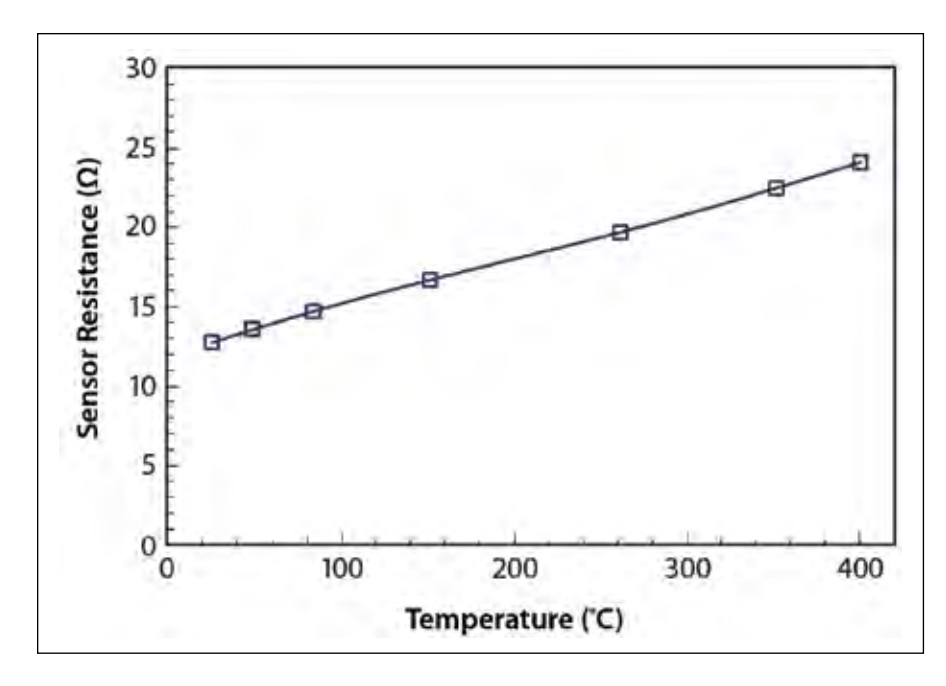
Project Description

The goal of this project is to develop advanced 3 sensors that can be tightly integrated with nuclear fuel system using advanced manufacturing methods to perform in pile thermal conductivity measurement. To determine the thermal conductivity, we will use the 3 method. A metal

sensor directly printed onto substrates representative of nuclear fuel materials serves as both a heater and a temperature sensor. The heater is driven by AC current at frequency, which produces a localized alternating temperature change through periodic Joule heating at frequency 2, with tunable heat penetration depth controlled by the current frequency. The 2 temperature change of the heater results in changes of its electrical resistance at frequency 2 and a corresponding third harmonic component of the heater voltage (3 voltage) which we can measure using a lock-in amplifier. This frequency-modulated thermal conductivity measurement offers real advantages over other methods for obtaining temperature-dependent thermal conductivity since we can confine the AC temperature field to the region of interest and minimize the influence of radiation heat loss.

The project outcome will advance

Figure 2. Microscope images of printed 3 sensors.



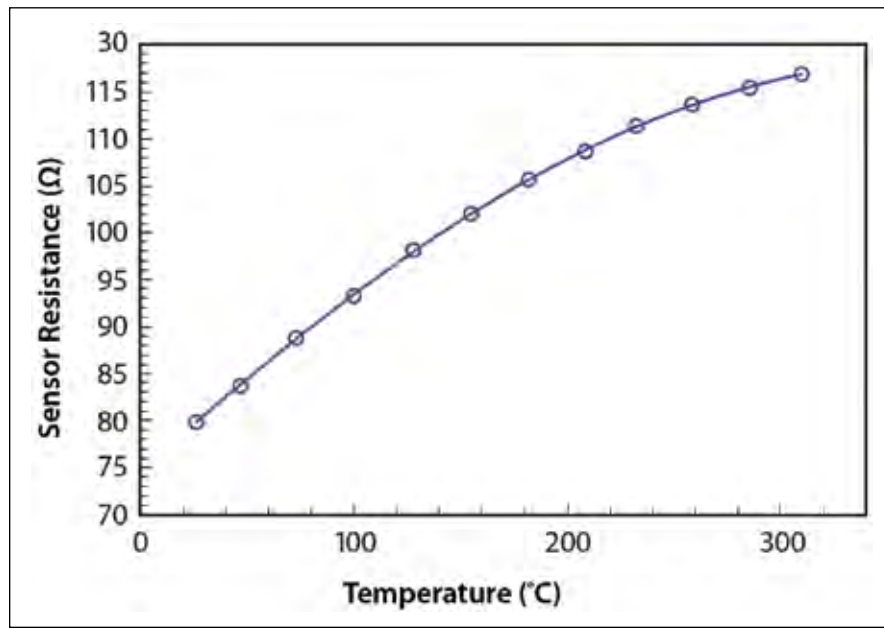


Figure 3. Resistance vs. temperature for aerosol jet printed silver (top) and platinum (bottom) 3 sensors.

scientific knowledge of the in-pile performance for sensors fabricated using additive manufacturing. Furthermore, the insight gained will significantly accelerate the deployment of additive manufacturing to fabricate a broad range of sensors and instrumentation for both in-pile and out-of-pile measurements. The research outcome will have a broad impact on a number of DOE-NE initiatives including Fuel Cycle Research and Development, the Transient Reactor Test Facility, and Advanced Modeling and Simulation. This transformative sensor manufacturing process will advance sensor research and development activities in various areas of importance to DOE including research associated with the Advanced Test Reactor (ATR) programs, the Transient Reactor Test Facility (TREAT) restart, Light Water Reactor (LWR) programs, and spent nuclear fuel storage.

Accomplishments

Silver and platinum are two sensor materials studied for this project. While silver ink is commercially available, there exists no commercial platinum (Pt) ink that can meet this project requirement. We synthesized the Pt nanoparticles using a wet-chemical bottom up approach. Pt nanocrystal was prepared by dissolving platinum precursor in an oleylamine, Oleic acid and 1-octadecene mixture. Pt inks were then prepared by dissolving 0.3 mmol of the-above-fabricated Pt nanoparticles in 2 mmol chlorobenzene. Thanks to the narrow size distribution of Pt nanocrystals, the Pt ink can be well printed using ultrasonic atomization in the aerosol jet printer. Figure 1 shows Transmission Electron Microscopy (TEM), and a Selected Area Diffraction Pattern (SAED) of the platinum nanoparticles, confirming

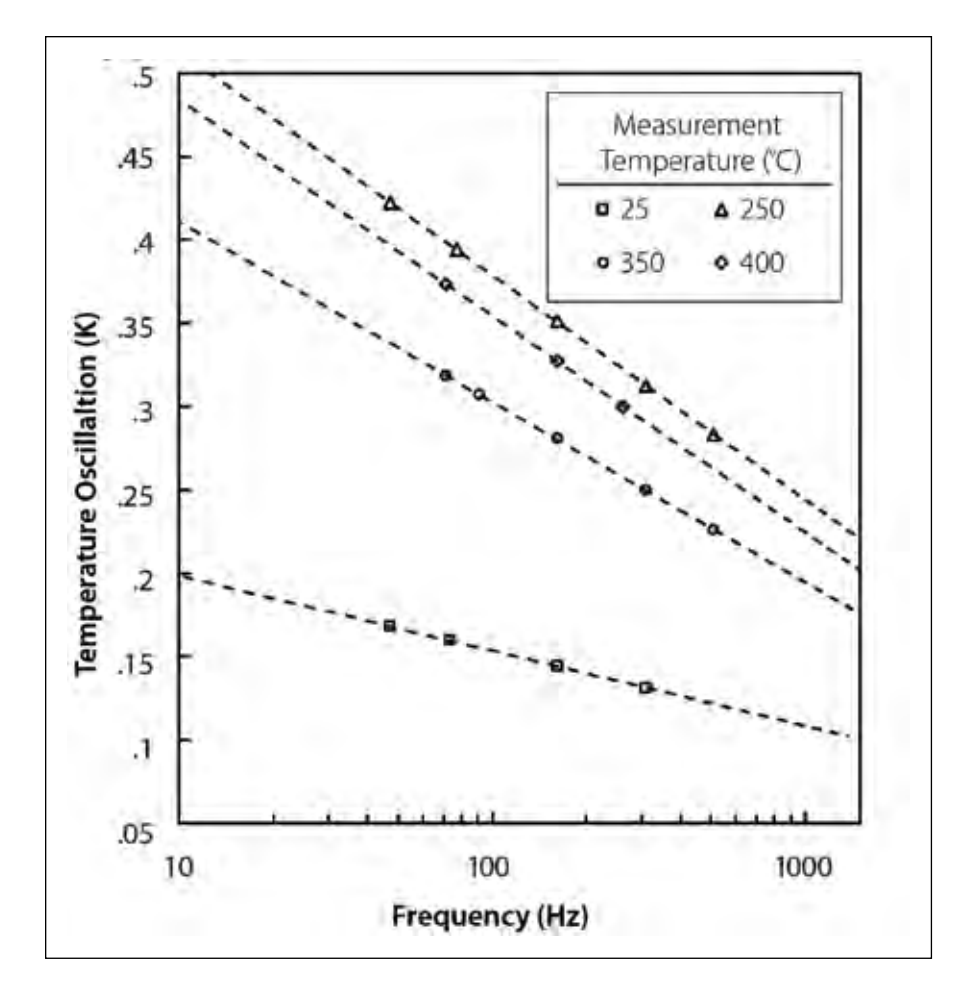


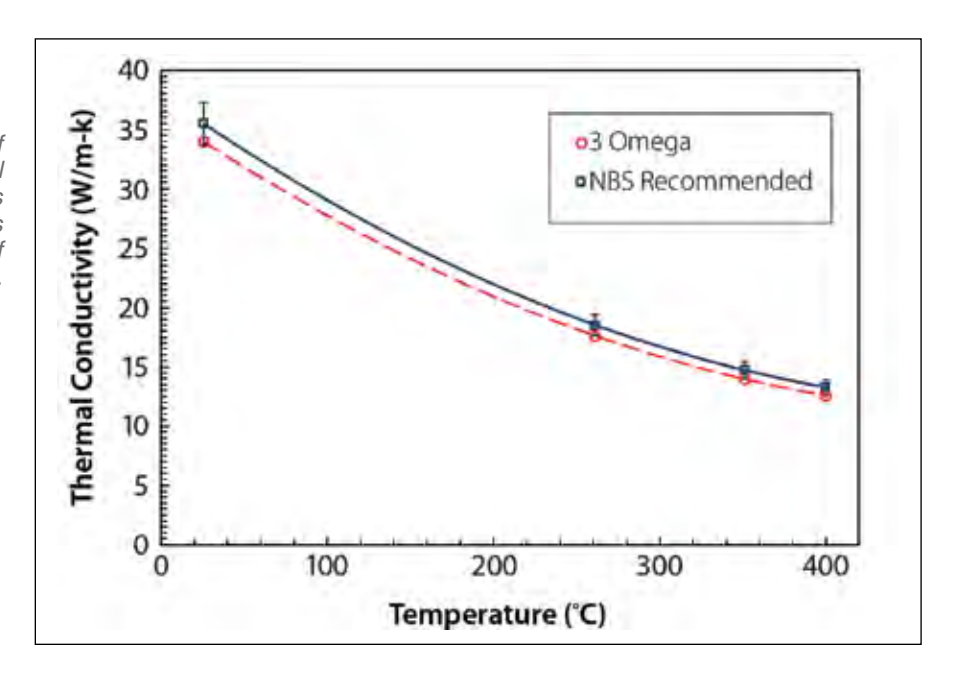
Figure 4. Temperature oscillation of the silver 3 sensor on alumina vs. applied frequency for various temperatures.

that Pt nanoparticles display good size and morphology uniformity with polyhedral structure.

In order to extract thermal conductivity with high accuracy, the width of the sensor must be much smaller than the thermal penetration depth. We optimized the aerosol jet printing parameter in order to print the 3-sensors with very fine microscale width. Figure 2 shows a printed silver sensor with 11.8 μ m width with a small degree of overspray and non-uniformity in the sensor line width. Since the overspray consists primarily of <1 μ m particles that are not in contact with the main sensor line, they do not influence the

sensor electrical signal and contribute insignificantly to heat transfer. Besides optimizing printing parameters, another important task is to sinter the nanoparticles to obtain bulk-like electrical conductivity. In the case of silver, this was accomplished by sintering for at least 6 hours at a temperature at least 100°C greater than the target operation temperature. The primary material property governing the performance of a 3 sensor is the temperature coefficient of resistance (TCR). Figure 3 shows electrical resistance as a function of temperature for a silver sensor and a platinum sensor. Room-temperature TCR values for aerosol jet printed silver sensors are

Figure 5. Thermal conductivity of alumina as measured by aerosol jet printed silver 3 sensors and the recommended values reported by the National Bureau of Standards (NBS) [5].



 $0.0025~{\rm K}^{-1}$ on average. This is lower than that of bulk silver (0.0038 K⁻¹), which is to be expected of the printed sensors due to their nanostructure and size. Similarly, the TCR of the printed platinum sensors is $\sim 0.0026~{\rm K}^{-1}$.

We have performed 3 thermal conductivity measurements on alumina substrates, which have thermal conductivity values roughly in the same range of advanced nuclear fuels. Based on the alumina substrate thickness of 635 µm and the sensor width of 15 µm, the range of frequencies applicable to the 3 slope method is ~60 to ~700 Hz. Figure 4 shows the temperature oscillation as a function of frequency for different temperature measurements. The results show an excellent linear dependence of temperature on the logarithm of applied frequency in the frequency range outlined above – a fundamental requirement of the 3 slope method. The amplitude of temperature oscillations varies slightly for the different temperatures studied because slightly

different current was used at each temperature. The thermal conductivity of the substrate can be determined based on the slope dV_3 d(In9)) of the third harmonic voltage V_3 to the natural logarithm of frequency using the following equation:

 $K = \frac{(TCR) V_{1\omega}^3}{\text{where } V_1 \text{ is} 4\pi l R \text{voltage } dV_{368} \text{ the}} \frac{d(ln(\omega))}{dV_{368}},$ sensor at the fundamental harmonic. I is the sensor length, and R is the sensor resistance at the temperature of interest. Figure 5 shows the temperaturedependent thermal conductivity measurement results up to 400°C. The thermal conductivity of 99.5% pure alumina measured using the printed 3 sensor agrees within about 5% of the value reported by the National Bureau of Standards. The excellent agreement validated the accuracy of the printed 3 sensor, and demonstrates promises of the printed sensors for in-pile thermal conductivity measurement.

Future Activities

We have completed the first round of irradiation on the printed sensors at NC State PULSTAR Reactor. Our future work will focus on post irradiation examination on the sensors irradiated at NC State. We will further improve sensor high-temperature thermal stability in order to extend the thermal conductivity measurement to higher temperatures. We will prepare sensors for irradiation experiment at MIT Research Reactor with significantly increased neutron flux and dose.

Publications

- [1.] B. Fox, H. Ban, J. L. Rempe, J. E. Daw, D. L. Knudson & K. G. Condie. In-Pile Thermal Conductivity Measurement Method for Nuclear Fuels. Thermal Conductivity 30:Thermal Expansion 18 30, 886 (2010).
- [2.] W. Z. Zhou, S. T. Revankar, R. Liu &

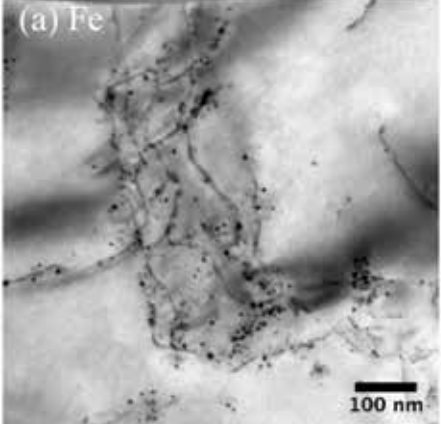
- M. S. Beni. Microstructure-Based Thermal Conductivity and Thermal Behavior Modeling of Nuclear Fuel UO2-BeO. Heat Transfer Engineering 39, 760 (2018).
- [3.] C. T. Walker, D. Staicu, M. Sheindlin, D. Papaioannou, W. Goll & F. Sontheimer. On the thermal conductivity of UO2 nuclear fuel at a high burn-up of around 100 MWd/kgHM. Journal of Nuclear Materials 350, 19 (2006).
- [4.] J. F. Villard, S. Fourrez, D. Fourmentel & A. Legrand. Improving high-temperature measurements in nuclear reactors with Mo/Nb thermocouples. International Journal of Thermophysics 29, 1848 (2008).
- [5.] Thermal conductivity of selected materials. U.S. Department of Commerce: National Bureau of Standards (1967).

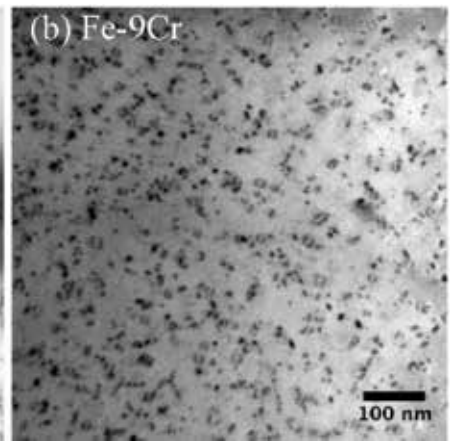
Distributed Partnership at a Glance			
NSUF and Partners	Facilities and Capabilities		
Center for Advanced Energy Studies	Microscopy and Characterization Suite		
Massachusetts Institute of Technology	Nuclear Reactor Laboratory		
North Carolina State University	PULSTAR Reactor Facility		
Collaborators			
Boise State University	Dave Estrada (co-principal investigator), Kiyo Fujimoto (collaborator)		
Idaho National Laboratory	Dave Hurley (co-principal investigator), Zilong Hua (collaborator)		
University of Notre Dame	Nick Kempf (collaborator), Yanliang Zhang (principal investigator)		

Neutron Irradiation Performance of Fe-Cr Base Alloys

James Stubbins - University of Illinois at Urbana-Champaign - jstubbin@illinois.edu

Figure 1. A comparison of (a) dislocation decoration in Fe irradiated to 1 dpa at 300, and (b) uniform dislocation loops in Fe–10Cr irradiated to 1 dpa at 300.





This project included several firsts including the first irradiations of low dose (0.01 and 0.1 dpa) specimens at ATR, first use of MR-CAT for in situ tensile tests of ATR specimens, and first use of NSUF facilities for Positron Annihilation Research.

dvanced nuclear reactors come with inherent safety Land improved energy efficiency, but they also require harsh operating conditions, such as elevated temperatures, high-dose neutron exposure, and corrosive environment. Fe-Cr-base ferritic/martensitic (F/M) alloys are considered lead candidate materials for in-core (cladding, ducts, and wrappers) and out-of-core (pressure vessel, piping) structural applications in advanced reactors. Compared to austenitic alloys, F/M alloys have higher thermal conductivity, a lower thermal expansion coefficient, and superior resistance to swelling and helium embrittlement. However, at relatively low temperatures, F/M alloys are susceptible to irradiation hardening and embrittlement.

The irradiation hardening and embrittlement in F/M alloys are known to be related to two types of defects created by neutron irradiation: (1) dislocation loops and (2) precipitates such as Cr-rich 'phase, Ni, Mn, Si-rich G-phase, and Cu-rich phase. It is critical to understand the microstructural evolution and governing mechanisms, in order to design advanced radiation-resistant alloys that can meet the requirements of next-generation reactors.

Project Description

In this research program, a coordinated set of ATR neutron-irradiation experiments with post-irradiation examination (PIE) on Fe–Cr base alloys were carried out, and several rapid-turnaround experiment (RTE) projects focusing on the PIE of irradiated specimens are ongoing. The suite of alloys ranges from pure

Table 1. Target irradiation alloy matrix, specimen types, and exposure conditions.

Alloy	Temp (C)	Dose (dpa)	Specimen Types
Model Alloys Fe, Fe-9Cr, Fe-12Cr, Fe-14Cr, Fe-19Cr, also Fe-9Cr & Fe-12Cr with 0.1, 0.2 or 0.5 wt% C	300, 450, 550	0.01, 0.1, 0.5, 1, 5, 10	TEM, Miniature Tensile
Commercial Alloys T91, HT-9	300, 450, 550	0.01, 0.1, 0.5, 1, 5, 10	TEM, Miniature Tensile
Developmental Alloys MA-957	300, 450, 550	0.01, 0.1, 0.5, 1, 5, 10	TEM, Miniature Tensile

iron to Fe—Cr binary model alloys to Fe—Cr—C ternary model alloys to commercial and developmental alloys. This spectrum of simple-to-complex Fe—Cr base alloys provide the basis for assessing the underlying radiation performance processes even in complex alloy systems. The new level of understanding on the irradiation performance of this alloy system will also facilitate the development of modeling capabilities to better predict future alloy performance and development.

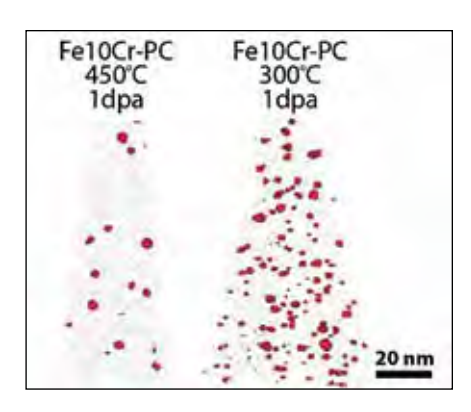
A set of state-of-the-art techniques has been used for the characterization of the irradiated alloys. Transmission electron microscopy (TEM), atom probe tomography (APT), and positron annihilation spectroscopy (PAS) were used to characterize the irradiated microstructure. Nanoindentation and in situ synchrotron wide-angle X-ray scattering (WAXS) were used

to study mechanical properties. Figure 1 is an example of TEM results comparing the loop structure of iron (Fe) and Fe–9Cr alloy that underwent the same neutron irradiation. It is clear that in Fe the dislocations are decorated by small black-dot dislocation loops, and in Fe–9Cr a homogeneous loop structure was observed. The reason is that the addition of chromium reduces the mobility of a/2 ⟨111⟩ loops and prevents them from migrating to pre-existing dislocations, resulting in a uniform loop distribution.

Another important feature commonly observed in irradiated high-Cr ferritic alloys are Cr-rich 'precipitates.

Previous studies indicated that 'precipitation is a radiation-enhanced process, rather than radiation-induced. Interestingly, the 'precipitation was found highly dependent on the bombarding radiation particles and

Figure 2. 20 at.% Cr isosurfaces showing the 'precipitates in neutron-irradiated Fe-10Cr samples.



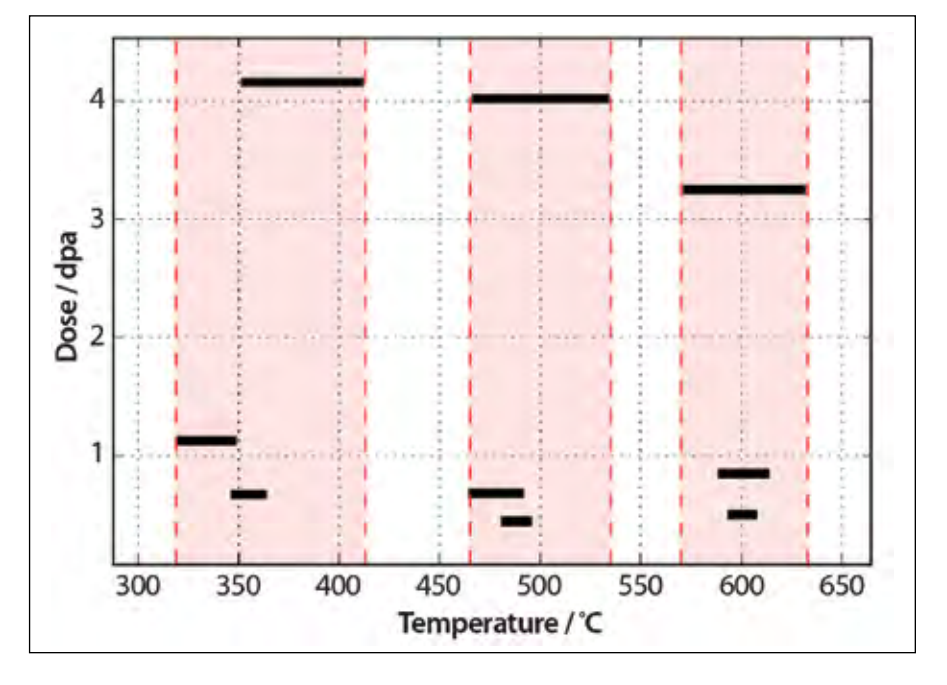
dose rate: 'precipitation was hardly observed in high-dose-rate heavy-ion-irradiated Fe—Cr alloys, but was observed in proton-, electron-, or neutron-irradiated Fe—Cr alloys. The chromium content of Cr-rich precipitates found in several studies is way below phase-diagram prediction, indicating strong effects due to ballistic mixing. Figure 2 shows the 'precipitates found in neutron-irradiated Fe—9Cr at two different irradiation temperatures. The decreasing number density of 'precipitates with

increasing irradiation temperature agrees with the phase diagram. However, the chromium content of these 'precipitates is also found to be considerably lower than the values predicted by the phase diagram.

Microstructure characterization of HT9 and T91

HT9 (12Cr) and T91 (9Cr) are high Cr F/M steels of great interest for applications in advanced reactors. In this project the specimens were irradiated to a relatively low dose level and then characterized using TEM and APT. The mechanical properties were measured by nanoindentation. A variety of radiation-induced microstructural changes were observed, including dislocation loops, radiation-induced precipitation, and segregation. The irradiation doses and thermal conditions were estimated using simulation methods, and the conditions investigated in this project are shown in Figure 3.

Figure. 3 Temperature and dose range of the irradiated HT9 and T91 specimens investigated.



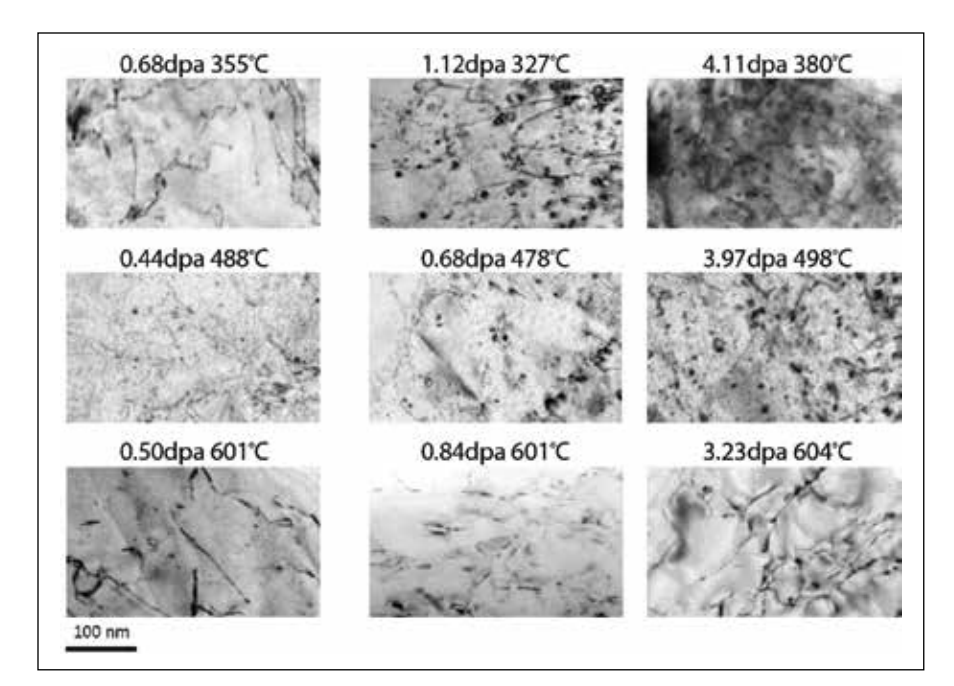


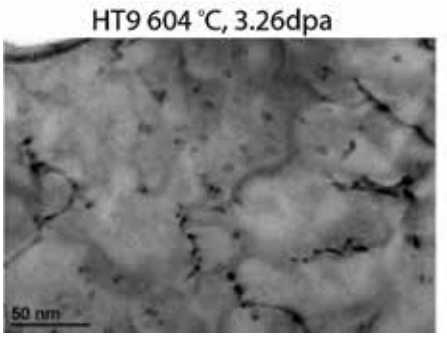
Figure 4. Effect of dose and temperature on the structure in T91.

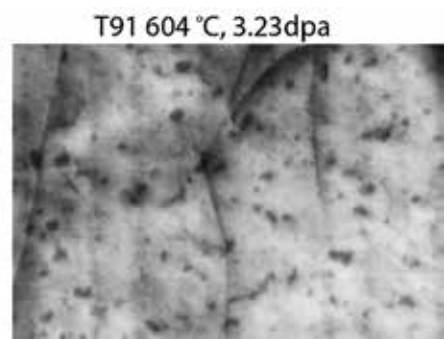
Radiation-induced defect microstructures
Both TEM and STEM were used to
characterize irradiation-induced
dislocation-loop structures in T91.
Most TEM samples were prepared using
an electropolishing technique. For
the conditions where electropolished
specimens were not available, the FIB
lift-out technique was used to prepare
the samples for TEM experiments.

The damage microstructures in T91 under various irradiation conditions are shown in Figure 4. The defect evolution in HT9 is similar to T91. The sizes of the dislocation loops strongly depend on the irradiation temperature, where the largest dislocation loops were observed at the highest temperature. Under the

similar dose level, at low temperature (around 350°C), damage was only visible above 1 dpa (except under special weak beam imaging conditions). At higher temperatures, visible loops were observed as early as 0.44 dpa. Considering the actual highest irradiation temperature is above 600°C, minimum irradiation damage was expected due to multiple factors including high-point defect recombination rate, low defect-cluster nucleation rate and thermal recovery above 600°C. On the contrary, significant irradiation damage was observed in this temperature regime. We also observed small loops with an average

Figure 5. Small loops observed in HT9 and T91 following high temperature high dose irradiation.





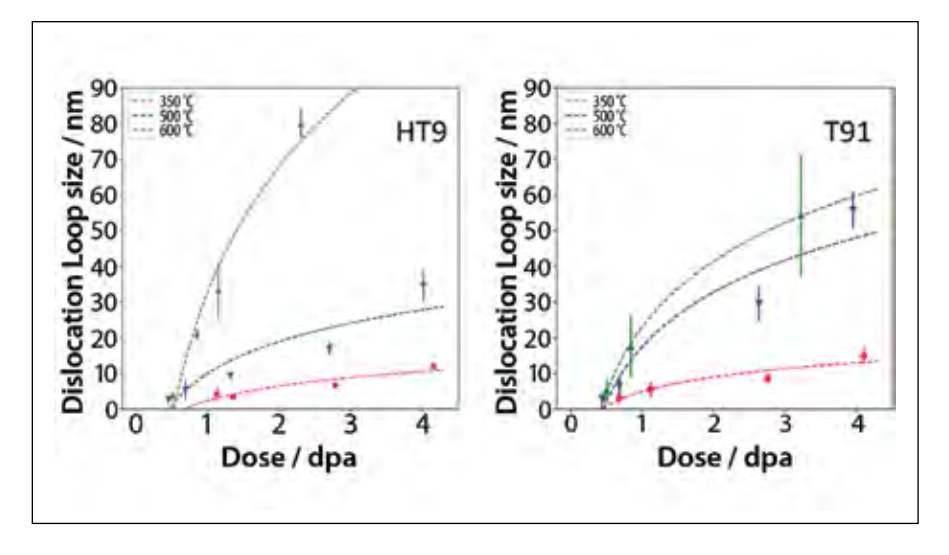
size of around 5 nm in the samples irradiated at highest temperature of 604°C and 3 dpa (see Figure 5).

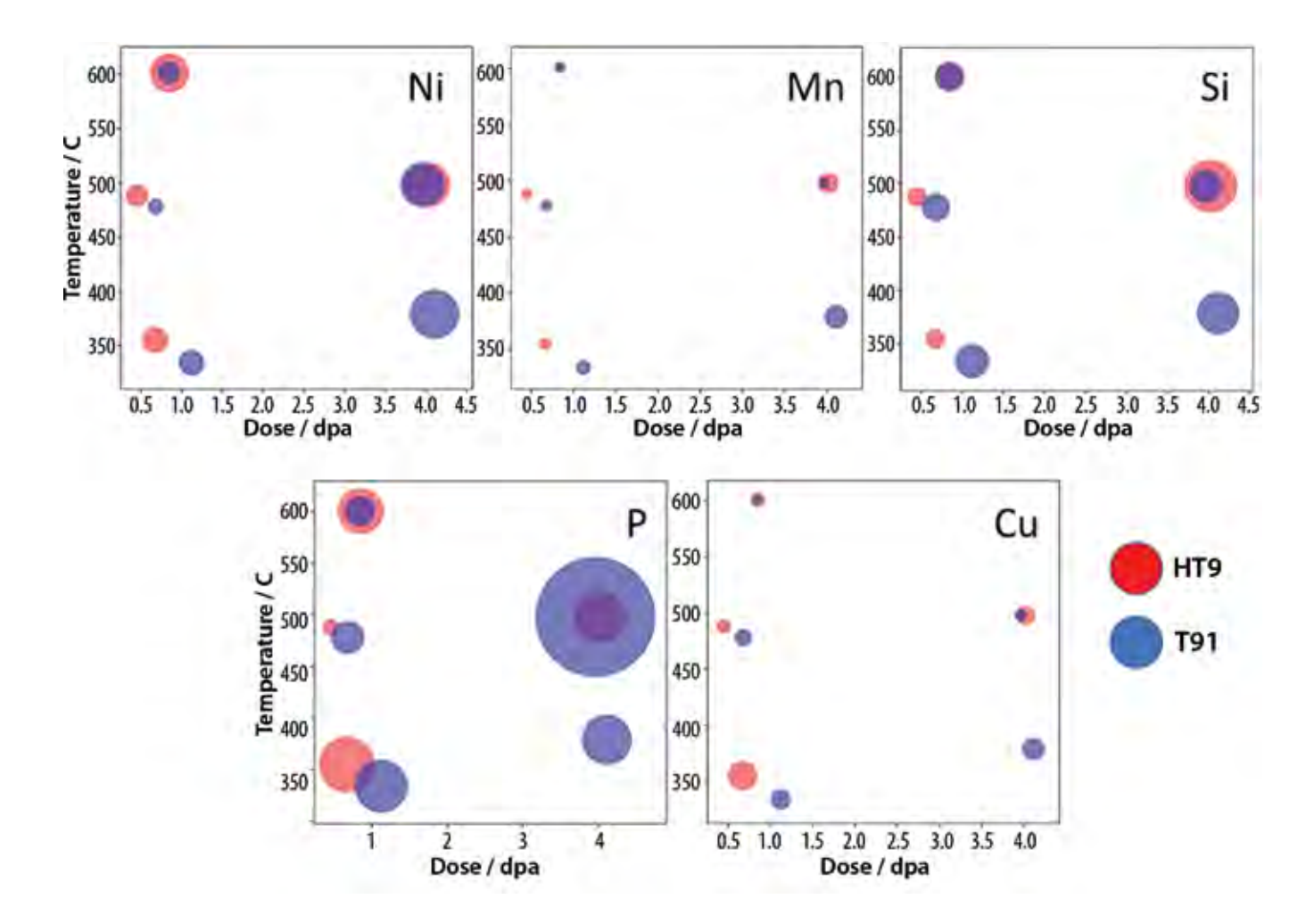
The abnormal defect structure is further illustrated by the multimodal size distribution of dislocation loops in samples irradiated for more than one cycle in the medium temperature range of 400 to 500°C. These phenomena can be explained by the lack of temperature control in reactor irradiation experiments. The specimens were sealed in capsules, and the main heating mechanism was by prompt gamma heating. The irradiation temperature was not well controlled during the experiment.

The samples may have experienced a fair amount of low-temperature irradiation, which leads to significant defect-cluster nucleation. These small clusters will then rapidly grow and develop into the scenario observed. The size of the dislocation loops is summarized in Figure 6 as a function of dose at 350°C. At low-temperatures, the loop sizes are similar in two materials, while the loops are significantly larger in T91 at higher temperatures, suggesting faster loop growth.

Radiation-induced segregation (RIS) STEM-EDS and APT were used to analyze radiation-induced segregation (RIS) and precipitation. Significant segregation of Cr, Si, Ni, Mn, P, and

Figure 6. Dislocation loop size in HT9 and T91 irradiation at 350, 500 and 600°C.





Cu was observed in some conditions at grain boundaries (Figure 7), second-phase boundaries, and dislocations. The dose dependency can be observed for Ni, Mn, Si, P, and Cu, but the temperature dependency is not clear. Strong segregation at the highest temperature might originate from the lack of temperature control. The highest RIS is observed for the element P, with the peak concentration 44 times higher than the bulk

concentration. The segregation of Ni, Mn and Si contributes to the precipitation of G-phase. The segregation of Cr to nitride surfaces facilitates the transformation of nitrides.

Radiation-induced Precipitation

A variety of radiation-induced modifications of the precipitation processes was observed, including the precipitation of G-phase, ', Cu-rich phase and modification of nitrides.

Figure 7. RIS of minor elements on GBs in HT9 and T91 as a function of dose and irradiation temperature. The radius of the circles is proportional to the percentage concentration increase.

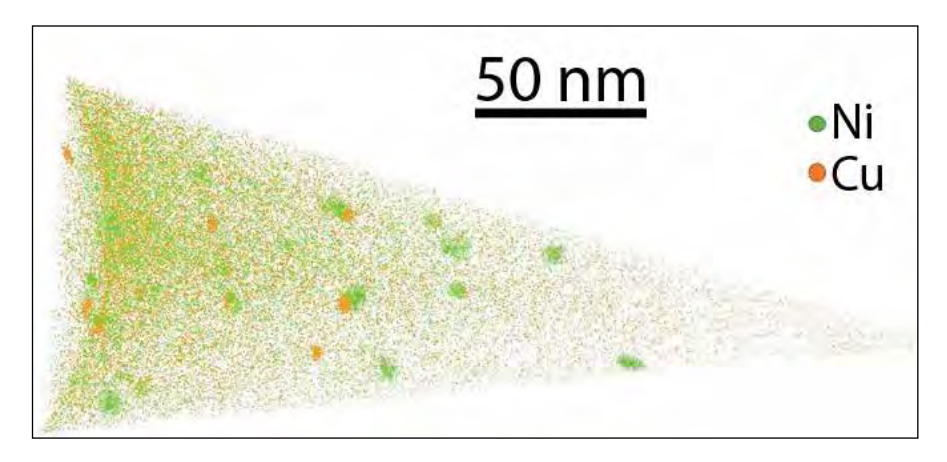


Figure 8. Ni atom maps showing the size and distribution of G-phase in irradiated HT9.

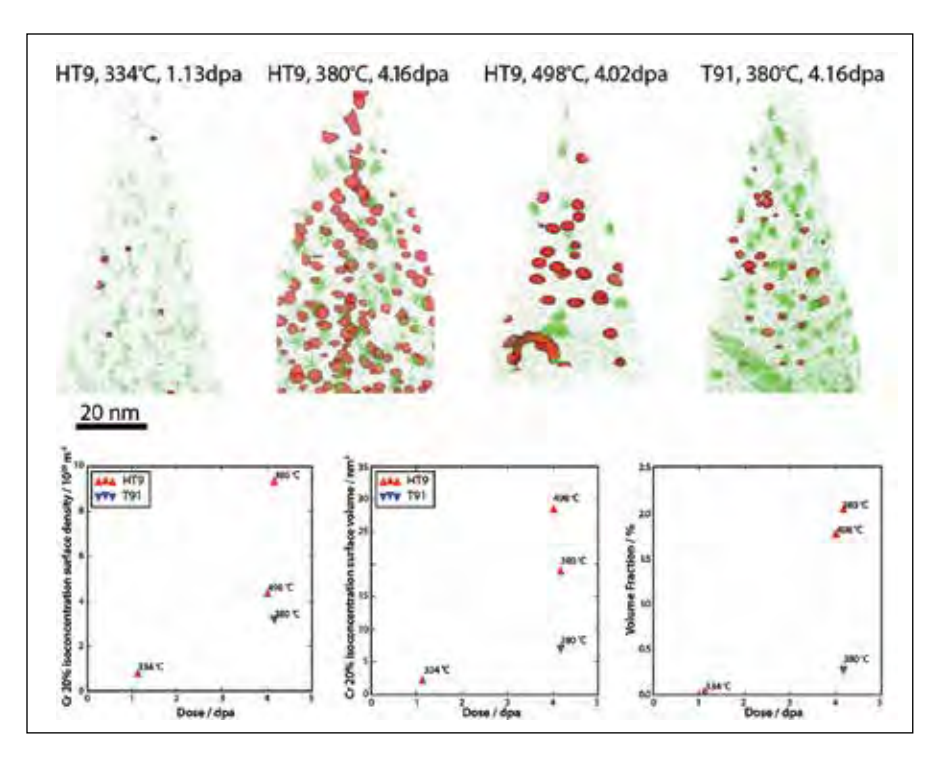


Figure 9. The distribution of ' visualized by 20% Cr isoconcentration surfaces. The size, density and volume fraction are also shown.

G-phase is a Ni-rich silicide frequently observed in irradiated steels due to the radiation-induced segregation of Ni, Mn and Si. The spatial distribution of G-phase particles is visualized in Figure 8 using APT Ni mapping. We

analyzed the particles using Ni, Si, Mn isoconcentration surfaces. The concentration evolution with irradiation is illustrated in Figure 9. The Ni, Si ratio is close to 1 for low-dose specimens, suggesting similar RIS for these two elements. The ratios then converge to the G-phase ratio, confirming that the particles are G-phase.

Cr-rich 'precipitates were also observed in HT9 and T91 under certain conditions. The precipitation of 'agrees well with the previously published results. In the 12Cr steel HT9, 'was observed in both low and medium temperature ranges, while in 9Cr steel T91, it was only observed in the low temperature range. The APT images and the size, density and volume fraction of 'are shown in Figure 9.

A Cu-rich phase was observed in T91 (Figure 11). Even though RIS of Cu was also observed in HT9, no clearly defined clusters of Cu were found in HT9. In T91 irradiated at high temperature to 3.23 dpa, Cu-rich particles were the only small-scale precipitates observed in APT. In the medium temperature range, G-phase and Cu-rich phase coexist and appear to have spatial correlations (See Figure 10). Nitrides are important precipitates in this type of steel. The most prominent type of nitrides in HT9 and T91 is vanadium nitride (VN). The thermodynamic calculation shows that VN is not a stable phase. Instead CrVN (Z phase) is the stable phase in high Cr steels. We observed the RIS of Cr on the VN phase boundary (Figure 12) and the modification of such phase. Cr₂N was also observed at both materials in low temperatures after long-term irradiation, up to 10 dpa.

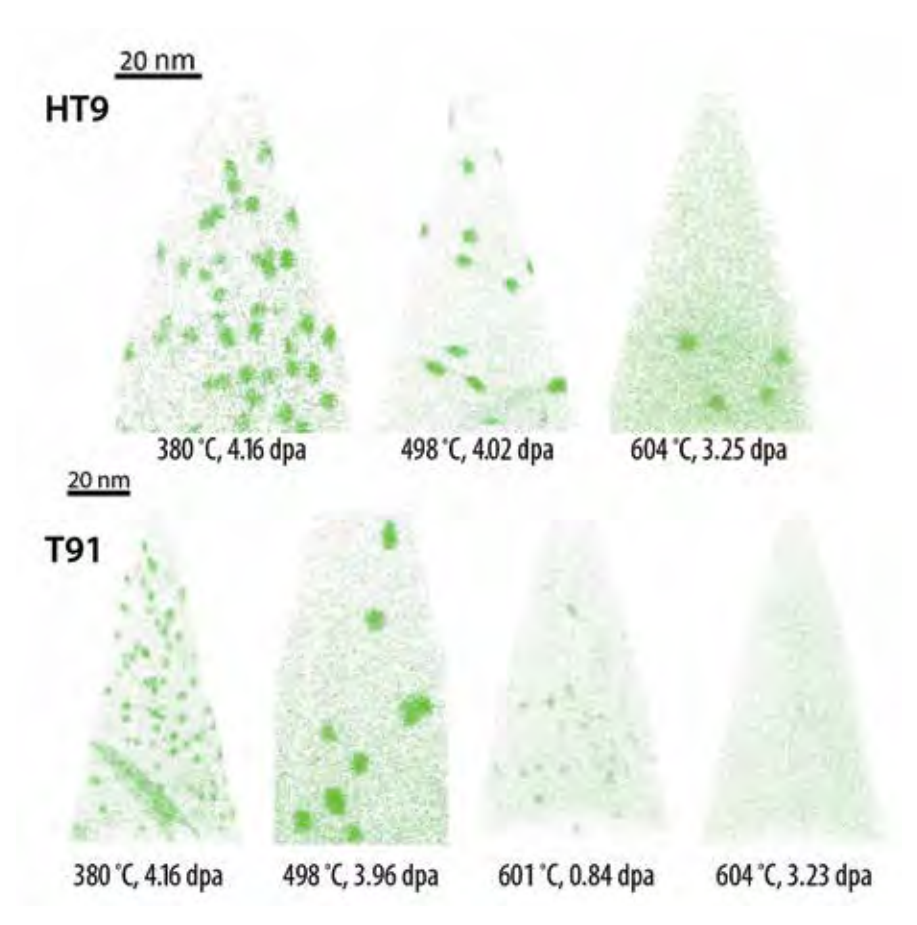


Figure 10. G-phase and Curich phase coexist in irradiated HT9 and T91 over the medium temperature range.

In general, three types of nitrides were identified in HT9 and T91, including VN, Z phase, and Cr₂N.

In addition to the model and F/M alloys, PIE work on an irradiated Fe–14Cr-base ferritic oxide dispersion strengthened (ODS) alloy MA957 has also started. Currently, microstructure characterization has been completed. Few dislocation loops were found in the lowest-dose specimens, and large loops were only found in the highest-dose specimens. The loops found in the intermediate dose (1.02 dpa at 340°C and 0.69 dpa at 478°C) were small black-dots. It might be possible to divide the

loop evolution into two regimes: loop nucleation below ~ 1 dpa, and loop growth above ~ 1 dpa.

Since MA957 is a Fe–14Cr alloy, the Cr content is above the threshold value for 'precipitation, which can be accelerated by neutron irradiation. Indeed, 'precipitation was observed in irradiated MA957 at several irradiation conditions. The 'precipitates can be readily seen from the Cr atom maps at the highest dose. More detailed analysis using Cr isosurfaces show that some 'precipitates can also be found in the ~ 1 dpa specimens.

In Situ tensile tests with

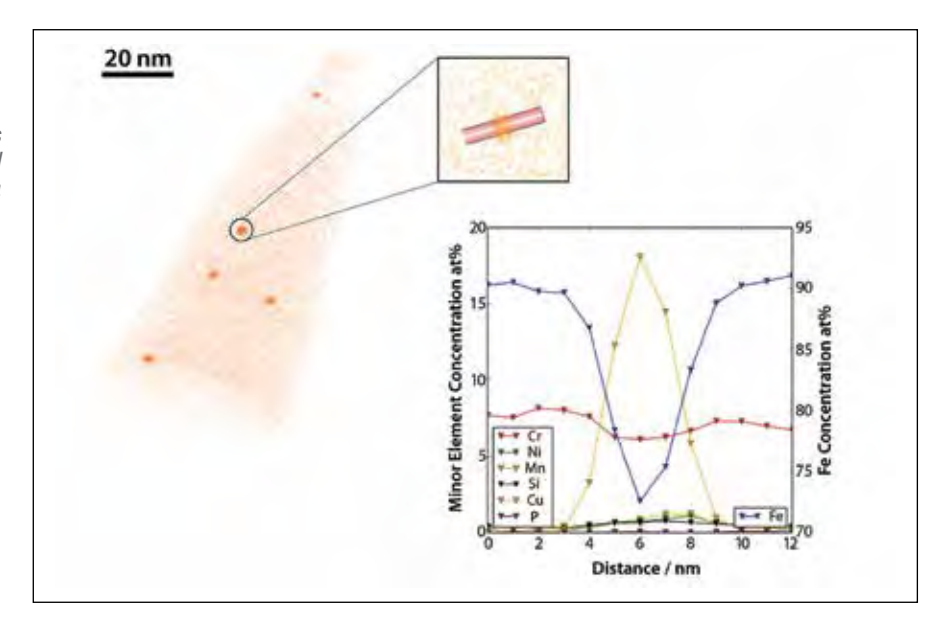


Figure 11. Cu-rich precipitates found in T91 irradiated around 600°C to 3.23 dpa

synchrotron X-ray diffraction

To study the irradiation embrittlement on F/M alloys, in situ synchrotron X-ray diffraction (XRD) measurements of the tensile deformation of irradiated samples were conducted. Because the samples were irradiated by neutron and activated with various radioactive isotopes, special confinement techniques were required to prevent radioactive contamination of the Advanced Photon Source (APS) beamline areas. Two types of radiationconfinement methods were developed for the in situ APS experiment. In APS beamline 1-ID, we employed doublecontained encapsulation for irradiated samples on the universal tensile machine. For the APS beamline 10-ID experiment, glovebox type confinement system was designed to enclose the samples and all experimental stages.

An in situ tensile test with high-energy X-ray provides more profound information over a conventional tensile test, including elastic and plastic behaviors with connections to specific crystal planes.

The lattice strains generated under applied stresses were mainly due to the elastic properties with hkl planes and plastic deformation with crystal slip planes and slip directions. Dislocation loops and the 'precipitation are the major contributors of irradiation hardenings. The theoretical contributions to irradiation hardening by dislocation

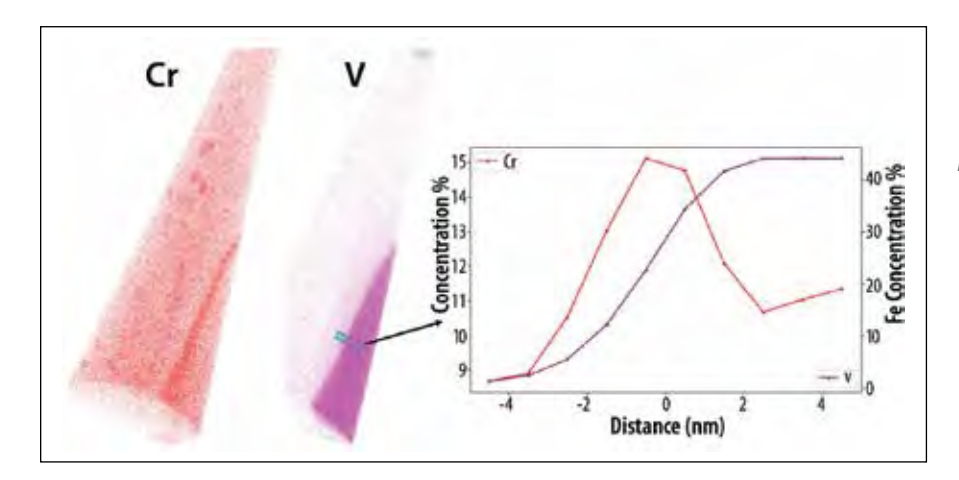


Figure 12. Cr RIS at VN phase boundary.

loops and the 'precipitation can be calculated by dispersed barrier hardening models.

The hardening contribution of the 'precipitation is a relatively simple function of density and average diameter of 'precipitations observed in APT. The calculation of irradiation hardening by dislocation loops, on the other hand, requires more-advanced modeling that consider the influence of critical resolved-shear stress on slip systems, habit planes of dislocation loops, and dislocation-density evolution during deformation.

Another major advantage of performing in situ synchrotron XRD tensile testing is that dislocation-density evolution during deformation can be obtained using the Williamson-Hall analysis. The in situ

tensile study shows similar plasticity behaviors in the low-dose samples and substantially increases dislocation densities at the higher dose samples.

HEDM (High-energy X-ray diffraction microscopy)

High-energy diffraction microscopy (HEDM) is a non-destructive three dimensional XRD technique that is suitable to characterize mechanical properties of neutron-irradiated samples. The APS 1-ID beamline has developed HEDM to obtain in situ grain-by-grain tensile behavior. Near-field high-energy diffraction microscopy (nf-HEDM) is used to obtain a crystallographic-orientation map of grains. Far-field high-energy diffraction microscopy (ff-HEDM) uses the high-resolution detector in ways similar to the WAXS detector to obtain grain-resolved lattice strains.

This spectrum of simpleto-complex Fe—Cr base alloys will provide the basis for assessing the processes underlying radiation performance even in complex alloy systems. The combination of nf-HEDM and ff-HEDM allows analyzing the distributions of orientations and strains at the scale of the sub-grain.

Because HEDM provides a crystallographic orientation map at microscale resolution, it is possible to obtain distributions of local misorientation in a grain. Local misorientations indicate local strains, usually plastic strains, because dislocations accompany residual strain and alter lattice orientations. Kernel average misorientation (KAM) is the popular approach to calculate variations of intergranular lattice orientations in electron backscatter diffraction, and it can be adapted to HEDM. KAM is numerically defined as the average misorentations between all neighboring kernels within the kernel. In the case that some kernels include grain boundaries, the kernels with KAM ≥5 degrees, for example, are excluded from the averaging calculation.

Positron annihilation studies
Positron Annihilation Spectroscopy
(PAS) provides a mechanism for
probing very small defect structures
produced during irradiation. This
technique is important since it is able
to measure defects with dimensions
smaller than those that can be imaged
using even the highest resolution
TEM techniques. PAS has the ability to

identify the presence of these tiny clusters, particularly vacancy clusters. This is critical to help develop a basis for understanding the void nucleation and void incubation processes, about which very little is presently known. Thus, PAS can provide an important link to the modeling of damage evolution. In addition to the role in damage structure evolution, the invisible defects, when they exist, can have an important impact on dislocation movement and overall deformation behavior.

This research is ongoing with the lowest-dose samples from the ATR irradiations.

Accomplishments

At present, a series of experimental and modeling work has been accomplished. Neutron irradiation on both disc specimens and miniature tensile specimens has been completed. The target doses range from 0.01 to 10 dpa (completed in six cycles), and the target temperatures were 300, 450, and 550 . For PIE on neutron-irradiated specimens, advanced characterization and testing techniques have been employed to explore the relationship between irradiated microstructure and mechanical properties.

Several RTE projects and a two-year

Nuclear Science User Facilities (NSUF)access-only project on microstructure characterization (TEM and APT) have been completed on neutron-irradiated Fe, Fe-Cr binary model alloy, Fe-9Cr-0.1C and Fe-9Cr-0.5C ternary model alloys, complex F/M alloys T91, HT9 and ODS MA957. The PIE work spans over 6 years, and TEM characterization was carried out using several electron microscopes at multiple facilities: MaCS (FEI Tecnai TF30-FEG STwin STEM) at the Center for Advanced Energy Studies (CAES), the Electron Microscopy Laboratory at Idaho National Laboratory (INL) (JEOL 2010 LaB6 TEM), Irradiated Materials Characterization Laboratory at INL (FEI Titan Themis 200 FEG-STEM), and the Low Activation Materials Design and Analysis Laboratory at Oak Ridge National Laboratory. The APT characterization was carried out using a LEAP 4000× HR at MaCS.

Collaborating with two beamlines (1-ID and MRCAT 10-ID) at Argonne National Laboratory's APS, in situ tensile tests with synchrotron WAXS and small-angle X-ray scattering (SAXS) have been completed on both control samples and neutron-irradiated Fe, Fe–9Cr, Fe–9Cr–0.1C, Fe–9Cr–0.5C, Fe–12Cr–0.2C, and Fe–12Cr–0.5C alloys. For the experiments at the Materials Research Collaborative

Access Team, a customized glovebox was built for the in situ tensile tests. This set of novel experiments will provide significant new insights on the effects of neutron irradiation on the microstructure and plastic deformation mechanisms.

An RTE project on measuring the nanohardness of neutron-irradiated Fe–Cr–C model alloys has also been completed, through collaboration with Dr. Peter Hosemann's Nuclear Materials Laboratory at University of California, Berkeley. The data are being used to correlate the irradiated microstructure with changes in mechanical property.

An NSUF-access-only project has also been initiated with North Carolina State University to measure the early stage of defect evolution in low-dose (e.g., 0.01 dpa and 0.1 dpa) specimens using PAS. At such low doses, a significant fraction of defects produced by neutron irradiation has not evolved into clustered form that can be resolved by conventional TEM. The PAS technique offers the possibility to examine small vacancy-type clusters. The experiments are ongoing at North Carolina State University.

Future Activities

Further investigations on the remaining neutron-irradiated specimens that will help bridge the knowledge gap from simple model alloys to complex F/M alloys will be carried out through future funding from NSUF RTE projects, NSUF-access-only projects, and Nuclear Energy University Program/Nuclear Energy Enabling Technology projects. Although efforts have been made to get microstructure data (including TEM, APT, PAS), nanoindentation, synchrotron WAXS/ SAXS tensile data on the same set of irradiated samples, there is still a long way to go to perform such coordinated experiments using the state-ofthe-art facilities at different national labs. We will push forward with the PIE efforts to make such experiments happen to advance the understanding of radiation effects in ferritic and F/M alloys.

Publications

- [1.] X. Liu, Y. Miao, Y. Wu, S.A. Maloy, J.F. Stubbins, "Stability of nanoclusters in an oxide dispersion strengthened alloy under neutron irradiation", Scripta Materialia 138 (2018) 57–61.
- [2.] X. Zhang, M. Li, J.-S. Park, P. Ken-

- esei, J. Almer, C. Xu, J.F. Stubbins, "In situ high-energy X-ray diffraction study of tensile deformation of neutron-irradiated polycrystalline Fe-9%Cr alloy", Acta Materialia 126 (2017) 67–76.
- [3.] W.-Y. Chen, Y. Miao, J. Gan, M.A. Okuniewski, S.A. Maloy, J.F. Stubbins, "Neutron irradiation effects in Fe and Fe–Cr at 300°C", Acta Materialia 111 (2016) 407–416.
- [4.] X. Liu, K. Mo, Y. Miao, K.-C. Lan, G. Zhang, W.-Y. Chen, C.A. Tomchik, R. Seibert, J. Terry, J.F. Stubbins, "Investigation of thermal aging effects on the tensile properties of Alloy 617 by in-situ synchrotron wide-angle X-ray scattering", Materials Science and Engineering: A 651 (2016) 55–62.
- [5.] W.-Y. Chen, Y. Miao, Y. Wu, C.A. Tomchik, K. Mo, J. Gan, M.A. Okuniewski, S.A. Maloy, J.F. Stubbins, "Atom probe study of irradiation-enhanced precipitation in neutron-irradiated Fe—Cr model alloys", Journal of Nuclear Materials 462 (2015) 242–249.

Distributed Partnership at a Glance			
NSUF and Partners	Facilities and Capabilities		
Argonne National Laboratory	The Intermediate Voltage Electron Microscopy (IVEM) — Tandem Facility		
Center for Advanced Energy Studies	Microscopy and Characterization Suite (MaCS)		
Idaho National Laboratory	Advanced Test Reactor (ATR), Irradiation Materials Characterization Laboratory (IMCL)		
Illinois Institute of Technology	Materials Research Collaborative Access Team (MRCAT) facility at Argonne National Laboratory's Advanced Photon Source		
North Carolina State University	PULSTAR Reactor Facility		
Oak Ridge National Laboratory	Low Activation Materials Design and Analysis Laboratory (LAMDA)		
University of California, Berkeley	Nuclear Materials Laboratory		
Collaborators			
Argonne National Laboratory	Carolyn Tomchik (collaborator), Jonathan Almer (collaborator), Jun-Sang Park (collaborator), Kun Mo (collaborator), Meimei Li (collaborator), Mike Billone (collaborator), Wei-Ying Chen (collaborator), Xuan Zhang (collaborator), Yinbin Miao (collaborator)		
Idaho National Laboratory	Assel Aitkaliyeva (collaborator), Collin Knight (collaborator), Jian Gan (collaborator), Lingfeng He (collaborator), Xiang Liu (collaborator),		
Illinois Institute of Technology	Jeff Terry (collaborator)		
North Carolina State University	Ayman Hawari (collaborator), Ming Liu (collaborator), Scott Lassell (collaborator)		
Los Alamos National Laboratory	Stu Maloy (collaborator)		
University of California, Berkeley	Peter Hosemann (collaborator)		
University of Illinois at Urbana-Champaign	James Stubbins (principal investigator)		

Post-irradiation examinations of annular mixed oxide (MOX) fuel pins for sodium fast reactors

Fabiola Cappia – Idaho National Laboratory – fabiola.cappia@inl.gov Jason Harp – Idaho National Laboratory – jason.harp@inl.gov

A more systematic study of the performance of annular fuel MOX pins has been undertaken in this project, with the specific objective both to ameliorate the understanding of the effects of irradiation temperature and burnup on the fuel microstructural evolution and to provide supporting data for validation of fuel-performance models.

The primary goal of Generation IV nuclear energy systems is to improve resource utilization and to minimize the nuclear waste burden while improving safety, reliability and proliferation resistance. In addition, through innovation aimed at reducing capital costs and financial risks, Gen IV technologies will provide clean energy at competitive costs compared to other energy sources [1].

The sodium-cooled fast reactor (SFR) is one of the six technologies that has been chosen as a next-generation nuclear energy system to meet these goals. SFR technology has been historically established both through pioneering experimental reactors (e.g., Fermi, Experimental Breeder Reactor-II, Rapsodie) and prototype reactors (e.g., Phenix, BN-600, Monju). Past experience is an essential asset and provides the basis to further develop advanced SFR concepts [2].

In terms of fuel for SFR, initial efforts in the fifties were focused on metallic fuels, due to the highest heavy-metal density favoring the highest breeding ratio. However, metal fuels struggled in achieving high burnup due to excessive swelling and dimensional instability. In a short time, uranium and plutonium mixed oxide (MOX) fuels became the reference fuel for SFR, thanks to their good stability under irradiation. Since the sixties, hundreds of thousands of pins have been successfully irradiated up to burnups exceeding 20% fission of initial heavy-metal atom [3]. High linear heat-generation rates (>30 kW/m) and high burnup, typically above 15%, were the main objectives of SFR fuel research and development, because it was shown that increasing fuel burnup offers significant cost advantages. Annular pellets, which lower the smear density to compensate for increasing pellet swelling as burnup progresses and maximize power rating for a prescribed margin to fuel melting [4], are one of the promising designs for SFR driver fuel.

Irradiation experiments of advanced MOX test assemblies were conducted in the Fast Flux Test Facility (FFTF) between 1980 and 1993 [5]. Assembly FO-2, which was one of the first assemblies to use HT-9 as cladding material, was designed to

Design parame	eters	K-type	L-type
Cladding	Material	HT-9	HT-9
	Outer diameter (mm)	6.858	6.858
	Cladding thickness (mm)	0.533	0.533
	Plenum volume (cm³)	23.6	23.6
Fuel Pellet	Material	MOX	MOX
	Outer diameter (mm)	5.59	5.59
	Inner diameter (mm)	1.397	1.397
	Pellet length range (mm)	6.27 to 8.66	6.27 to 8.66
	Gap width (mm)	0.203	0.203
	Smeared density (%TD)	80±1	80±1
	Pellet density (%TD)	91.7	91.7
	Oxygen-to-metal ratio	1.96±0.010	1.96±0.010
	Pu content (Pu/(Pu+U) wt%)	22	26

evaluate the effects of fuel form (i.e. annular vs solid) and fuel-design variables on pin performance. The test assembly was irradiated for 312 equivalent full power days at peak power of 45.6 kW/m, peak burnup of 65.2 GWd/tHM and peak fast fluence of 9.9×10^{22} n/cm². Initial post-irradiation examination (PIE) of the overall assembly and selected pins showed good and predictable performance of MOX with HT-9 cladding [6]. However, data remain limited to two studies of single pins [6,7]. A more systematic study of the performance of MOX annular fuel pins has been undertaken in this project, with the specific objective both to ameliorate the understanding of the effects of irradiation temperature and

burnup on the fuel microstructural evolution and to provide supporting data for validation of fuel-performance models.

Project Description

In the FO-2 assembly, there were 12 different fuel variants. Ten variants were solid MOX pellets and 2 were annular MOX pellets. This work focuses only on the annular variants. Four pins of two different types were selected: two of the L-type and two of the K-type. Design parameters of each pin are summarized in Table 1. The two types of pins have the same nominal design data, except for the initial Pu content, which is 26 wt% for the L-type and 22 wt% for the K-type.

Table 1. Design parameters of the FFTF pins.

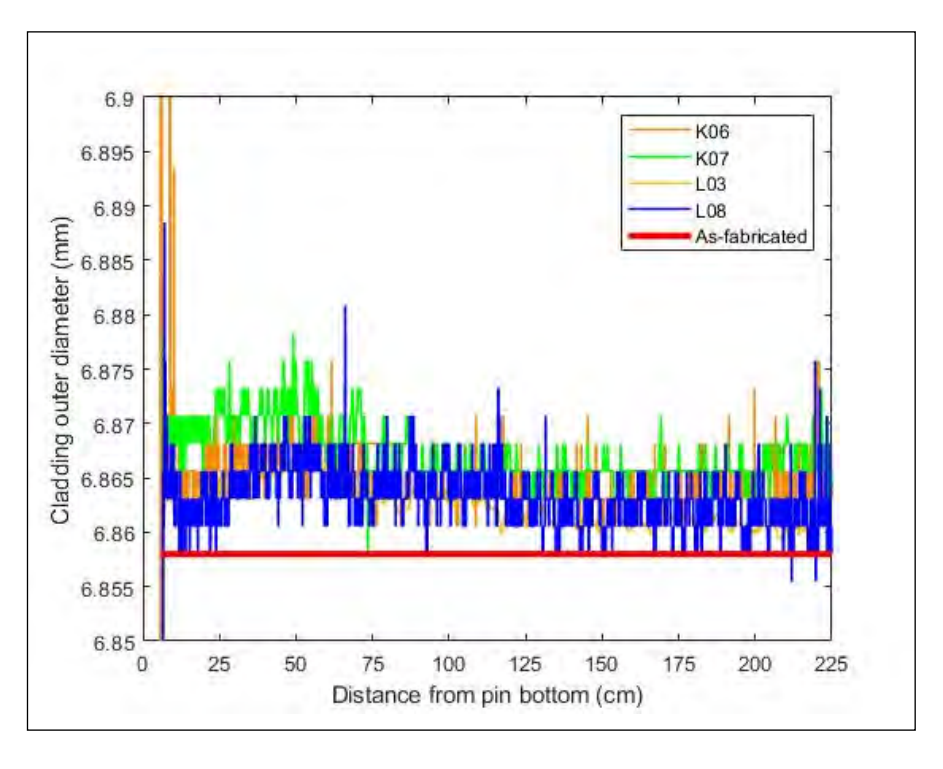


Figure 1. Cladding profilometry results of the four pins.

PIEs are primarily performed at the Hot Fuel Examination Facility (HFEF) of Idaho National Laboratory (INL). All non-destructive PIEs were completed, and destructive baseline PIEs are currently ongoing. Baseline non-destructive PIEs performed included neutron radiography, gamma spectroscopy, and dimensional inspection. Baseline destructive PIEs comprise fission-gas release, burnup analysis, and optical microscopy, including image analysis and microhardness testing.

PIE highlight and discussion Non-destructive PIE

Spiral profilometry scans were collected utilizing the in-cell element contact profilometer (ECP). The diameter was measured at intervals of 2.54 mm, starting at the top of each fuel pin. Results are reported for all four pins in Figure 1. The nominal as-fabricated diameter is also shown

in red. The results of all four pins are similar, with a uniform and limited strain along the full pin length. A more pronounced swelling of the cladding is noticeable in the part corresponding to the active column length, which is expected.

Gamma spectroscopy was performed with the precision gamma scanner (PGS) at HFEF. Only long-lived fission products Eu-154 and Cs-137 were detectable. Eu-154 and Cs-137 axial profiles are presented in Figure 2 and 3, respectively. The Eu-154 profiles follow the fission density of the fuel, indicating that the pins achieved similar burnup values, with pin L-08 having slightly higher burnup value. The depressed signals above and below the active fuel stack (see red arrows in Figs. 2 and 3) correspond to the blanket portions of the stack. According to fuel-performance-code calculations, burnup values at peak

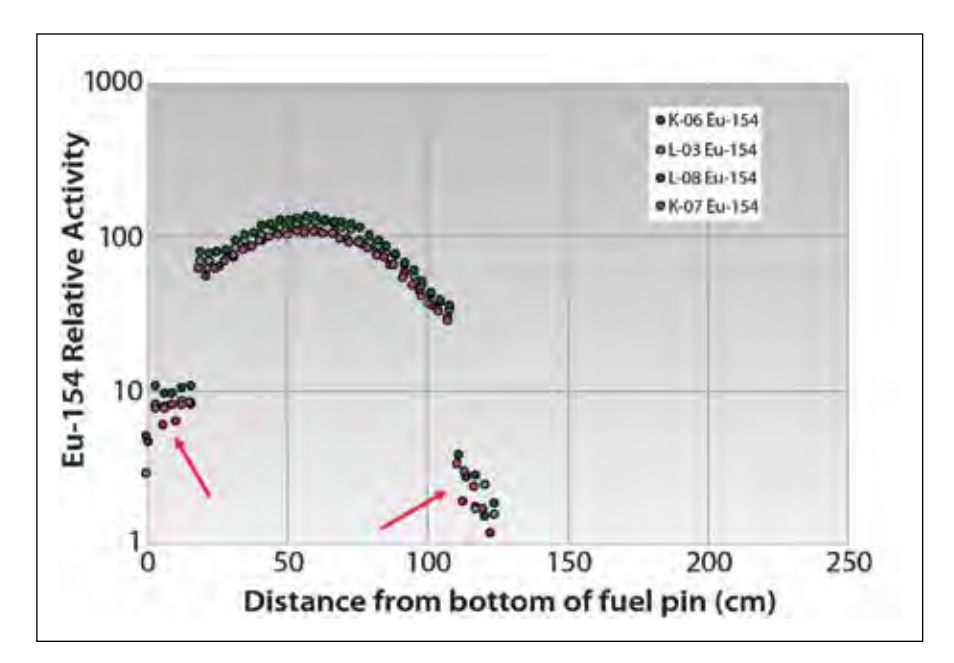


Figure 2. Axial gamma scanning (Eu-154) of the four pins.

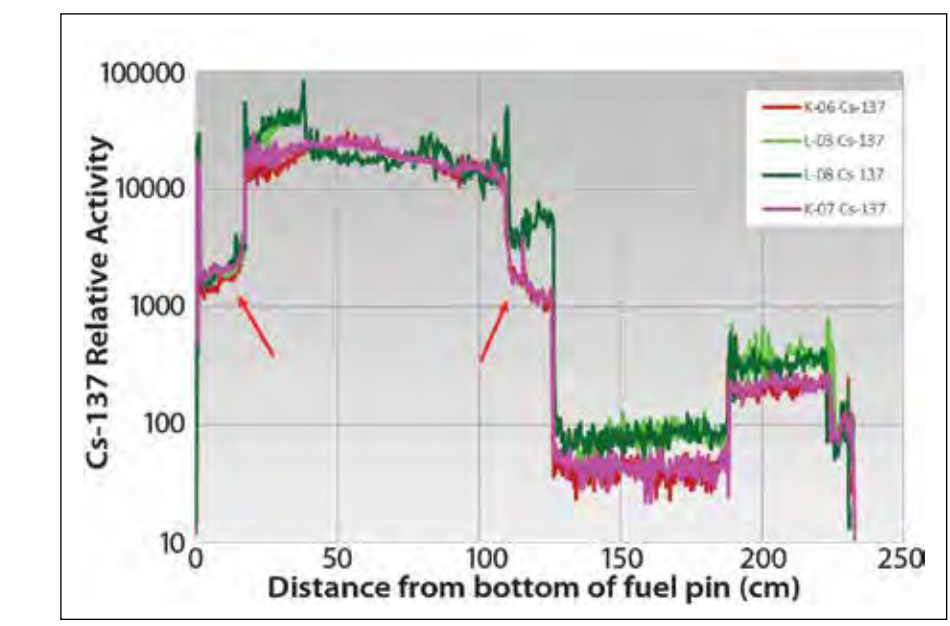
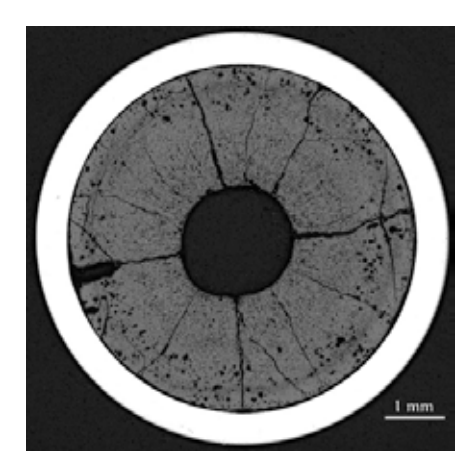


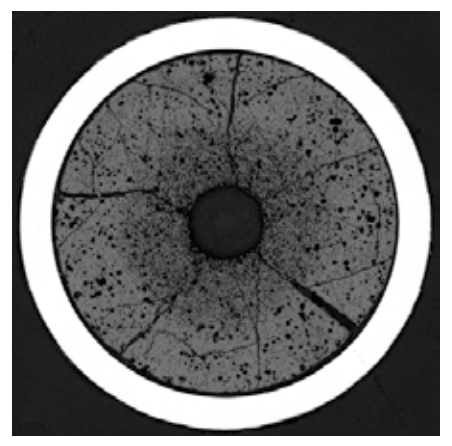
Figure 3. Axial gamma scanning (Cs-137) of the four pins.

power node are 59.4 GWd/tHM for K06 and K07, 59.5 GWd/tHM for L03 and 62 GWd/tHM for L08. Burnup analyses are ongoing in order to compare and verify the calculations. The Cs profiles of the K-type pins are consistent and resemble the as-generated profile. A remarkable

difference is visible in the behavior of Cs in the L-type pins, compared to the other two pins. Depletion of Cs has occurred in the central part of the active column, and Cs redistribution has occurred towards the end of the fuel, particularly towards the first 1/3 of the fuel length.

Figure 4. Low magnification cross section images (50x) from pin K06 at different axial positions. (a) Relative axial position 0.5 (peak power node) and (b) 0.05.



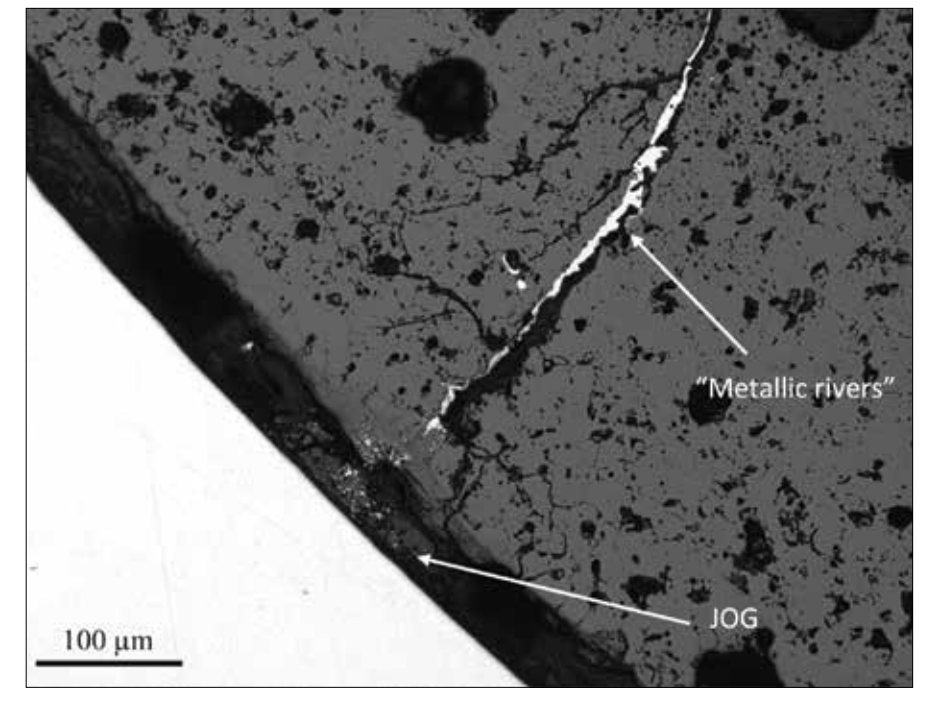


Destructive PIE

Major changes were implemented in the procedure to prepare metallography samples for these pins as compared to previous PIE investigations carried out on FO-2 pins. It is known that with increasing burnup, part of the fission products, particularly cesium and molybdenum, leave the fuel matrix and accumulate in the fuel-to-cladding gap, forming the so-called joint oxyde gaine (JOG)

[3]. Historical electron probe microanalyzer (EPMA) data [8] and thermodynamic calculations [9] suggest Cs₂MoO₄ as one of the major components of the JOG. The compound is highly hygroscopic and tends to dissolve rapidly when in contact with water, which was the main cutting fluid used in the past. The new sample preparation procedure uses non-water-based solutions and cleaning with ethanol—thus allowing

Figure 5. High-magnification image (200×) showing the formation of JOG and metallic rivers around one of the fuel cracks.



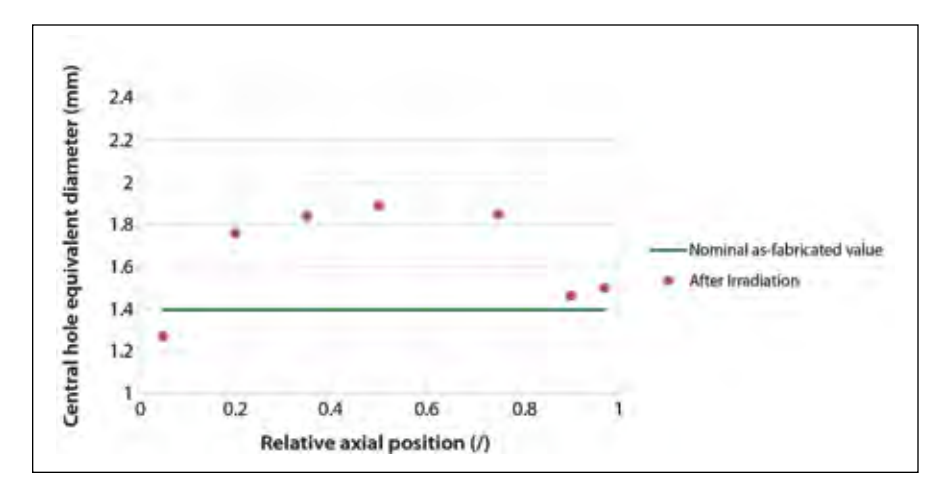


Figure 6. Evolution of the central void size after irradiation in pin K06. Increase of the void size is a consequence of pore migration induced by thermal gradients. Decrease of the size is due to possible material relocation or migration towards the coldest part of the pin.

better sample preparation compared to the past [10] and preserving both the JOG and the fission products accumulating in the fuel-cladding chemical interaction (FCCI) layer (Figure 5).

From optical microscopy images, engineering-scale measurements of the fuel microstructure features can be obtained. For instance, central void dimension and its evolution along the pin axis are reported in Figure 6. This type of quantitative information is fundamental to validate models of pore migration used in fuel performance codes [11].

Accomplishments

PIE results highlighted very good and comparable performance among the pins under similar irradiation conditions. Cesium redistribution has occurred in two of the pins, as shown in Figure 3. Cesium migration is a known phenomenon in SFR MOX fuels, induced by radial and axial temperature gradients. Cesium becomes volatile in the hottest parts of the fuel and migrates by successive evaporation and condensation to the colder regions, where lower temperatures allow formation of Cs compounds with low Cs vapor pressure [12]. Despite increased cesium concentration

at specific axial locations, no enhanced cladding strain was measured, as shown in Figure 1, suggesting no detrimental impact on the cladding following cesium accumulation, at least at intermediate burnup.

Fuel microstructure evolution occurs both radially and axially, depending on the local temperatures and burnup levels. At peak-power axial-node positions (i.e., at intermediate relative axial positions), formation of columnar grains occurs where temperatures exceed 1800-1900°C [4], as shown in Figure 4a. An enlargement of the as-fabricated annulus occurs due to pore migration, driven by steep temperature gradients (Figure 6). At the beginning of the fuel column, where power and burnup levels remain lower, no columnar grain formation occurs (Figure 4b), but the central part of the pellet shows a different texture, probably related to the enhanced diffusion-driven precipitation of fission products on grain boundaries.

Analysis of the optical microscopy mounts at different axial locations showed that the gap is still open. Partially, the gap is filled with fission Regarding the destructive
tests, a major accomplishment
has been obtained by
implementing a new samplepreparation methodology,
which considerably improved
the quality of the samples.

products that migrated radially. Present data confirmed that formation of the JOG occurs already at intermediate burnup, as indicated in Figure 5. The FCCI includes metallic precipitates (white particles in Figure 5) that could be either metallic fission products or cladding components. In addition, metallic rivers [13] are observed along fuel cracks. Advanced PIE such as scanning electron microscopy and energy-dispersive X-ray spectroscopy are foreseen to determine the chemical composition of the observed phases.

PIE results on four pins with advanced annular MOX and HT-9 cladding have been gathered. The non-destructive examination did not reveal anomalous behavior of the pins and are in line with previous investigations on similar pins.

Regarding the destructive tests, a major accomplishment has been obtained by implementing a new sample-preparation methodology, which considerably improved the quality of the samples. In particular, the JOG and FCCI have been preserved for the first time in FFTF annular MOX

fuels. While the JOG and the FCCI have been extensively characterized at very high burnup [8], less it is known about the composition and structure of these phases at intermediate burnup. The present data will allow the characterization of the FCCI at intermediate burnup and comparison with published literature.

Publications

- [1.] OECD Nuclear Energy Agency, Technology Roadmap Update for Generation IV Nuclear Energy Systems, 2014.
- [2.] K. Aoto, P. Dufour, Y. Hongyi, J.P. Glatz, Y. Kim, Y. Ashurko, R. Hill, N. Uto, Prog. Nucl. Energy 77 (2014) 247–265.
- [3.] Y. Guerin, in:, Compr. Nucl. Mater., Elsevier, 2012, pp. 547–578.
- [4.] N.E. Todreas, M.S. Kazimi, in:, Taylor & Francis, 1990, p. 317.
- [5.] J. Perez-Carter, N.J. Graves, B.C. Gneiting, Irradiation History Report for Advanced Oxide Fuel Assembly FO-2, 1993.
- [6.] L.L. Gilpin, R.B. Baker, S.A. Chastain, in:, ANS Annu. Meet. 1989, Atlanta, 1989.

- [7.] M. Teague, B. Gorman, J. King, D. Porter, S. Hayes, J. Nucl. Mater. (2013).
- [8.] M. Tourasse, M. Boidron, B. Pasquet, J. Nucl. Mater. (1992).
- [9.] J.-C. Dumas, Etude Des Conditions de Formation Du Joint-Oxyde-Gaine Dans Les Combustibles Oxydes Mixtes Des Reacteurs a Neutrons Rapides, Observations et Proposition D'un Modele de Comportement Des Produits de Fission Volatils, Institut National Polytechnique de Grenoble, 1995.
- [10.] M. Teague, Post Irradiation Examination of Legacy FFTF Oxide Fuel, 2012.
- [11.] S. Novascone, P. Medvedev, J.W. Peterson, Y. Zhang, J. Hales, J. Nucl. Mater. 508 (2018) 226–236.
- [12.] W. Breitung, G. Schumacher, The Significance of Cesium in LMFBR and LWR Safety Analysis, 1984.
- [13.] R.B. Fitts, E.L. Long, J.M. Leitnaker, in:, Fast React. Fuel Elem. Technol., 1971, pp. 431–458.

Distributed Partnership at a Glance	
NSUF and Partners	Facilities and Capabilities
Idaho National Laboratory	Hot Fuel Examination Facility (HFEF)
Collaborators	
Idaho National Laboratory	Fabiola Cappia (principal investigator), Jason Harp (principal investigator)

Availability of well-characterized, highly irradiated 304 stainless steel for NSUF-supported studies

Frank Garner – Radiation Effects Consulting – frank.garner@dslexteme.com Paula Freyer – Westinghouse – freyerpd@westinghouse.com

It was successfully
demonstrated that ultrasonic
measurements were in full
agreement with densitychange and microscopy
measurements.

tainless steels serve as the major structural components in both I fast reactors and thermal power reactors, not only in the U.S., but in Russia, China, Japan, most European countries and other nations. Therefore, intense international interest is growing in the response of these steels to increasing radiation exposure, especially in the light-water reactor (LWR) power-generation community, where government-granted operation licenses for 30 years (Russia, Japan) or 40 years (U.S.) are approaching or exceeding these lifetime limits. Requests in the U.S. for life extension to 60 years are now being considered and, in many cases, granted, generating new interest in research on radiation response of these steels.

In the U.S., Western Europe and Asia, the major construction steel employed in reactor construction was AISI 304, produced 45–60 years ago, but with then-current technology, which produced steels with less stringent specifications than currently required, especially with respect to minor deleterious elements such as sulphur and phosphorous—important in corrosion and welding—or with respect to gases such as oxygen and nitrogen, which are important initiators of void swelling.

Studies to support plant life extension require sufficient material of the 60-year-old vintage, subjected to well-characterized neutron irra-

diation at high enough exposures to enter material-degradation regimes involving transmutation, segregation, precipitation, helium generation, void swelling, irradiation creep, embrittlement, etc. Most currently available specimens in the NSUF Nuclear Fuels and Materials Library (NFML) are relatively small in size with the exception of a few specimens produced from AISI 304.

Project Description

For activities such as training of students, development of new microstructural and microchemical interrogation techniques, or exploration of various degradation mechanisms on LWR-relevant material, the NSUF NFML contains rather large singleheat volumes of AISI 304 stainless steel of the appropriate vintage and technology. These cover a wide, wellcharacterized range of temperature, dose, dose rate and helium levels. Specimens range from forearm-sized blocks and fist-sized chunks, inchthick plates, cm-size cubes, mm-thick plates to smaller sizes such as 3 mm-diameter microscopy disks. Most importantly, a number of published studies have been conducted on these materials so that, in new studies, the researchers will know in advance the microstructural and microchemical characteristics of their specimens, as well as their exposure doses, temperatures, helium content, radioactivity levels and radioisotope content.

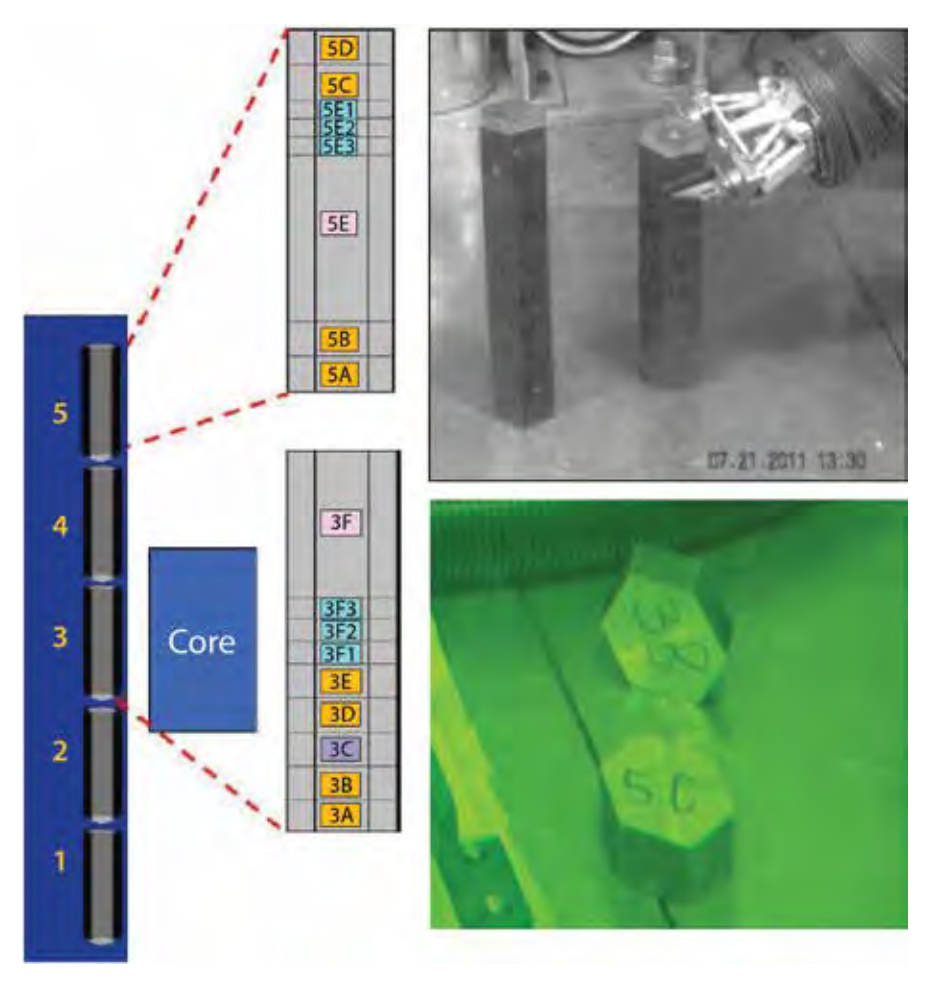


Figure 1. Schematic diagram of the U9807 assembly and its relationship to the EBR-II fueled core. The core is 30 cm tall so Block 3 is the only one fully within the elevation range of the core. Also shown are the two blocks chosen for extensive evaluation at Westinghouse—Block 3 below and above—with the first stage of destructive examination being the production of hex-coins with thicknesses of either 1.2 or 2.5 cm. The mid-block exposures of 3 and 5 were ~30 dpa and ~2.5 dpa, respectively.

These AISI 304 materials were retrieved from the Idaho National Laboratory (INL) Experimental Breeder Reactor II (EBR-II) near Idaho Falls. As shown in Figure 1, the EBR-II fast reactor Row 8 reflector assembly designated U9807 comprised a stack of six hexagonal cross-section blocks (hex-blocks), with sodium flowing outside the wrapper duct (hex-can)

and also flowing in the gaps between the outer surface of the hex-blocks and the inner surfaces of the hex-can. There are both radial and axial variations in temperature and neutron exposure in these blocks, determined by ambient coolant temperature and gradients in gamma heating within the block.

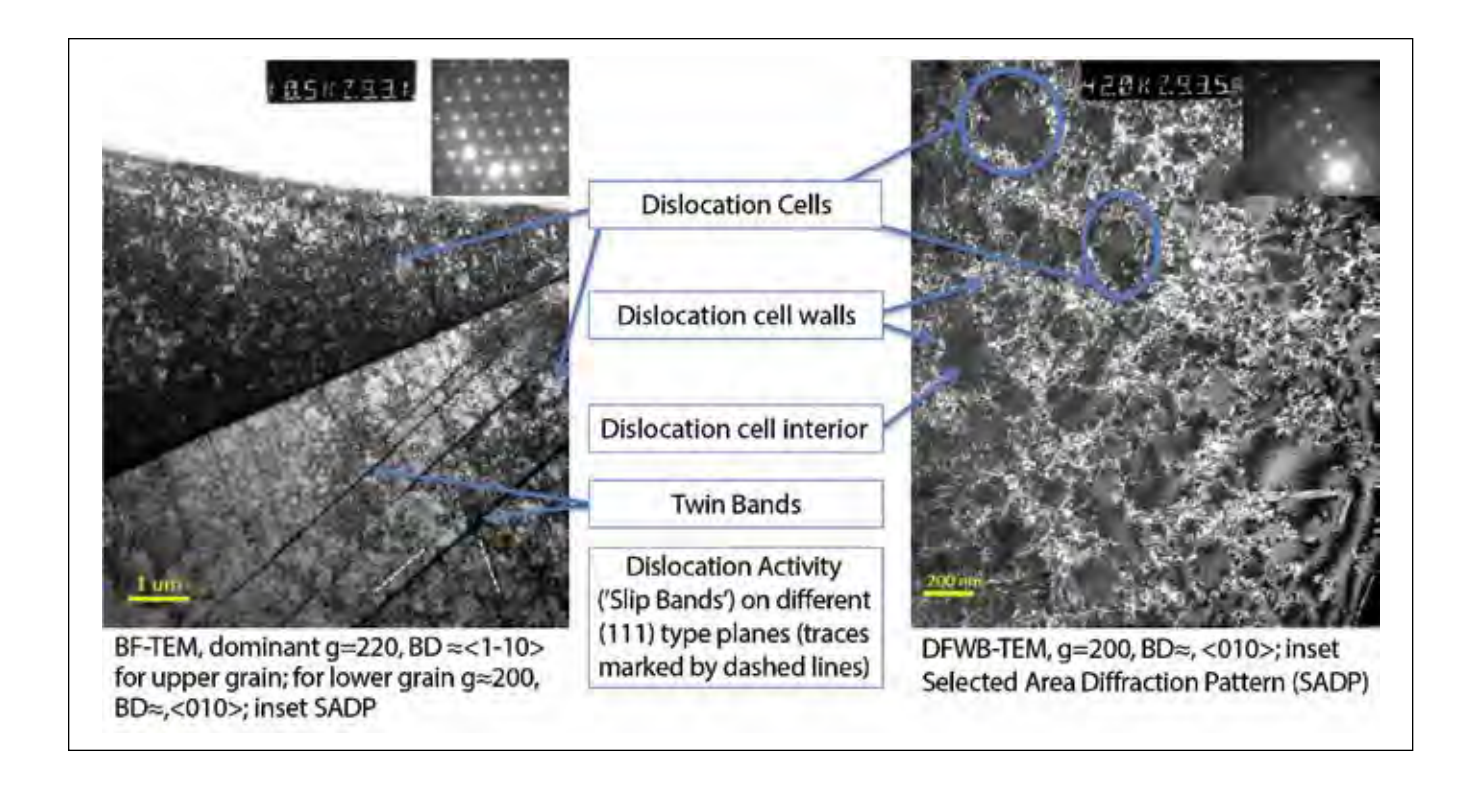


Figure 2. Cold-worked microstructure of an archive block, showing deformation-induced twin bands and dislocation cells existing prior to irradiation.

As shown in Figure 2 the as-produced microstructure of the blocks is typical of \sim 5% cold-working, all traces of which disappear during irradiation. Most importantly, this Row 8 reflector assembly operated over the range of dpa rates that are characteristic of the baffle-former assembly of pressurized water reactors (PWRs).

With the exception of the discarded, much longer (395.3 mm) Block 1, located far below the core, each of the four hex-blocks in the NSUF NFML had initial dimensions of 52.2 mm flat-to-flat cross-sectional thickness and a length of either 217.5 (for Blocks 5 and 6) or 243.3 mm (Blocks 2,3,and 4). Block 6 was also discarded and is not in the NFML. Blocks 2–5 are currently maintained in the NSUF

NFML, with Blocks 2 and 4 located at INL in fully intact form, with profilometry data available to describe their dimensional changes.

Blocks 3 (mid-core) and 5 (far abovecore) were shipped to the Westinghouse hot cells in Pittsburgh and have since been extensively sectioned into smaller segments with a wide range of sizes and geometries. Large portions of both blocks still remain in Pittsburgh, but various subsets of smaller specimens have been shipped to several national laboratories, to the Center for Advanced Energy Studies (CAES) and a number of universities. Some of these previously shipped specimens have been tested to destruction, but others remain intact at Westinghouse or their current location for further use or for shipment to other laboratories.

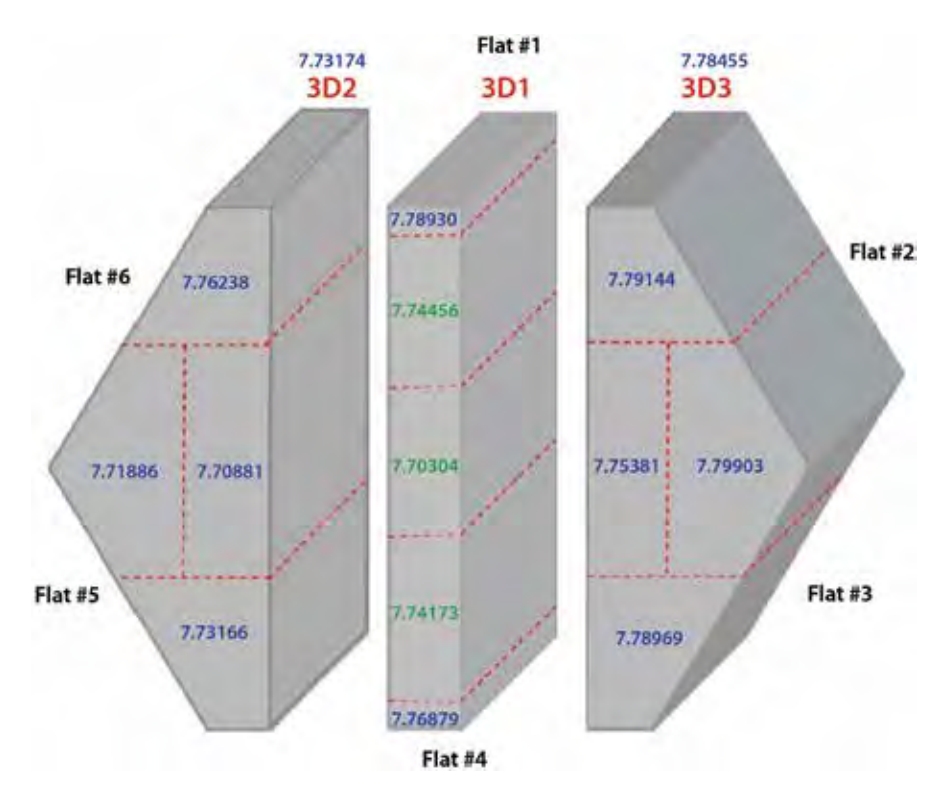


Figure 3. Second stage of cutting after ultrasonic and density measurements were completed on the three-dimensional hex-coin, with measured densities of each piece shown. Slice 3D1 is an iso-dose (28 dpa) strip such that the only variable is the temperature which peaks near the center. Both microscopy and density measurements confirm that void swelling peaks in the center of the strip. The NSUF inventory contains a number of intact, uncut coins.

Previous studies on hex blocks have involved the University of Wisconsin, University of Michigan, Boise State University, University of Pittsburg, Massachusetts Institute of Technology, Texas A&M, Purdue University, CAES, Electric Power Research Institute, MicroXact Inc., Radiation Effects Consulting, LLC, INL, Oak Ridge National Laboratory, Pacific Northwest National Laboratory, as well as two Japanese entities, the University of Tokyo and Nuclear Fuel Industries-Osaka. A wide range of mechanical, microstructural, microchemical, and dimensional studies have been conducted by these groups. Results of these studies are available to guide the definition and interpretation of new studies, and are listed below. Other publications are in preparation. Currently ongoing studies include

welding-induced crack formation, scanning electron microscopy of deformation-induced phase stability, laser and acoustic interrogation of radiation-induced microstructure, non-linear ultrasonic testing of microstructure, and subsequent ion irradiation on neutron-preconditioned specimens. A full description of the available specimen inventory and current location of each specimen can be found on the NSUF website.

Accomplishments

In typical PWRs, the structural components range from \sim 2–4 cm in thickness and experience significant gradients in neutron-flux spectra, dpa, temperature, and helium generation, potentially producing complex internal distributions in void swelling. The development of new experimental

Highest dpa rate on faces 5-6

Coolant temperature increasing

100

150

Figure 4. Average throughthickness swelling determined between flats 1 and 4 of Block 3 using time-of-flight ultrasonic measurements. Dotted lines indicate the cutting locations that will be used later to produce the 2.5-cm-thick hex coins.

50

techniques involving ultrasonic or laser interrogation will require similarly thick materials. Likewise studies on welding or corrosion are best conducted using thick specimens. Other studies on mechanical properties or physical properties are better studied using thinner specimens. The current hex-block specimen inventory covers this full range of sizes.

Before sectioning of the two blocks at Westinghouse, each was extensively measured using non-destructive profilometry techniques to assess carbide-induced shrinkage, void-induced swelling, and block bending. Non-destructive time-of-flight ultrasonic measurements were then used to identify the average levels of void swelling and carbide precipitation across opposing flats of the two blocks. The first round of cutting to produce 0.5 and 1.0 inch thick "hex-coins" was followed by density measurements and more ultrasonic

measurements across the new cut faces. Subsequent sectioning of the hex-coins was followed by additional density measurements and the production of specimens for measurement of various mechanical and physical properties, microstructure and microchemistry. Figure 3 provides an example of the second stage of cutting of one coin, to be followed later by cutting of smaller specimens for microscopy, shear punch, and other tests.

200

250

The original major goal of the hexblock program was to demonstrate that ultrasonic measurements could be used to assess the internal distribution of void swelling and carbide densification in thick components. It was successfully demonstrated that ultrasonic measurements were in full agreement with density-change and microscopy measurements. Some examples of these results are shown in Figures 4-6.

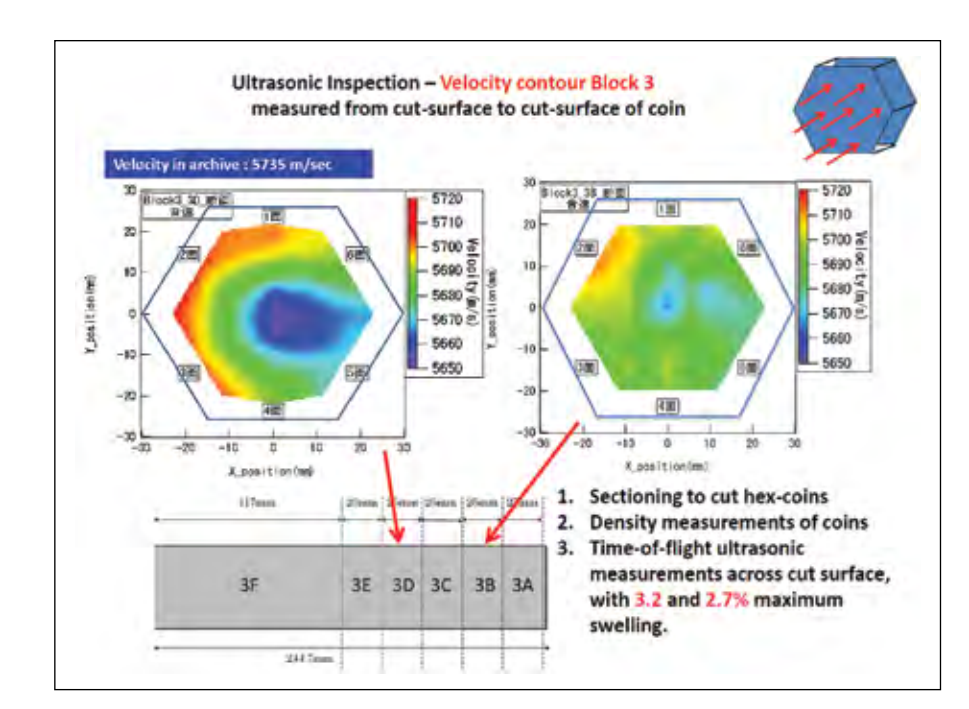


Figure 5. Time-of-flight measurements of internal swelling distribution in two Block 3 hex-coins. Coin 3D experienced both higher dose and temperature compared to coin 3B. The asymmetry of swelling is the consequence of a gradient in gamma heating rate, moving from right to left.

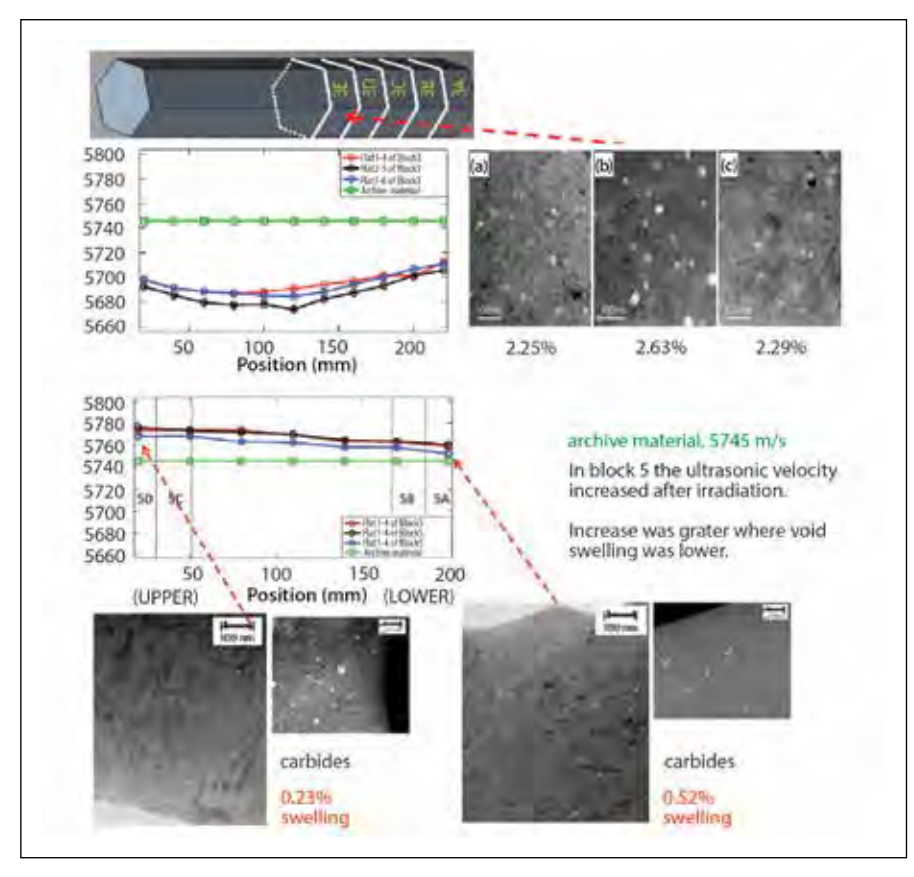


Figure 6. Time-of-flight throughthickness measurements showing the effect of competing effects of carbide densification and void swelling in high-dose Block 3 and low-dose Block 5. Carbide precipitation increases the flight time while void swelling decreases it. Swelling peaks in the hotter center of Block 3.

Publications

- [1.] J. Etoh, M. Sagisaka, T. Matsunaga, Y. Isobe, F. A. Garner, P. D. Freyer, Y. Huang, J. M. K. Wiezorek, T. Okita, "Development of a nondestructive inspection method for irradiation-induced microstructural evolution of thick 304 stainless steel blocks", J. Nucl. Mater., 440 (2013) 500-507.
- [2.] Y. Isobe, J. Etoh, M. Sagisaka, T. Matsunaga, P. D. Freyer, F. A. Garner, T. Okita, "Using UT to assess neutron-induced damage", Nuclear Engineering International, April 24, 2014, 36-39.
- [3.] F. A. Garner, P. D. Freyer, D. L.
 Porter, J. Wiest, C. Knight, T. Okita,
 M. Sagisaka, Y. Isobe, J. Etoh, T.
 Matsunaga, Y. Huang, J. Wiezorek,
 "Void swelling and resultant
 strains in thick 304 stainless steel
 components in response to spatial
 gradients in neutron flux-spectra
 and irradiation temperature",
 Proceedings of 16th International
 Conference on Environmental Degradation of Materials in
 Nuclear Power Systems Water
 Reactors, 2013, in CD format, no
 page numbers.
- [4.] F. A. Garner, "Assessment of the swelling equation used for predict swelling of AISI 304 stainless steel in LWR and LMR environments" Proceedings of 16th International Conference on Environmental Degradation of Materials in Nuclear Power Systems Water Reactors, 2013, in CD format, no page numbers.

- [5.] F. A. Garner, T. Okita, Y. Isobe, J. Etoh, M. Sagisaga, T. Matsunaga, P. D. Freyer, Y. Huang, J.M.K. Wiezorek, D. L. Porter, "Measurement of void swelling in thick non-uniformly irradiated 304 stainless steel blocks using nondestructive ultrasonic techniques ", Proceedings of Fontevraud 8 Contributions of Materials Investigations and Operating Experience to LWR's Safety, Performance and Reliability, Avignon, France, 2014.
- [6.] T. Okita, J. Etoh, M. Sagisaka, T. Matsunaga, Y. Isobe, P. D. Freyer, J. M. K. Wiezorek, F. A. Garner, "Validation of ultrasonic velocity measurements in first wall structural materials", Fusion Science and Technology 66 (2014) 77-82.
- [7.] J. Etoh, M. Sagisaka, T. Matsunaga, Y. Isobe, T., "A simulation model of ultrasonic wave changes due to irradiation-induced microstructural evolution of thick 304 stainless steel blocks", Journal of Nuclear Materials 441 (2013) 503–509.
- [8.] E. M. Rabenberg, B. J. Jaques, B.H. Sencer, F. A. Garner, P. D. Freyer, T. Okita, D. P. Butt, "Mechanical behavior of AISI 304SS determined by miniature test methods after neutron irradiation to 28 dpa,", J. Nucl. Mater. 448 (2014) 315-324.
- [9.] J.M.K. Wiezorek, Y. Huang, F.A. Garner, P.D. Freyer, M. Sagisaka, Y. Isobe, T. Okita, "Transmission Electron Microscopy of 304-type

- Stainless Steel after Exposure to Neutron Flux and Irradiation Temperature Gradients, Proceedings of Microscopy & Microanalysis 2014, Hartford, CT, August 3-7, 2014, pp. 1822-1823.
- [10.] Y. Huang, J.M.K. Wiezorek, F. A. Garner, P. D. Freyer, T. Okita, M. Sagisaka, Y. Isobe, T. R. Allen, "Microstructural characterization and density change of 304 stainless steel reflector blocks after long-term irradiation in EBR-II", J. Nucl. Mater, 465 (2015) 516-530.
- [11.] Y. Dong, B. H. Sencer, F. A. Garner, E. A. Marquis, "Microchemical and microstructural evolution of AISI 304 stainless steel irradiated in EBR-II at PWR-relevant dpa rates", J. Nucl. Mater. 467 (2015) 692-702.

- [12.] V.I. Pastukhov, S. . verin, V.L. Panchenko, I. . Portnykh, P.D. Freyer, L.A. Giannuzzi, F. . Garner, "Application of backscatter electrons for large area imaging of cavities produced by neutron irradiation", J. Nucl. Mater. 480 (2016) 289-300.
- [13.] K. Mao, P. D. Freyer, L. A. Giannuzzi, J. K. Tatman, F. C. Gift, F. A. Garner, J. P. Wharry, "Microstructure evolution of laser weld repairs of 304SS at high dose ion irradiation", Proceedings of Fontevraud 9 Contributions of Materials Investigations and Operating Experience to Light Water NPPs' Safety, Performance and Reliability, Avignon, France, 2018.

Distributed Partnership at a Glance		
NSUF and Partners	Facilities and Capabilities	
Westinghouse	Materials Center of Excellence (MCOE) Laboratories	
Collaborators		
Radiation Effects Consulting	Frank Garner (principal investigator)	
Westinghouse	Paula Freyer (principal investigator)	

Disc Irradiation for Separate Effects Testing (DISECT) with Control of Temperature

Walter Williams – Purdue University – will1793@purdue.edu Maria Okuniewski – Purdue University – mokuniew@purdue.edu

The DISECT project includes the design and fabrication of a uniquely instrumented, separate effects testing vehicle; specimen fabrication and pre-characterization; irradiation; and post-irradiation examination to enable a more comprehensive understanding of in-pile phenomena.

s modern advanced reactors, such as those proposed within the Versatile Test Reactor and the Advanced Fuel Cycle programs, envision the use of metallic fuels, there is renewed interest in examining these fuel systems in order to comprehensively understand in-pile fuel behavior and maximize fuel performance while maintaining fuel integrity in a stable and predictable manner. Metallic fuels and materials require immediate and extensive testing that expands upon the historical knowledge amassed over decades [1-4] in order to provide a more fundamental and scientific understanding of metallic fuels, assess their material performance, and to validate models. Investigation into the fundamental, nano- and microscale phenomena that impact bulk fuel behavior is critical to the understanding of future fuel systems and reactor development. Historical hindrances to

this effort included convoluted experimental parameters that are challenging to isolate during neutron irradiation, such as temperature, alloy composition, and power rate. These variable experimental conditions are compounded by the coexistence of various in-pile phenomena, such as constituent redistribution, swelling, and fuel/cladding chemical interaction. Separate effects testing has the ability to isolate these parameters and competing phenomena within single irradiation campaigns of relatively short duration.

Uranium-zirconium (U-Zr) and uranium-molybdenum (U-Mo) are the two most-commonly utilized and historically studied metallic fuel systems that are also under consideration for advanced reactor use. To address the aforementioned gaps that exist within the metallic fuel body of knowledge, these two metallic fuels will be irradiated utilizing a separate-

effects approach to isolate alloy composition, irradiation temperature, burnup, and power. This investigation is termed the Disc Irradiation for Separate Effects Testing with Control of Temperature (DISECT) project. The research involves a collaborative effort with the Studiecentrum voor Kernenergie, Centre d'Étude de l'énergie Nucléaire (SCK • CEN) in Mol, Belgium and the Nuclear Science User Facilities (NSUF) utilizing capabilities at Idaho National Laboratory, Purdue University, and the Belgian Nuclear Research Center. In order to improve the mechanistic understanding of fuel behavior and performance. This international collaboration will be a first-of-a-kind NSUF experiment that will conduct irradiations in the Belgian Reactor 2 (BR2), located at SCK • CEN and shown in Figure 1, that have been designed, fabricated, and characterized at U.S. facilities (i.e., INL and Purdue University).

Project Description

The DISECT project includes the design and fabrication of a uniquely instrumented, separate effects testing vehicle; specimen fabrication and pre-characterization; irradiation; and post-irradiation examination

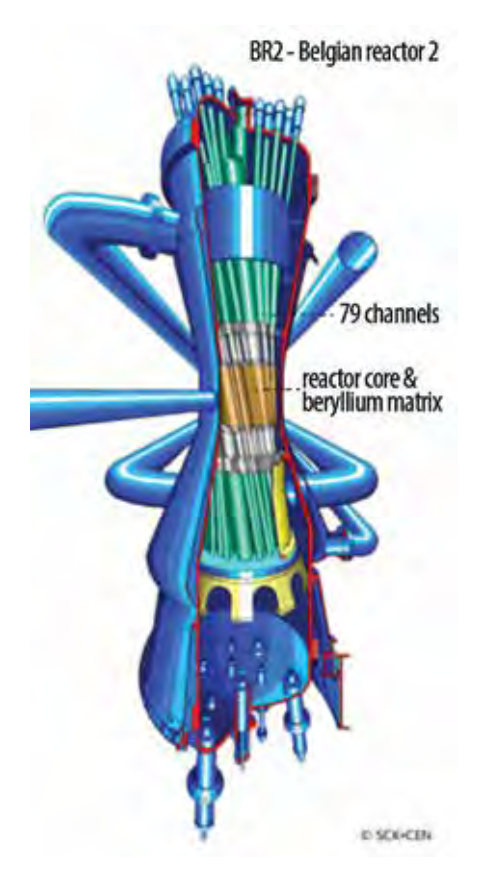
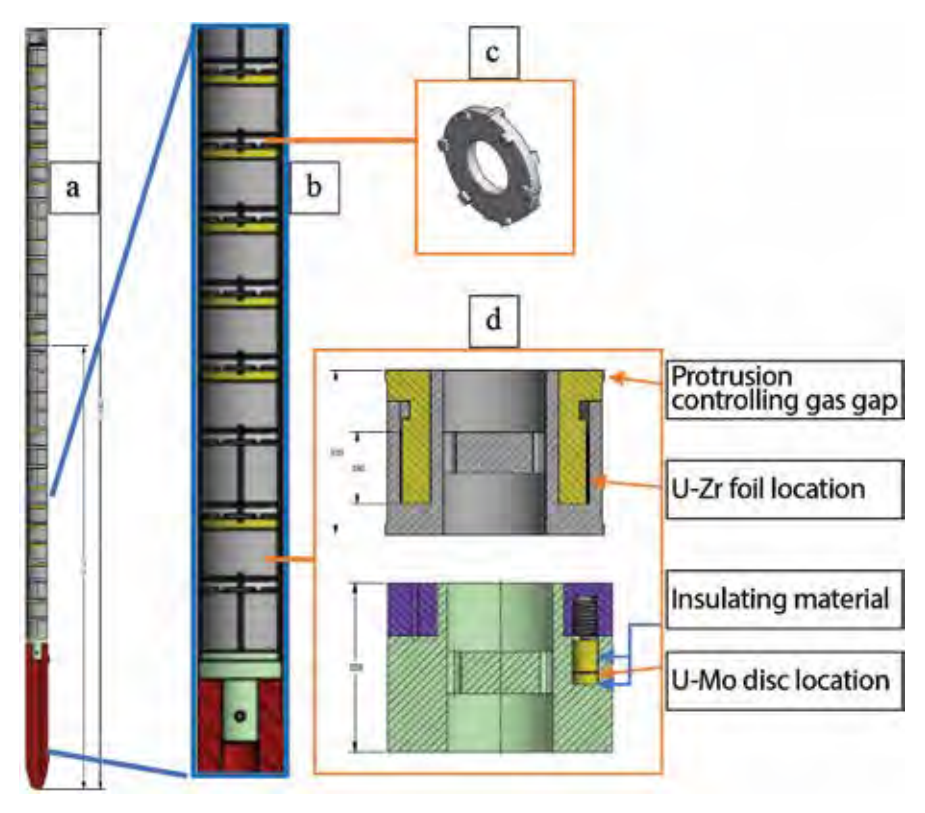


Figure 1. Cutaway illustration of the BR2 reactor. The hyperboloidal arrangement of the 79 channels provides a closely arranged core while retaining a large working space on the extremities. This feature is exceptional for the insertion of complex and instrumented vehicles [5].

Figure 2. a) In-core portion of the test vehicle. b) Enlarged section of vehicle illustrating the stack-up of specimen holders separated by insulators. c) Insulators utilizing gas gaps to isolate specimen holders. d) Specimen holders for the U-Zr alloy foils (top) and the U-Mo alloys disks (bottom).



to enable a more comprehensive understanding of in-pile phenomena. The instrumented in-pile irradiation vehicle designed for insertion into BR2 is shown in Figure 2. The test vehicle is comprised of an outer capsule that serves as the housing for individual fuel samples and customizable instrumentation, such as thermocouples or other developmental in-pile instrumentation requiring testing. The in-core portion of the device is shown in Figure 2 (label a).

A unique aspect of the device is the customizable internals that keep individual samples isolated from one another in sealed sample enclosures separated by insulators that utilize gas

gaps to isolate thermal effects from adjacent specimens, shown in Figure 2 (label b and c). This allows for in-pile conditions, such as atmosphere, temperature, composition, geometry, and power, to vary between samples in a single device. Such a device is able to provide the unique capability to target various phenomena of interest on a per sample basis. It also has the ability to be implemented for future work without a large-scale redesign or qualification. Figure 2 (label d) shows the sample enclosures for the U-Zr alloy foils (top) and the U-Mo alloys disks (bottom).

Low-enriched (19–20% weight U-235) U-Mo and U-Zr alloys of varying compositions were selected as the alloy compositions for this

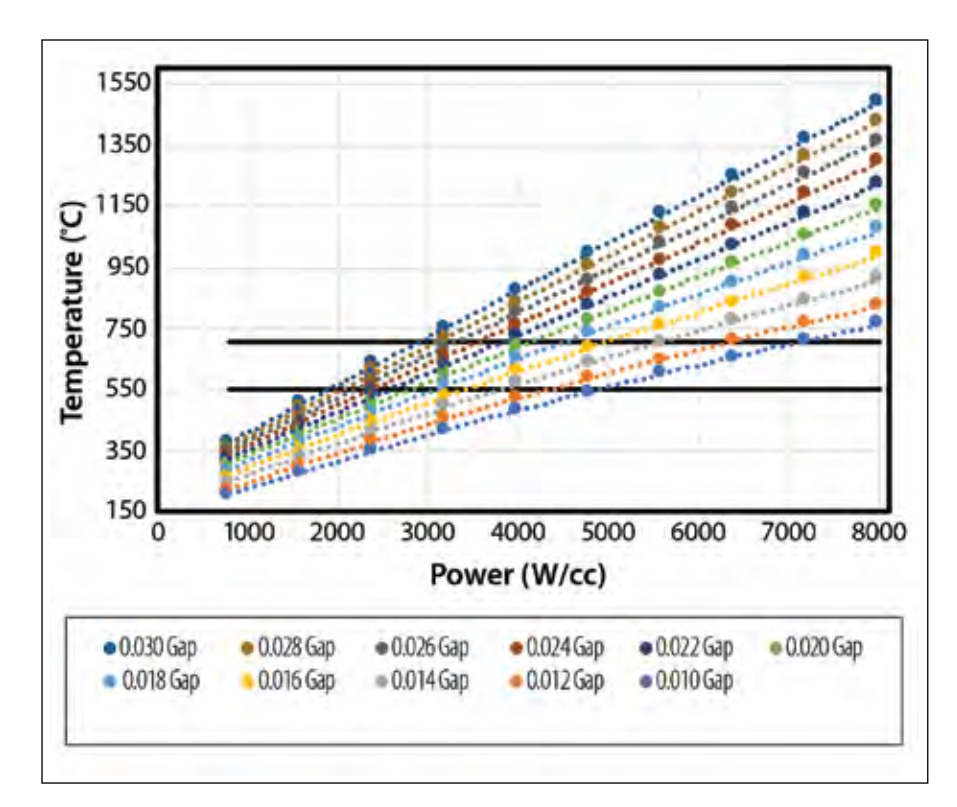


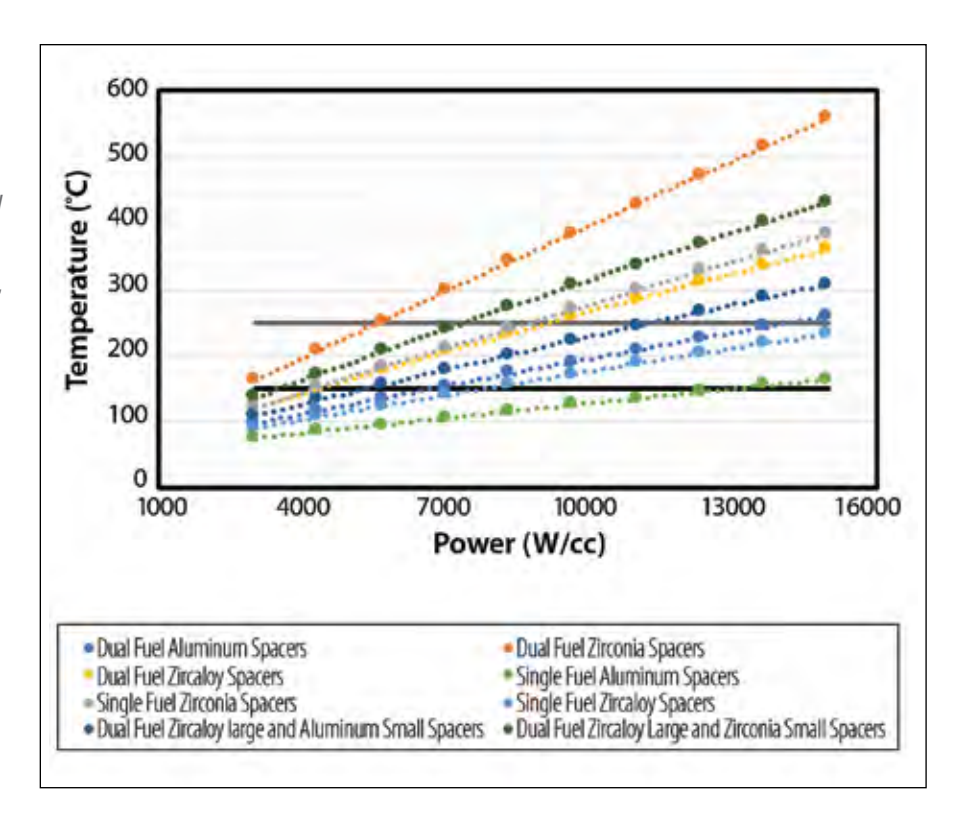
Figure 3. U-Zr foil temperature as a function of power for 1.5 W/g gamma heating. The black horizontal lines represent target specimen irradiation temperatures. The gap refers to the gas gap between specimen holder and vehicle wall in inches.

experiment. Fuel compositions for U-Mo include 7, 10, and 12 weight percent Mo, fabricated as discs (3 mm in diameter and 250 μ m in height). The compositions for U-Zr include 6, 10, 20, and 30 weight percent Zr, fabricated as foils (180 μ m thick, 72.75 mm long, and 8.9 mm wide), with the first irradiation including only U-10Zr and U-30Zr.

The U-Zr foil specimen holder design allows for a discrete sample temperature to be obtained by varying the insulating gas gap between the holder and vehicle wall. This feature allows for otherwise identical fuel samples to reach different temperatures without modifications to power, specimen geometry, alloy composition, or enrichment. Figure 3 indicates the ideal gas gap required for a target temperature and a given power.

In contrast, the desired irradiation temperature for the U-Mo discs is obtained by optimizing the spacer material surrounding the specimens with varying thermal conductivities to obtain desired irradiation temperatures. This method allows for higher power densities to be achieved at lower temperatures due to the contact of the specimen holder with the outer wall

Figure 4. U-Mo disc temperature as a function of power for 1.5 W/g gamma heating. The black horizontal lines represent target specimen irradiation temperatures. Various materials are considered for spacers, including aluminum, zirconia, and zircaloy, to achieve the desired irradiation temperatures.



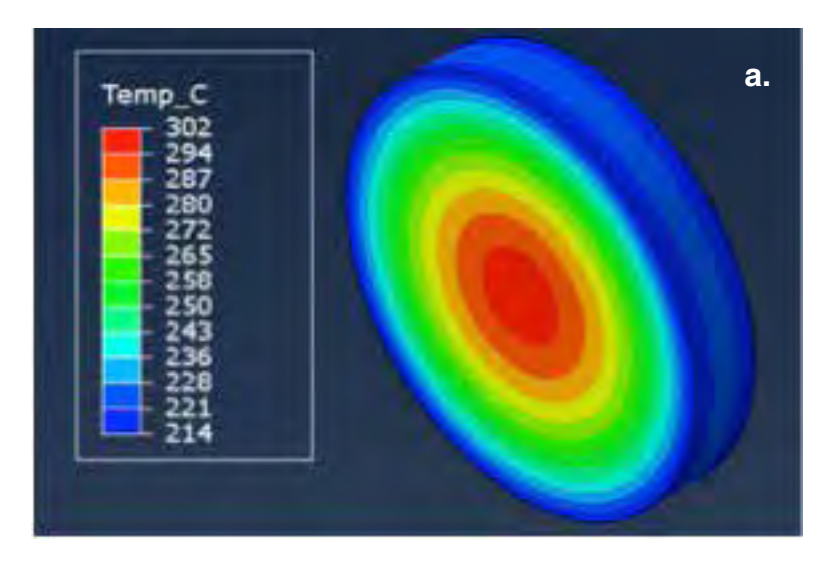
of the irradiation vehicle. This contact is ensured by the use of ball detents on the side of the specimen holder opposite the specimens. Figure 4 shows the optimization of desired irradiation temperatures for the U-Mo alloys with varying powers and spacer materials.

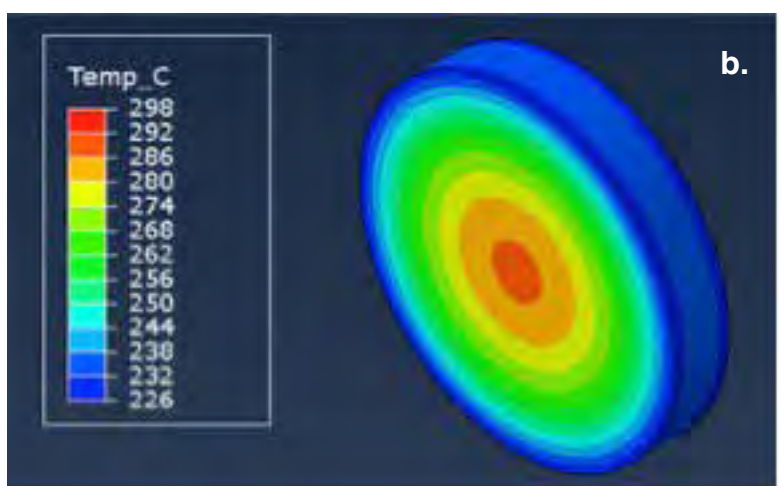
Accomplishments

A Phenomenon Identification and Ranking Table (PIRT) analysis was performed on both fuel systems to identify the phenomena to investigate and select the in-pile parameters to isolate. Following the PIRT findings, the DISECT project has completed the design review (INL) and the first stage of the committee for the evaluation of experiments for reactor insertion (SCK • CEN). The preliminary neutronics, preliminary thermal analysis, fuel fabrication, and precursory characterization of the U-Zr and U-Mo alloys were

completed in FY 2018. Detailed thermal models are shown in Figure 5 for both the U-Mo disc and the U-Zr foil. These models were built with ABAQUS (v. 6.14-2) and using nominal neutronics information for the estimated insertion cycle. This model will be used to guide the specific irradiation-temperature conditions for post-irradiation characterization. Moreover, these localized models allow for discrete identification and, thus, a further understanding of phenomena such as constituent redistribution, porosity growth, fuel polygonization, and fission-gas superlattice formation as functions of temperature and/or power.

The fuel was fabricated at INL based on thermal and neutronics calculations and designs. Preliminary characterization has been conducted on both the U-Zr and U-Mo alloys.





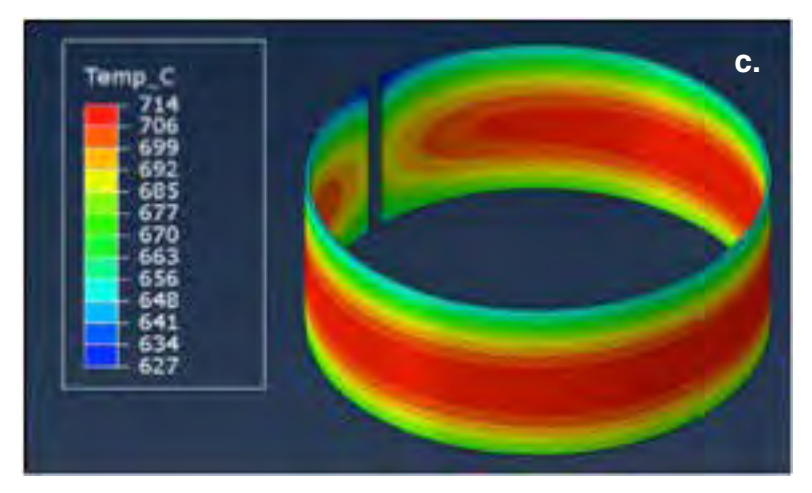
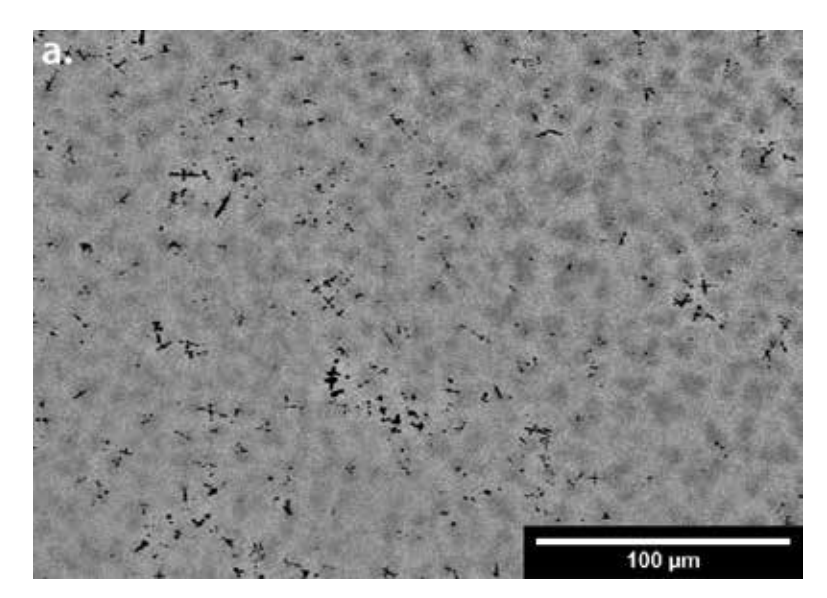


Figure 5. The estimated cost at INL for installation is \$200K which should be the expected cost at other labs

Metallic fuels and materials require immediate and extensive testing that expands upon the historical knowledge amassed over decades in order to provide a more fundamental and scientific understanding of metallic fuels, assess their material performance, and to validate models.



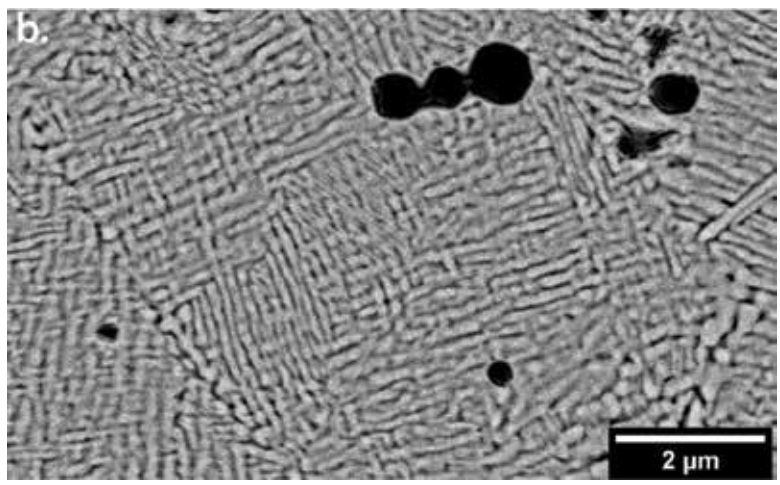


Figure 6. Scanning electron microscopy backscatter micrograph of U-Zr samples following fabrication from an (a) as-cast and (b) rolled and annealed foil. The dark regions are Zr-rich while the light regions are U-rich.

Figure 6 (label a) shows the as-cast microstructure of U-10Zr, which exhibits in-solution variation of U and Zr content. Figure 6 (label b) shows the rolled and annealed U-10Zr alloy exhibiting a typical lamellar microstructure. The irradiation-vehicle fabrication is currently underway. An example of a U-Zr foil that is loaded into a Zr specimen holder is pictured in Figure 7.

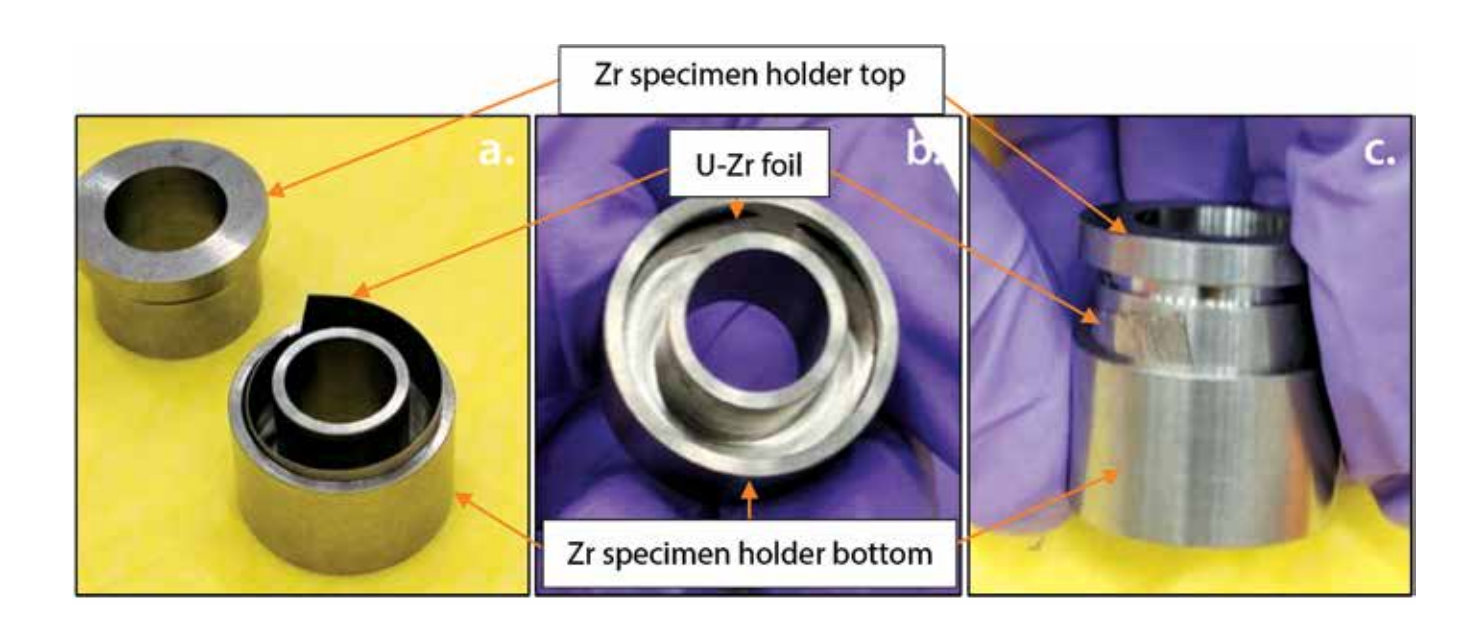
Future Activities

The irradiation vehicle is slated for irradiation in the BR2 reactor in the

fall of 2019. Prior to this, multiple awarded rapid-turnaround experiments (RTEs) are scheduled. These RTEs include in situ neutron-diffraction experiments to investigate texture, crystallography, and microstrain evolution, as well as phase transitions during thermal cycling. Following this experiment, in situ thermal treatments during transmission electron microscopy will be carried out on identical samples to investigate phase-transformation kinetics. This pre-irradiation characterization will provide a reference point for the post-irradiation characterization of this fuel, as well as provide a more in-depth understanding of the crystallography and kinetics of the U-Zr and U-Mo fuel systems.

Publications

- [1.] M.K. Meyer, J. Gan, J.F. Jue, D.D. Keiser, E. Perez, A.B. Robinson, D.M. Wachs, N. Woolstenhulme, G.L. Hofman, Y.S. Kim, "Irradiation performance of U-Mo monolithic fuel," Nucl. Eng. Technol. Vol. 46 (2014), pp. 169–182.
- [2.] S. van den Berghe, P. Lemoine, "Review of 15 years of high-density lowenriched UMo dispersion fuel development for research reactors in Europe," Nucl. Eng. Technol. Vol. 46 (2014), pp. 125–146.
- [3.] D.E. Janney, S.L Hayes, "Experimentally Known Properties of U-10Zr Alloys: A Critical Review," Nucl. Technol. Vol. 203 (2018), pp. 109–128.
- [4.] G.L. Hofman, L.C. Walters, T.H. Bauer, "Metallic fast reactor fuels," Prog. Nucl. Energy. Vol. 31 (1997), pp. 83–110.
- [5.] SCK-CEN, BR2 refurbishment operation, (2019) http://science.sckcen.be/en/News/20150325_BR2_refurbishment.



Distributed Partnership at a Glance		
NSUF and Partners	Facilities and Capabilities	
Center for Advanced Energy Studies	Microscopy and Characterization Suite	
Idaho National Laboratory	Fuels and Applied Sciences Building, Experimental Fuels Facility, and Electron Microscopy Laboratory	
Purdue University	Interaction of Materials with Particles and Components Testing (IMPACT) Experimental Facility	
SCK•CEN	Belgian Reactor 2	
Collaborators		
Idaho National Laboratory	Cody Hale (collaborator), Daniel Wachs (co-principal investigator), Mike Sprenger (collaborator), Tom Maddock (collaborator)	
Purdue University	Maria Okuniewski (co-principal investigator), Walter Williams (co-principal investigator)	
SCK•CEN	Ann Leaners (collaborator), Emre Sikik (collaborator), Geert Van den Branden (collaborator), Gitte Borghmans (collaborator), Patrice Jacquet (collaborator), Steven Van Dyck (collaborator), Sven van den Berghe (co-principal investigator)	

Figure 7. (a) Loading of a U-10Zr fuel foil into the Zr specimen holder. (b) U-Zr foil placed in bottom of specimen holder. (c) Holder top inserted prior to being welded shut for atmospheric containment. (Foil protrusion shown for visualization only.)

NSUF LIST OF ACRONYMS

APSAdvanced Photon Source
APT Atom Probe Tomography
ATR Advanced Test Reactor
BMG bulk metallic glass
BR2Belgian Reactor 2
CAES Center for Advanced Energy Studies
CINRConsolidated Innovative Nuclear Research
CRPCu-rich precipitate
DBHdispersed barrier hardening
DISECT Disc Irradiation for Separate Effects Testing with Control of Temperature
DOE Department of Energy
dpadisplacements per atom
DTRADefense Threat Reduction Agency
EBR-II Experimental Breeder Reactor II
ECP element contact profilometer
EDS energy dispersive spectroscopy
EELSElectron Energy Loss Spectrometer
EMLElectron Microscopy Laboratory
EPMA Electron Probe Micro-Analyzer
EPRI Electric Power Research Institute
F/M ferritic/ martensitic
FCCI fuel-cladding chemical interaction
FFT Fast Fourier Transform
FIBFocused Ion Beam
FSWfriction stir welded
HEDM High-Energy X-Ray Diffraction Microscopy

HFEF Hot Fuel Examination Facility
IMCL Irradiated Materials Characterization Laboratory
INLIdaho National Laboratory
IVEMIntermediate Voltage Electron Microscope
IYNCInternational Youth Nuclear Congress
JOGjoint oxyde-gaine
KAM Kernel Average Misorientation
LAMDALow Activation Materials Development and Analysis
LANLLos Alamos National Laboratory
LEAPLocal Electrode Atom Probe
LWRlight water reactor
MaCSMicroscopy and Characterization Suite
MFC Materials and Fuels Complex
MITR Massachusetts Institute of Technology Reactor
MMLC multimetallic layered composite
MNSPMn-Ni-Si precipitate
MOX mixed oxide
NE Office of Nuclear Energy
NEETNuclear Energy Enabling Technologies
NEUPNuclear Energy University Program
NFAnanostructured ferritic alloy
NIFS National Institute for Fusion Science
NITEnano infiltration transient eutectic ceramic
NSUF Nuclear Science User Facilities
ODSoxide dispersion strengthened
ORNI Oak Ridge National Laboratory



PALSpositron annihilation lifetime spectroscopy
PASpositron annihilation spectroscopy
PFCplasma-facing components
PGSPrecision Gamma Scanner
PIprincipal investigator
PIEpost-irradiation examination
PIRTPhenomenon Identification and Ranking Table
PNNLPacific Northwest National Laboratory
PPMSPhysical Property Measurement System
RISradiation-induced segregation
RTE Rapid Turnaround Experiment
RPVreactor pressure vessels
SANSsmall-angle neutron scattering
SAXsmall-angle X-ray scattering
SCCstress corrosion cracking

SEMScanning Electron Microscope
SFR Sodium-cooled Fast Reactor
SiC silicon carbide
SSPAShielded Sample Preparation Area
STEM scanning transmission electron microscopy
TEMTransmission Electron Microscope
TRISOtristructural-isotropic
UCSB University of California, Santa Barbara
ULTRAULtrasonic TRAnsducer
U-MoUranium-Molybdenum
U-ZrUranium-Zirconium
UTultrasonic thermometer
WAXSwide-angle X-ray scattering
XRDX-ray diffraction
7rN Zirconium nitrida

NSUF INDEX

NSUF & Partner Institutions: Facilities & Capabilities

Argonne National Laboratory (ANL): 10, 11, 34, 35, 37, 38, 39, 40, 42, 44, 45, 101, 103, 130, 132

Argonne National Laboratory: The Intermediate Voltage Electron Microscopy (IVEM) — Tandem Facility, 44,103,128,130,132

Argonne National Laboratory's: Advanced Photon Source (APS), 98, 99,101, 103,128

Australian Nuclear Science and Technology Organisation: 65

Boise State University: 11, 34, 42, 89, 115

Brookhaven National Laboratory (BNL): 10,35,36,39,42,45,65,130

Brookhaven National Laboratory: National Synchrotron Light Source II, 130

Center for Advanced Energy Studies (CAES): 10, 25, 26, 27, 34, 36, 37, 39, 40, 41, 42, 44, 45, 89, 101, 103, 114, 115, 127, 128, 130

Center for Advanced Energy Studies (CAES): Microscopy and Characterization Suite (MaCS), 23, 25, 26, 89, 103, 127, 128, 130

General Atomics: 11, 42, 83

Idaho National Laboratory (INL): 2, 4, 5, 6, 7, 10, 11, 12, 13, 18, 19, 20, 21, 25, 26, 28, 34, 35, 36, 37, 39, 40, 41, 42, 43, 44, 45, 46, 47, 51, 52, 65, 66, 68, 72, 73, 74, 75, 89, 101, 103, 104, 106, 111, 112, 113, 114, 115, 121, 124, 125, 127, 128, 129, 130, 132

Idaho National Laboratory: Advanced Test Reactor (ATR), 12, 21, 34, 45, 51, 52, 54, 65, 73, 74, 86, 90, 100, 103, 128, 130

Idaho National Laboratory: Analytical Laboratory (AL), 130

Idaho National Laboratory: Electron Microscopy Laboratory (EML), 20, 21, 101, 127, 128, 130

Idaho National Laboratory: Experimental Fuels Facility, 127

Idaho National Laboratory: Fuels and Applied Sciences Building (FASB), 127, 130

Idaho National Laboratory: Gamma Irradiation Test Loop, 130

Idaho National Laboratory: Hot Fuel Examination Facility (HFEF), 2, 12, 15, 106, 111, 128, 130

Idaho National Laboratory: Irradiated Materials Characterization Laboratory (IMCL) Facility, 3, 12, 13, 14, 15, 16, 17, 21, 26, 101, 103, 128, 130

Illinois Institute of Technology: 10, 103, 130

Illinois Institute of Technology: Materials Research Collaborative Access Team (MRCAT), 90, 101, 103, 130

Lawrence Livermore National Laboratory (LLNL): 10, 130

Lawrence Livermore National Laboratory: Center for Accelerator Mass Spectrometry, 130

Los Alamos National Laboratory (LANL): 10, 11, 21, 36, 39, 40, 41, 64, 103, 128, 130, 132,

Los Alamos National Laboratory: Chemical and Metallurgical Research Facility (Wing 9), 130

Los Alamos National Laboratory: Lujan Center at Los Alamos Neutron Science Center (LANS), 130

Los Alamos National Laboratory: Plutonium Surface Science Laboratory, 130

Massachusetts Institute of Technology (MIT): 10, 11, 29, 35, 36, 39, 42, 44, 45, 47, 69, 72, 75, 89, 115, 128, 130, 132

Massachusetts Institute of Technology: Nuclear Reactor Laboratory, 75, 89, 130

North Carolina State University (NCSU): 10, 11, 35, 41, 44, 89, 101, 103, 130

North Carolina State University: PULSTAR Reactor Facility, 89, 103, 130

Oak Ridge National Laboratory (ORNL): 10, 11, 30, 31, 33, 34, 35, 36, 37, 39, 40, 41, 42, 44, 45, 48, 49, 76, 83, 101, 103, 115, 128, 130, 132, 133

Oak Ridge National Laboratory: Gamma Irradiation Facility, 130, 131

Oak Ridge National Laboratory: High Flux Isotope Reactor (HFIR) 79, 83, 130

Oak Ridge National Laboratory: Irradiated Materials Examination and Testing Facility (IMET) Hot Cells, 83

Oak Ridge National Laboratory: Low Activation Materials Design and Analysis Laboratory (LAMDA), 83, 101, 103, 128, 130

The Ohio State University (OSU): 10, 11, 34, 39, 40, 42, 47, 131

Pacific Northwest National Laboratory (PNNL): 11, 33, 36, 40, 48, 115, 129, 131



Pacific Northwest National Laboratory: Materials Science & Technology Laboratory (MSTL), 131

Pacific Northwest National Laboratory: Radiochemistry Processing Laboratory (RPL), 131

Purdue University: 10, 11, 36, 37, 41, 45, 115, 120, 121, 127, 131

Purdue University:

Interaction of Materials with Particles and Components Testing (IMPACT) experimental facility, 127, 131

Radiation Effects Consulting: 112, 115. 119

Sandia National Laboratories (SNL): 10, 36, 37, 44, 131

Sandia National Laboratories: Gamma Irradiation Facility, 131

Sandia National Laboratories: In-Situ Ion Irradiation Transmission Electron Microscope (13TEM) Facility, 131 Studiecentrum voor Kernenergie/ Centre d'Étude de l'énergie nucleaire (SCK CEN): 11,74, 121, 124, 126, 127

Texas A&M University (TAMU): 10, 11, 21, 45, 131

Texas A&M University: Accelerator Laboratory, 131

University of California, Berkeley (UCB): 10, 11, 34, 37, 39, 101, 103, 131, 132

University of California, Berkeley: Nuclear Materials Laboratory, 101, 103, 131

University of California, Santa Barbara (UCSB): 11, 34, 45, 52, 54, 55, 56, 58, 59, 60, 62, 63, 64, 65, 129, 132

University of Florida: 10, 11, 29, 34, 36, 37, 40, 42, 44, 48, 131, 132

University of Florida:

Nuclear Fuels and Materials Characterization Facility, 131

University of Illinois at Urbana-Champaign: 90, 103 University of Michigan (UM): 10, 11, 25, 26, 34, 40, 45, 55, 56, 65, 115, 131, 132

University of Michigan:

Michigan Ion Beam Laboratory, 24, 25, 131

University of Nevada, Las Vegas: 10, 131

University of Nevada, Las Vegas: University of Notre Dame: 11, 47, 84, 89

University of Wisconsin (UW): 10, 11, 29, 39, 40, 41, 44, 65, 115, 131

University of Wisconsin: Characterization Laboratory for Irradiated Materials, 131

University of Wisconsin: Tandem Accelerator Ion Beam, 131

Westinghouse: 10, 11, 35, 41, 112, 113, 114, 116, 119, 131

Westinghouse: Churchill Site, 131

Westinghouse: Materials Center of Excel-

lence (MCOE) Laboratories, 119

Collaborators

Aitkaliyeva, Assel

Idaho National Laboratory 42, 48, 103, 132

Almer, Jonathan

Argonne National Laboratory 102, 103

Almirall, Nathan

University of California, Santa Barbara 34,

64,65

Back, Christina General Atomics 83

Bhattacharyya, Dhriti

Australian Nuclear Science and Technology

Organisation 55, 65

Billone, Mike

Argonne National Laboratory 103

Borghmans, Gitte

Studiecentrum voor Kernenergie/Centre d'Étude

de l'énergie nucleaire (SCK CEN) 127

Cappia, Fabiola

Idaho National Laboratory 2, 42, 104, 111

Chen, Wei-Ying

Argonne National Laboratory 102, 103, 132

Cole, Jim

Idaho National Laboratory 64, 65

Daw, Joshua E.

Idaho National Laboratory 66, 69, 75, 89

Deck, Christian P.

General Atomics 42, 82, 83

Ecker, Lynne

Brookhaven National Laboratory 64, 65

Estrada, David

Boise State University 34, 42, 89

Freyer, Paula D.

Westinghouse 112, 118, 119

Fujimoto, Kiyo

Boise State University 89

Gan, Jian

Idaho National Laboratory 18, 21, 26, 35,

43, 102, 103, 126, 132

Garner, Frank

Radiation Effects Consulting 112, 118, 119

Hale, Cody

Idaho National Laboratory 127

Harp, Jason

Idaho National Laboratory 104, 111

Hawari, Ayman

North Carolina State University 103

He, Lingfeng

Idaho National Laboratory 26, 35, 39, 46,

103, 132

Hosemann, Peter

University of California, Berkeley 64, 65,

101, 103, 132

Hu, Xunxiang

Oak Ridge National Laboratory 83

Hua, Zilong

Idaho National Laboratory 89

Hurley, Dave

Idaho National Laboratory 89

Jacquet, Patrice

SCK CEN 127

Katoh, Yutai

Oak Ridge National Laboratory 3, 30, 31, 32,

33, 35, 76, 82, 83, 132

Kempf, Nick

University of Notre Dame 89

Knight, Collin

Idaho National Laboratory 4,103,118

Koyanagi, Takaaki

Oak Ridge National Laboratory 35, 44, 82,

83, 132

Lassell, Scott

North Carolina State University 103

Leaners, Ann

SCK CEN 127

Li, Meimei

Argonne National Laboratory 102, 103, 132

Liu, Ming

North Carolina State University 103

Liu, Xiang

Idaho National Laboratory 44, 102, 103

Maddock, Tom

Idaho National Laboratory 4, 127

Maloy, Stuart A.

Los Alamos National Laboratory 64, 65, 102,

103.132

Marquis, Emmanuelle A.

University of Michigan 55, 64, 65, 119

McDuffee, Joel L.

Oak Ridge National Laboratory 82, 83

Miao, Yinbin

Argonne National Laboratory 35, 38, 40,

102, 103

Mo, Kun

Argonne National Laboratory 102, 103

Morgan, Dane

University of Wisconsin 64, 65

Odette, G. R.

University of California, Santa Barbara 52,

64, 65, 132, 127

Okuniewski, Maria A.

Purdue University 36, 102, 120, 127

Park, Jun-Sang

Argonne National Laboratory 102, 103

Petrie, Christian M.

Oak Ridge National Laboratory 40, 82, 83, 133

Sikik, Emre

SCK CEN 127

Singh, Gyanender

Oak Ridge National Laboratory 82, 83

Sprenger, Mike

Idaho National Laboratory 127

Sprouster, D. J.

Brookhaven National Laboratory 64, 65

Stubbins, James F.

University of Illinois at Urbana-Champaign

36, 40, 90, 102, 103

Terrani, Kurt A.

Oak Ridge National Laboratory 82, 83



Terry, Jeff Illinois Institute of Technology 102, 103

Tomchik, Carolyn A.

Argonne National Laboratory 102, 103

Van den Berghe, Sven SCK CEN 126, 127

Van den Branden, Geert SCK CEN 127

Van Dyck, Steven SCK CEN 127 Wachs, Daniel M. Idaho National Laboratory 126, 127

Wang, Hsin Oak Ridge National Laboratory 83

Wells, Peter University of California, Santa Barbara 55, 64, 65, 132

Williams, Walter Purdue University 41, 45, 120, 127 Yamamoto, Takuya University of California, Santa Barbara 45,64, 65

Zhang, Xuan Argonne National Laboratory 45, 102, 103

Zhang, Yanliang University of Notre Dame 84, 89, 111

